UNIVERSITÀ
DEGLI STUDI
DI PADOVA

Sede Amministrativa: Università degli Studi di Padova
Dipartimento di Scienze Chimiche

SCUOLA DI DOTTORATO DI RICERCA IN SCIENZE CHIMICHE
INDIRIZZO: SCIENZE MOLECOLARI
CICLO XVII

ORGANIZATION AND SIGNAL REGULATION IN COMPLEX CHEMICAL SYSTEMS

Direttore della Scuola: Ch.mo Prof. Antonino Polimeno
Coordinatore d'indirizzo: Ch.mo Prof. Antonino Polimeno
Supervisore: Ch.mo Prof. Leonard J. Prins

Dottorando: Cristian Pezzato

Dedico questo lavoro a tutte le persone
intellettualmente oneste rimaste in questo paese.

A tutti i colleghi e amici che con passione, coraggio e
dedizione si misurano ogni giorno nel mondo della ricerca.

A mamma,
lavoratrice infaticabile, stella polare della mia vita.

A papà,
genio ribelle, incompreso ma comprensivo.

A Sara,
sorella meravigliosa, amica sensibile e genuina.

But why, some say, the moon? Why choose this as our goal?
And they may well ask why climb the highest mountain?
Why, 35 years ago, fly the Atlantic? Why does Rice play Texas?
We choose to go to the moon. We choose to go to the moon
in this decade and do the other things, not because they are easy,
but because they are hard, because that goal will serve
to organize and measure the best of our energies and skills,
because that challenge is one that we are willing to accept,
one we are unwilling to postpone, and one which we intend to win,
and the others, too.

John Fitzgerald Kennedy, September 12, 1962

Table of Content

Chapter 1

Chapter 2

Chapter 3

Chapter 4

Chapter 5

Chapter 6

Chapter 7

Chapter 8

Chapter 1

General introduction

1.1 Supramolecular chemistry

The Nobel prize awarded to Lehn, Cram, and Pedersen in 1987 marked the official recognition of supramolecular chemistry as "chemistry beyond the molecule": a new branch of chemistry focused on the study and development of chemical systems that rely on non-covalent interactions between molecules. Molecular chemistry (i.e. the chemistry of the covalent bond) concerns the uncovering and mastering of the rules that govern the structure, properties and transformation of molecules.[1] Supramolecular chemistry combines all the resources provided by molecular chemistry together with the controlled manipulation of non-covalent interactions for the formation of "supermolecules",[2] which are organized complex entities of molecular subunits. The process by which supermolecules are formed has been referred to as self-assembly, i.e. the spontaneous association of either a few or many components resulting in the formation of either discrete supermolecules or extended supramolecular assemblies.[3] Alternatively, self-assembly can be defined as the autonomous organization of components into precise structures without human intervention.[4] Self-assembly is undoubtedly at the core of supramolecular chemistry, where the "instructions" of how to assemble larger entities are "encoded" in the structure of the individual molecules. The main

challenge is then to "program" the molecular building blocks such that they organize into the desired structure.[5-7] Over the past decades, chemists have learned the rules that govern self-assembly processes benefitting from the numerous examples provided by Nature. A thorough understanding of natural self-assembly processes has been decisive for implementing self-assembly as a viable tool for the construction of synthetic architectures.

1.2 Self-assembly in Nature

Self-assembly is a ubiquitous process in biology, where it plays an important role in numerous processes and underlines the formation of a wide range of functional complex structures.[8] Self-assembly is of crucial importance in life as it is involved in many of the functional processes of the living cell. The specificity and precision displayed by biological systems is derived from the highly directed mutual recognition displayed by the components of a structure.[9]

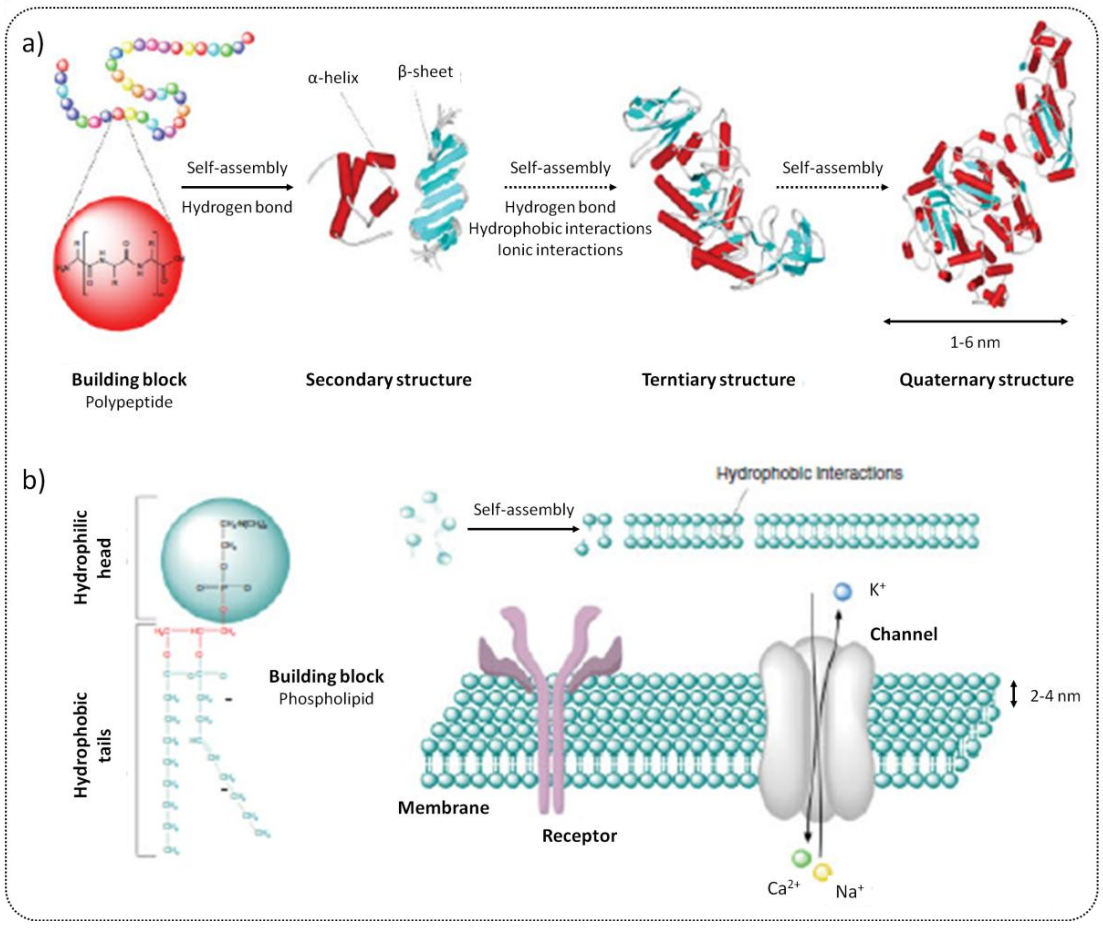

Figure 1.1. Schematic representation of (a) the protein folding process and (b) the 2D mosaic fluid.[13]

For example, protein folding clearly illustrates how the number and type of non-covalent interactions (e.g. hydrogen bonds, hydrophobic and ionic interactions, etc.) determines the conformations of a given structure (from secondary to quaternary), ultimately leading to the formation of functional domains (e.g. catalytic and binding points) (Figure 1.1a). Nonetheless, it is the specific order of amino acids in the peptide sequence (primary structure) that dictates how protein folding will occur.[10] Another example of a biological self-assembled system is represented by the cytoplasmic membrane, which is a phospholipid bilayer that serves to create a confined space isolated from the external environment: the cell. The phospholipid bilayer is composed of phospholipids, whose structure generally consists of hydrophobic tails and a hydrophilic head group. The bilayer results from the self-assembly of these amphiphilic building blocks, which are arranged so that the polar heads form the outermost and the innermost of the membrane, while the hydrophobic tails cluster in the apolar region of the membrane. The resulting 2D mosaic fluid[11] structure is selectively permeable to ions (e.g. Ca^{2+}, Na^{+}, K^{+}, etc.) and organic molecules and has the fluidity to allow the entrance of other solutes inside the cell by endocytosis.[12,13] Among others, these two examples highlight how biological systems display a diverse array of functional nanoscale structures in various length scale (from 1 to 10^4 nm). Their beauty reflects the art of making stable functional systems of large dimensions by the summation of many weak noncovalent interactions between chemical entities.

1.3 Supramolecular synthesis

From the chemists' point of view, the research in self-assembly has evolved as an important step forward to overcome the conceptual limits of chemical synthesis, with the aim to design and control the formation of synthetic structures that approach the size and complexity of biological systems.[9,14-16] This has led to an impetuous development of so-called s*upramolecular synthesis* (i.e. the creation of multicomponent supramolecular architectures utilizing non-covalent interactions). A broad range of new highly ordered and molecularly defined structures have been achieved, ranging from inclusion complexes to ordered oligo- and polymolecular entities held together using intermolecular bonds.[16] In particular, the subdiscipline

of *metallo-supramolecular chemistry* has provided beautiful examples that illustrate the potential of this approach. Discrete multicomponent supermolecules such as supramolecular cages,[17-19] macrocycles,[20,21] grids,[22] racks,[23] ladders,[24] clusters[25] and helices have been synthesized through self-assembly using predominantly coordination bonds.[26] Other beautiful achievements are represented by supramolecular systems built from strong and cooperative hydrogen-bonding interactions characteristic of melamine with other complementary molecules such as barbituric acid.[27] On the other hand, self-assembly has been used as a tool to mediate the formation of mechanical bonds, resulting in completely new chemical entities, whose structure is unattainable using the available repertoire of covalent-bond-making tools. Examples are interlocked entities such as catenanes, rotaxanes and interwoven cages to name a few.[28-30]

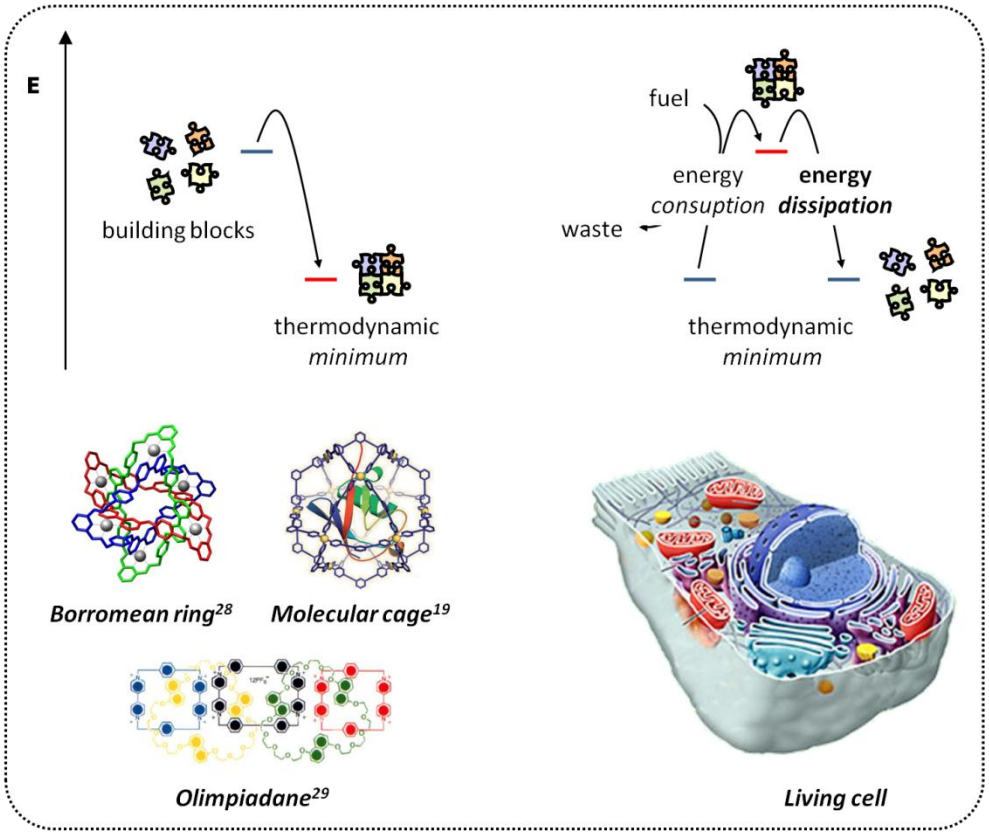

Figure 1.2 Crucial difference between synthetic and natural systems

However, notwithstanding the achievements made over the past decades, fundamental differences exist between natural and synthetic systems. [31] First, most of synthetic systems regard symmetric, hierarchically well-defined molecular

architectures, whose complexity is still much less advanced compared to natural systems. Second, natural assemblies are built up for carrying out precise functions, while most of those described above, although beautiful, were born merely for a synthetic challenge rather than for being used concretely. A final crucial difference regards the concepts of *self-assembly* and *self-organization*, which are often used interchangeably, but they are not. Both refer to the spontaneous formation of ordered structures but they are distinguished on a thermodynamic basis: self-assembly is a spontaneous process that leads toward equilibrium, whereas self-organization is a non-equilibrium process. Natural systems operate *out-of-equilibrium*, in a regime in which the infusion of energy is of crucial importance for maintaining the mutual organizations of large structures.[32] On the contrary, synthetic self-assembled systems still concern spontaneous processes tending *toward equilibrium* (Figure 1.2). Once made, they cannot be either further adjusted/reconfigured or respond to changes in the external environment as happens in the biological world.[31] Consequently, further efforts are still needed to fill up these gaps.

1.4 Toward complex supramolecular architectures

In order to overcome such limitations, chemists have recalibrate their target trying to develop *functional* supramolecular systems starting from *simple* building blocks (bottom-up approach).[14,33] A wide range of different building blocks can be used to form large supramolecular structures in a variety of different conditions. A key prerequisite is the possibility of the builiding blocks to form multiple non-covalent interactions in a given solvent. Probably, one of the most widespread class of building blocks used are amphiphilic molecules that can assemble into a variety of nanosized structures (Figure 1.3).[34,35] Examples of frequently used amphiphiles are simple surfactants,[36] dendritic molecules,[37,38] and synthetic block copolymers.[39,40] Based on parameters such as amphiphile geometry and concentration a wide variety of assemblies[41] can be formed: from micellar aggregates (e.g. micelles,[42] micellar rods[43]) to bilayer structures such as vesicles (e.g. liposomes[44]) as well as supramolecular polymers. The latter include even more sophisticated constructs such as nanofibers, twisted nanoribbons and nanotubes.[45-48] In this case, most of

the structures can be precisely designed to exhibit stimuli responsive behaviour in reponse to changes in the environment (e.g. pH, temperature, solvent). This has been exploited for developing new approaches toward drug delivery and smart materials.[38,49,50]

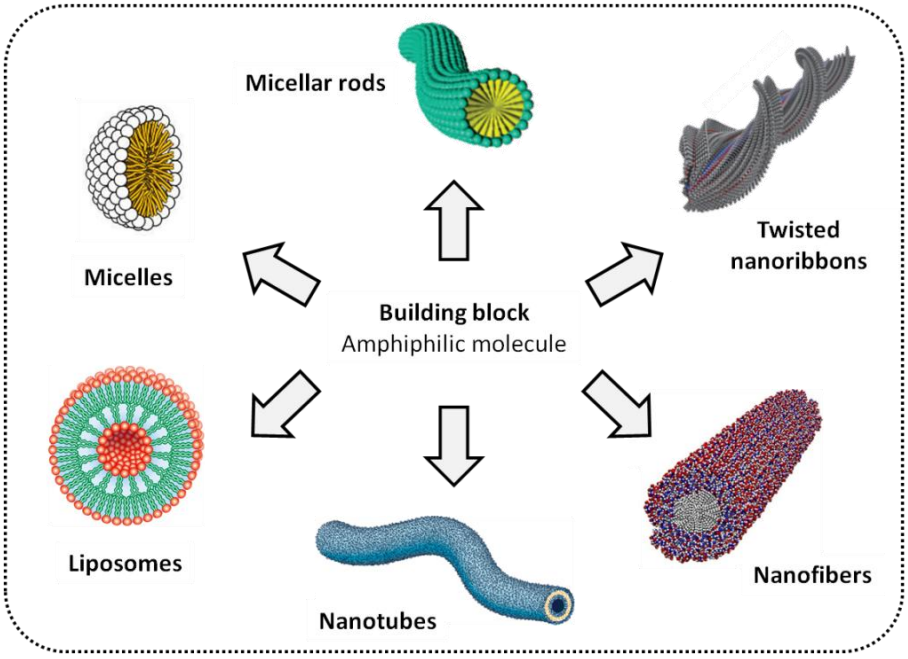

Figure 1.2. Representation of the various structures accessible using amphiphilic build blocks.

A common feature of amphiphile-based supramolecular structures is the use of fully organic molecules as building blocks. Nonetheless, the scientific community has been increasingly interested to combine the modularity of organic functionalities together with the robustness of metals and semiconductors. On this way, highly ordered architectures built from inorganic clusters have started to emerge,[51,52] whose enhanced stability (both thermodynamic and kinetic)[53] associated with unique optical, electronic and magnetic properties[54] have opened new ways for a wide range of appliciations.

1.5 Functionalized gold nanoparticles

Amongst other type of noble metal colloids, monolayer protected gold clusters (Au NPs) have attracted major interest originating from a combination of unique physical and chemical attributes.[36] Au NPs are composed of a gold core of nanosized dimensions (d = 1 -25 nm) covered by a monolayer of organic molecules, typically

thiols.[55,56] The organic monolayer is obtained through a self-assembly process driven by the formation of (most frequently) a stable Au-S bond. The result is a multivalent system with a very high stability, even at very low concentrations under physiologically relevant conditions. Reproducible synthetic protocols have been developed that allow a functionalization with a large variety of head groups, either for use in aqueous or organic media.[57-59] The optoelectronic properties of the gold core, such as surface plasmon resonance absorption, conductivity, or redox behavior, can be used for signal generation as these are typically sensitive to recognition processes occurring at the monolayer surface. For these reasons, Au NPs have represented a key component for the development of sensing applications as they offer a platform for multifunctionalization with a wide range of organic or biological ligands for the selective binding and detection of small molecules and biological targets.[60-62]

1.5.1 Au NPs containing metal binding sites

A particular subgroup of Au NPs is represented by those that contain metal binding sites in the monolayer. In this case the chemical nature of the binding sites determines which metal ions will be complexed, thus provides for an easy way to tune the selectivity of the system for the sensing of certain metal ions.[63-67] However, metal ions complexed in the monolayer can themselves act as recognition units for the selective interaction with small molecules[68,69] or larger (bio)macromolecules.[60,62] Nonetheless, the attractiveness of this kind of Au NPs results from the possibility to create in a straightforward and controlled manner multivalent surfaces with a very high density of recognition elements able to develop strong interactions with external molecules. This aspect is extremely important to achieve complexity both in terms of structure and function, which is the great lack of synthetic systems compared to the natural ones. Recently, the Prins' group has shown that this concept can be used as alternative approach toward the formation of complex supramolecular structures with minimal synthetic efforts.[70,71] In particular, gold nanoparticles Au NP **1**•Zn^{2+} (d_{Au} = 1.8 ± 0.4 nm) containing 1,4,7-triazacyclononane (TACN)•Zn^{2+} head groups have proved to be highly attractive building blocks for the assembly of multivalent structures. The

ability of gold clusters to quench the fluorescence of bound fluorophores[72] has been exploited for studying the binding of fluorescent anions (Figure 1.4). It was found that biologically relevant oligoanions, such as nucleotides or peptides, have such a high affinity for Au NP **1**•Zn^{2+} that binding occurs under saturation conditions at low micromolar concentrations in water. In particular, an apparent binding constant of $2.4x10^8$ M^{-1} has been calculated for 2-aminopurine riboside-5'-O-triphosphate (**A**), a fluorescent analogue of ATP.[71] In addition, it was shown that the surface composition can be modulated simply by varying the ratio of anionic probes, giving important perspectives for a post-synthetic regulation of the supramolecular functions.

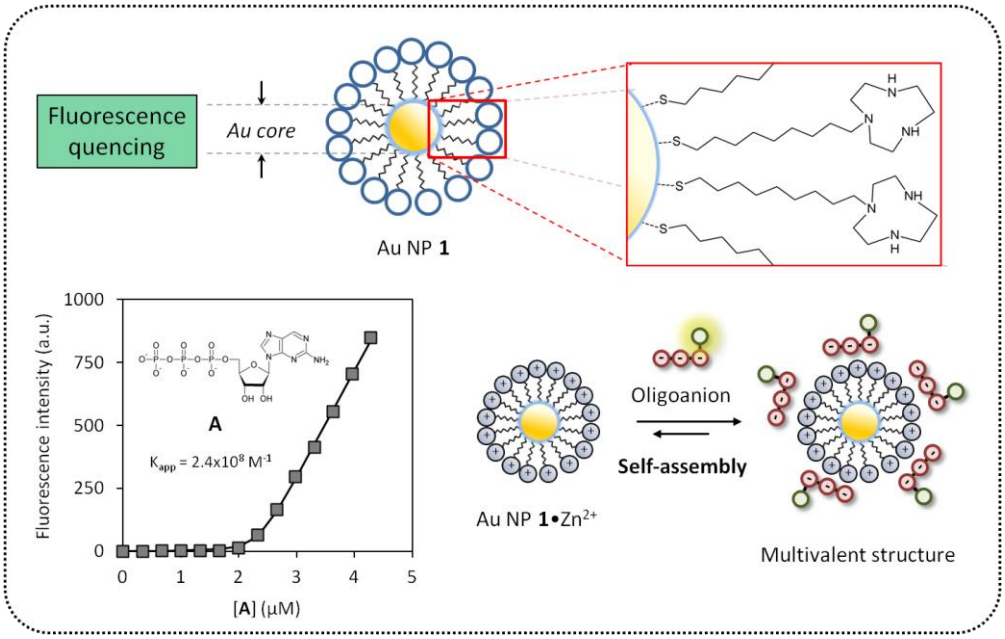

Figure 1.4 Schematic representation of the structure of Au NP **1**. On the bottom are reported a general representation of the self-assembly of oligoanions on the surface of Au NP **1**•Zn^{2+} together with the binding profile obtained adding increasing amount of **A** to a buffered aqueous solution ([HEPES] = 10 mM, pH 7.0) of Au NP **1**•Zn^{2+} (10 μM).

1.6 Concept of this Thesis

As mentioned in the paragraph 1.3, there are still fundamental differences between natural and synthetic systems. This thesis extends the use of Au NP **1**•Zn^{2+} as multivalent scaffolds for the development of complex functional systems. Particular emphasis is dedicated to study the self-assembly of various small anionic molecules on the monolayer surface, within the challenge to approach behaviours characteristic of natural systems.

Chapter 2 deals with the study of the valency of a self-assembled system comprising many small molecules bound to the surface of Au NP **1** as a function of different experimental conditions. It is shown that the metal ions in the monolayer can be used as regulatory elements of the self-assembly process, giving the possibility to control the valency of the system in a reversible manner.

Chapter 3 introduces the use of a series of commercially available fluorescent anions with the aim to rationalize the structural factors that govern the interaction between Au NP 1 and small molecules. It is shown that the presence of hydrophobic moieties able to penetrate into the apolar part of the monolayer significantly enhance the the binding affinity.

In **Chapter 4** a primitive form of compartmentalization is developed It is shown that a mixture of two different oligoanions, with the same number of negative charges but with different anionic groups (phosphate *vs* carboxylate), spontaneously self-sorted on two different monolayer surfaces, creating two discrete topological domains in a homogeneous system. In **Chapters 5** and **6** the obtained knowledge is exploited for the development of supramolecular sensors able to detect small molecules and enzymes. It is shown that the self-assembly of multiple fluorescence indicators on the monolayer surface resulted in a dynamic responsive surface able to generate finger-print patterns upon the addition of eight different di- and tri-nucleotides. The ability of the system to discriminate between ATP and ADP was then used for the development of a protein kinase assay relying on the monitoring of ATP→ADP conversion.

Chapter 7 deals with the study of the catalytic activity of Au NP **1**•Zn^{2+} with the aim to improve the sensitivity of the protein kinase assay. Is shown that ATP→ADP conversion can be potentially be detected by means of catalytic signal amplification.

Chapter 8 unifies all the concepts emerged before and describes a *life-like* supramolecular system able to generate a transient signal, whose duration is determined by the amount of ATP added to the system. It is shown that the methodology provides a straightforward way to gain temporal control over supramolecular processes in general, reflecting important analogies with the behaviour of natural signalling pathways.

1.7 References

(1) "Jean-Marie Lehn - Nobel Lecture: Supramolecular Chemistry - Scope and Perspectives: Molecules - Supermolecules - Molecular Devices". Nobelprize.org. Nobel Media AB 2014. Web. 27 Jan 2015.

(2) from the german term "übermolekule", K. L. Wolf, R. Wolff, *Angew. Chem.* **1949**, *61*, 191

(3) Lehn, J. M. *Supramolecular Chemistry*; Wiley, **1995**.

(4) Whitesides, G. M.; Grzybowski, B. *Science* **2002**, *295*, 2418.

(5) Lehn, J. M. *Proc. Natl. Acad. Sci. USA* **2002**, *99*, 4763.

(6) Whitesides, G. M.; Boncheva, M. *Proc. Natl. Acad. Sci. USA* **2002**, *99*, 4769.

(7) Grzybowski, B. A.; Wilmer, C. E.; Kim, J.; Browne, K. P.; Bishop, K. J. M. *Soft Matter* **2009**, *5*, 1110.

(8) Boncheva, M; Whitesides, G.M. *MRS Bull*, **2005**, *30*, 736-742

(9) Philp, D.; Fraser Stoddart, J. *Angew. Chem. Int. Ed.* **1996**, *35*, 1154.

(10) Fasman, G. D. *Prediction of Protein Structure and the Principles of Protein Conformation*; Springer, **1989**.

(11) Singer, S. J.; Nicolson, G. L. *Science* **1972**, *175*, 720.

(12) Alberts, B.; Johnson, A.; Lewis, J.; Walter, P.; Raff, M.; Roberts, K. *Molecular Biology of the Cell 4th Edition: International Student Edition*; Routledge, **2002**.

(13) Mendes, A. C.; Baran, E. T.; Reis, R. L.; Azevedo, H. S. *WIREs Nanomed Nanobiotechnol*. **2013**, *5*, 582–612.

(14) Whitesides, G. M.; Mathias, J. P.; Seto, C. T. *Science* **1991**, *254*, 1312.

(15) Whitesides, G. M.; Simanek, E. E.; Mathias, J. P.; Seto, C. T.; Chin, D.; Mammen, M.; Gordon, D. M. *Acc. Chem. Res.* **1995**, *28*, 37.

(16) Fyfe, M. C. T.; Stoddart, J. F. *Acc. Chem. Res.* **1997**, *30*, 393.

(17) Fujita, M.; Oguro, D.; Miyazawa, M.; Oka, H.; Yamaguchi, K.; Ogura, K. *Nature* **1995**, *378*, 469.

(18) MarquisRigault, A.; DupontGervais, A.; Baxter, P. N. W.; VanDorsselaer, A.; Lehn, J. M. *Inorg. Chem.* **1996**, *35*, 2307.

(19) Fujita, D.; Suzuki, K.; Sato, S.; Yagi-Utsumi, M.; Yamaguchi, Y.; Mizuno, N.; Kumasaka, T.; Takata, M.; Noda, M.; Uchiyama, S.; Kato, K.; Fujita, M. *Nat. Commun.* **2012**, *3*, 1093.

(20) Fujita, M.; Sasaki, O.; Mitsuhashi, T.; Fujita, T.; Yazaki, J.; Yamaguchi, K.; Ogura, K. *Chem. Commun.* **1996**, 1535.

(21) Whiteford, J. A.; Lu, C. V.; Stang, P. J. *J. Am. Chem. Soc.* **1997**, *119*, 2524.

(22) Baxter, P. N. W.; Lehn, J. M.; Fischer, J.; Youinou, M. T. *Angew. Chem. Int. Ed.* **1994**, *33*, 2284.

(23) Hanan, G. S.; Arana, C. R.; Lehn, J. M.; Baum, G.; Fenske, D. *Chem. Eur. J.* **1996**, *2*, 1292.

(24) Baxter, P. N. W.; Hanan, G. S.; Lehn, J. M. *Chem. Commun.* **1996**, 2019.

(25) Beissel, T.; Powers, R. E.; Raymond, K. N. *Angew. Chem. Int. Ed.* **1996**, *35*, 1084.

(26) Funeriu, D. P.; Lehn, J. M.; Baum, G.; Fenske, D. *Chem. Eur. J.* **1997**, *3*, 99.

(27) Zerkowski, J. A.; Seto, C. T.; Wierda, D. A.; Whitesides, G. M. *J. Am. Chem. Soc.* **1990**, *112*, 9025.

(28) Chichak, K. S.; Cantrill, S. J.; Pease, A. R.; Chiu, S. H.; Cave, G. W.; Atwood, J. L.; Stoddart, J. F. *Science* **2004**, *304*, 1308.
(29) Amabilino, D. B.; Ashton, P. R.; Reder, A. S.; Spencer, N.; Stoddart, J. F. *Angew. Chem Int. Ed.* **1994**, *33*, 433.
(30) Ashton, P. R.; Collins, A. N.; Fyfe, M. C. T.; Glink, P. T.; Menzer, S.; Stoddart, J. F.; Williams, D. J. *Angew. Chem. Int. Ed.* **1997**, *36*, 59.
(31) Fialkowski, M.; Bishop, K. J.; Klajn, R.; Smoukov, S. K.; Campbell, C. J.; Grzybowski, B. A. *J. Phys. Chem. B* **2006**, *110*, 2482.
(32) Halley, J. D.; Winkler, D. A. *Complexity* **2008**, *14*, 10.
(33) Zhang, S. *Nat. Biotechnol.* **2003**, *21*, 1171.
(34) Velonia, K. *Polym. Chem.* **2010**, *1*, 944.
(35) Lim, Y.-b.; Moon, K.-S.; Lee, M. *J. Mater. Chem.* **2008**, *18*, 2909.
(36) Reynhout, I. C.; Cornelissen, J. J.; Nolte, R. J. *Acc. Chem. Res.* **2009**, *42*, 681.
(37) Smith, D. K. *Chem. Commun.* **2006**, 34.
(38) Zeng, F.; Zimmerman, S. C. *Chem. Rev.* **1997**, *97*, 1681.
(39) Lohmeijer, B. G.; Schubert, U. S. *Angew. Chem. Int. Ed.* **2002**, *41*, 3825.
(40) Blanazs, A.; Armes, S. P.; Ryan, A. J. *Macromol. Rapid. Commun.* **2009**, *30*, 267.
(41) Lowik, D. W.; van Hest, J. C. *Chem. Soc. Rev.* **2004**, *33*, 234.
(42) Roks, M. F. M.; Visser, H. G. J.; Zwikker, J. W.; Verkley, A. J.; Nolte, R. J. M. *J. Am. Chem. Soc.* **1983**, *105*, 4507.
(43) Velonia, K.; Rowan, A. E.; Nolte, R. J. *J. Am. Chem. Soc*. **2002**, *124*, 4224.
(44) Zhang, S.; Sun, H. J.; Hughes, A. D.; Moussodia, R. O.; Bertin, A.; Chen, Y.; Pochan, D. J.; Heiney, P. A.; Klein, M. L.; Percec, V. *Proc. Natl. Acad. Sci. USA* **2014**, *111*, 9058.
(45) Zheng, B.; Wang, F.; Dong, S.; Huang, F. *Chem. Soc. Rev.* **2012**, *41*, 1621.
(46) de Greef, T. F.; Meijer, E. W. *Nature* **2008**, *453*, 171.
(47) Aida, T.; Meijer, E. W.; Stupp, S. I. *Science* **2012**, *335*, 813.
(48) Hartgerink, J. D.; Beniash, E.; Stupp, S. I. *Proc. Natl. Acad. Sci. USA* **2002**, *99*, 5133.
(49) Allen, T. M.; Cullis, P. R. *Adv, Drug Deliv. Rev.* **2013**, *65*, 36.
(50) Tanner, P.; Baumann, P.; Enea, R.; Onaca, O.; Palivan, C.; Meier, W. *Acc. Chem. Res.* **2011**, *44*, 1039.
(51) Mirkin, C. A.; Letsinger, R. L.; Mucic, R. C.; Storhoff, J. J. *Nature* **1996**, *382*, 607.
(52) Li, M.; Schnablegger, H.; Mann, S. *Nature* **1999**, *402*, 393.
(53) Jin, R. *Nanoscale* **2010**, *2*, 343.
(54) Hayat, A. *Colloidal Gold: Principles, Methods, and Applications*; Academic Press, 1989.
(55) Templeton, A. C.; Wuelfing, M. P.; Murray, R. W. *Acc. Chem. Res.* **2000**, *33*, 27.
(56) Daniel, M. C.; Astruc, D. *Chem. Rev.* **2004**, *104*, 293.
(57) Zhao, P. X.; Li, N.; Astruc, D. *Coord. Chem. Rev.* **2013**, *257*, 638.
(58) Brust, M.; Walker, M.; Bethell, D.; Schiffrin, D. J.; Whyman, R. *Chem. Commun.* **1994**, 801.
(59) Jana, N. R.; Peng, X. G. *J. Am. Chem. Soc.* **2003**, *125*, 14280.

(60) Giljohann, D. A.; Seferos, D. S.; Daniel, W. L.; Massich, M. D.; Patel, P. C.; Mirkin, C. A. *Angew. Chem. Int. Ed.* **2010**, *49*, 3280.
(61) Bunz, U. H. F.; Rotello, V. M. *Angew. Chem. Int. Ed.* **2010**, *49*, 3268.
(62) Saha, K.; Agasti, S. S.; Kim, C.; Li, X. N.; Rotello, V. M. *Chem. Rev.* **2012**, *112*, 2739.
(63) Russell, L. E.; Pompano, R. R.; Kittredge, K. W.; Leopold, M. C. *J. Mater. Sci.* **2007**, *42*, 7100.
(64) Norsten, T. B.; Frankamp, B. L.; Rotello, V. M. *Nano Lett.* **2002**, *2*, 1345.
(65) Chai, F.; Wang, C.; Wang, T.; Li, L.; Su, Z. *ACS Appl. Mater. Interfaces* **2010**, *2*, 1466.
(66) Krpetic, Z.; Guerrini, L.; Larmour, I. A.; Reglinski, J.; Faulds, K.; Graham, D. *Small* **2012**, *8*, 707.
(67) Lisowski, C. E.; Hutchison, J. E. *Anal. Chem.* **2009**, *81*, 10246.
(68) Zhang, S.; Wang, J.; Han, L.; Li, C.; Wang, W.; Yuan, Z. *Sensor. Actuat. B - Chem.* **2010**, *147*, 687.
(69) Massue, J.; Quinn, S. J.; Gunnlaugsson, T. *J. Am. Chem. Soc.* **2008**, *130*, 6900.
(70) Zaramella, D.; Scrimin, P.; Prins, L. J. *J Am Chem Soc* **2012**, *134*, 8396.
(71) Pieters, G.; Cazzolaro, A.; Bonomi, R.; Prins, L. J. *Chem. Commun.* **2012**, *48*, 1916.
(72) Dulkeith, E.; Mortcani, A. C.; Niedereichholz, T.; Klar, T. A.; Feldmann, J.; Levi, S. A.; Van Veggel, F. C. J. M.; Reinhoudt, D. N.; Möller, M.; Gittins, D. I. *Phys. Rev. Lett.* **2002**, *89*, 2030021.

Chapter 2

Reversible control over the valency of a nanoparticle-based supramolecular system*

*In this chapter, the valency (i.e. the number of bound molecules) of a self-assembled system comprising small molecules bound to the surface of Au NP **1** is studied under different conditions, such as the presence of metal ions (i.e. Zn^{2+}, Cu^{2+}) in the monolayer and the pH of the bulk solution. It will be shown that metal ions increase the valency of the self-assembled nanosystem, independent of the pH. On the contrary, in the absence of metal ions, the valency of the system varies as a function of pH, reflecting the different protonation states of the free TACN-ligands. This behaviour was used to reversibly control the valency of the system in situ, through the addition and removal of metal ions. The release rate of the bound molecules was pH-dependent and could be further controlled by altering the ratio of different metal ions in the monolayer. These results are important as they give new perspectives for a post-synthetic regulation of the valency of supramolecular systems.*

* Part of this Chapter was published in: G. Pieters, C. Pezzato, L. J. Prins *J. Am. Chem. Soc.* **2012**, *134*, 15289-15292.

2.1 Introduction

Multivalency has become a key concept in the fields of biorecognition,[1] catalysis,[2] supramolecular chemistry[3] and nanotechnology.[4,5] Consequently, there is a strong interest in the functionalization of synthetic multivalent structures such as polymers,[6] dendrimers,[7] and nanoparticles.[8] In particular, gold nanoparticles (Au NPs) have emerged as attractive scaffolds, because of their straightforward preparation and functionalization. This, in combination with appealing intrinsic optical and electronic properties and a high biocompatibility, has led towards numerous applications in nanomedicine[9] and diagnostics.[10] Nonetheless, a common feature of most systems, including Au NPs, is that their valency is determined during synthesis. Systems that permit a 'post-synthetic' control over valency offer the important perspective of permitting an active regulation of the strength of interaction with the target, including a controlled dissociation if requested. An enormous progress has been made in the development of supramolecular aggregates, such as micelles, peptide amphiphiles, supramolecular polymers, etc. that indeed show adaptive behavior of their valency to the target as a spontaneous process originating from the dynamic nature of these systems.[11-13] An attractive alternative approach relies on the modification of monolayer surfaces on nanoparticles through supramolecular interactions, which permits the tunability of the valency of discrete assemblies.[14-16] In this chapter, the effect of metal ions in determining the valency of the monolayer will be emphasized. It will be shown that small molecules can be *captured* and *released* in a controlled manner from the surface of Au NPs through the addition and removal of metal ions from the monolayer, respectively. This process is fully reversible and it will be shown that both the change in valency and the release rate are pH-dependent.

2.2 Results and discussion

2.2.1 The role of Zn^{2+} metal ions

As already mentioned in the introduction, gold nanoparticles Au NP **1**•Zn^{2+} (d_{Au} = 1.8 ± 0.4 nm) containing 1,4,7-triazacyclononane (TACN)•Zn^{2+} head groups are attractive scaffolds for the formation of multivalent supramolecular structures

(Figure 2.1). It was found that oligoanions, such as ATP, ADP, or Ac-DDD-OH, have such a high affinity for Au NP **1**•Zn^{2+} that binding occurs under saturation conditions at low micromolar concentrations in water.

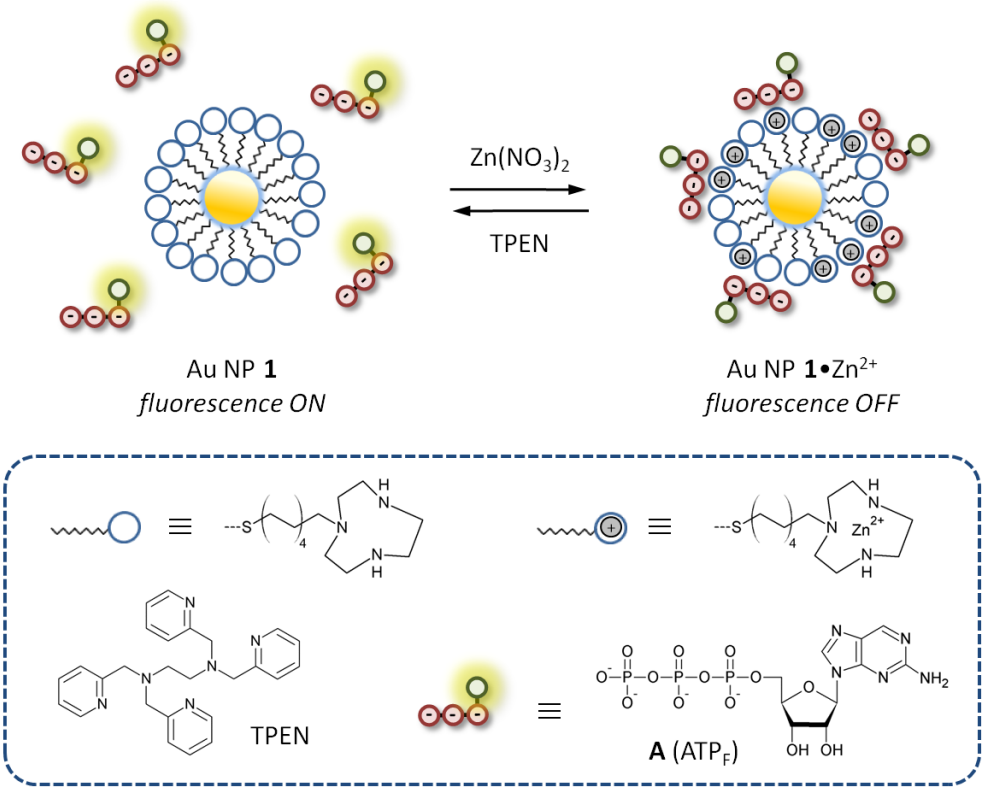

Figure 2.1. Schematic representation of metal-mediated control over the valency of the supramolecular system composed by Au NP **1** and probe **A**. On the bottom are reported the molecular structures of the components used in this chapter.

Compared to Au NP **1**, *i.e.* the same Au NP but in the absence of Zn^{2+}, the presence of the Zn^{2+}-metal ions in the self-assembled monolayer (SAM) caused an increase of the surface saturation concentration (SSC) of the oligoanions and, thus, the valency of the obtained structure. It was estimated that around 18 molecules of **A**, which is a fluorescent analogue of ATP,[17] were bound to the surface of Au NP **1**•Zn^{2+} at saturation against around 4 for Au NP **1**.[18] This is intriguing, because the difference in SSC between Au NP **1** and Au NP **1**•Zn^{2+} suggests that Zn^{2+} can potentially act as a regulatory element of the valency of the system. This hypothesis was verified by adding increasing amounts of $Zn(NO_3)_2$ to a solution of Au NP **1** ([TACN] = 10 μM) and 2.0 μM of **A** at pH 7.0 (Figure 2.2a). Considering the surface saturation concentration of 0.8 μM for **A** at this pH (Figure 2.2d) this implies that initially 1.2

µM of **A** is free in solution. The addition of Zn^{2+} results in the metalation of the TACN-ligands and a corresponding 'capture' of unbound **A** by Au NP **1**•Zn^{2+}.

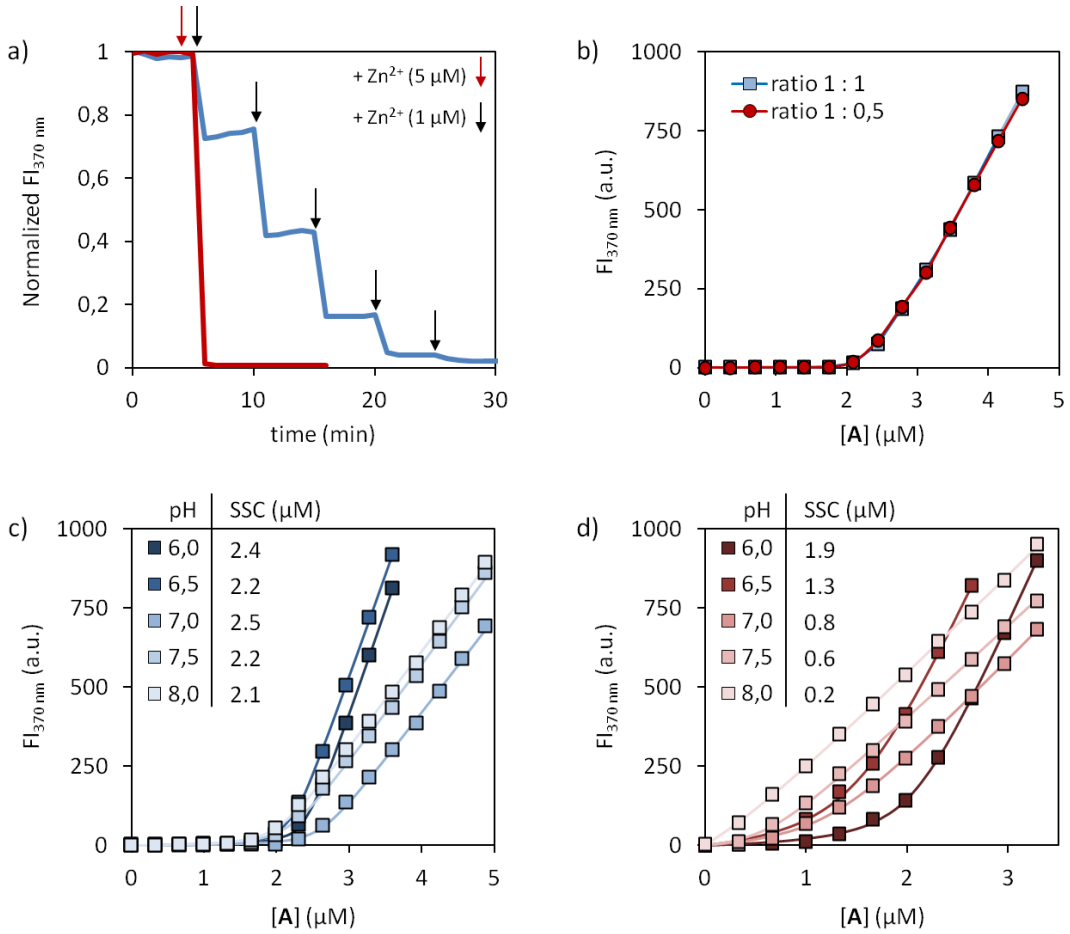

Figure 2.2. (a) Normalized fluorescence intensity at 370 nm as a function of the addition of aliquots of Zn^{2+} to a solution of Au NP **1** and **A** (2.0 µM) at pH = 7.0 (b) Fluorescence intensity at 370 nm as a function the concentration of **A** added to a solution of Au NP **1** in the presence of 10 µM (blue) or 5 µM (red) of Zn^{2+} at pH 7.0. (c-d) Fluorescence intensity at 370 nm as a function the concentration of **A** added to a solution of (c) Au NP **1**•Zn^{2+} or (d) Au NP **1** at different pHs. See the experimental section for a detailed description of the determination of SSCs. Experimental conditions (where not specified differently): [TACN] = 10 ± 1 µM, [$Zn(NO_3)_2$] = 5 µM [HEPES] = 10 mM (for pH = 7.0-8.0), [MES] = 10 mM (for pH = 6.0 and 6.5), 37°C.

Complex formation was detected by fluorescence spectroscopy, taking advantage of the ability of Au nanoparticles to quench the fluorescence of surface bound fluorophores.[19] The plot of the fluorescence intensity at 370 nm as a function of the amount of Zn^{2+} added shows several features. First, the decrease in fluorescence intensity is a clear indication that the formation of TACN•Zn^{2+} complexes on the surface of Au NP **1** results in the 'capture' of unbound **A**. Second, a complete

quenching requires the addition of only 5 μM of $Zn(NO_3)_2$ instead of the 10 μM required to metalate all TACN-ligands. An independent binding titration indeed confirmed that the **A** surface saturation concentration did not change in case 5 μM instead of 10 μM $Zn(NO_3)_2$ was added (Figure 2.2b). Third, the 'capture' of unbound **A** occurs almost instantaneously upon the addition of Zn^{2+}, in particular for the first additions. Interestingly, the addition of 5 μM of $Zn(NO_3)_2$ in a single batch resulted in a complete quenching of fluorescence within 3 minutes (Figure 2.2a, red trace). This either suggests that neighbouring TACN-ligands are selectively metalated to form bimetallic binding pockets or that the formation of binding sites composed of a single TACN•Zn^{2+} complex in combination with a neighboring protonated TACN-head group is sufficient to cause an increase in the surface saturation concentration.

In order to clarify the possible role of protonated TACN-ligands we decided to study the SSC of **A** on Au NP **1** as a function of the pHs. As before, SSC values were determined by measuring the fluorescence intensity at 370 nm as a function of the amount of **A** added to a solution of Au NP **1** ([TACN] = 10 μM) at pH values ranging from 6.0 – 8.0. This study revealed a strong pH dependence of the saturation concentrations of **A** on Au NP **1** with values decreasing from 1.9 μM at pH = 6.0 to 0.2 μM at pH = 8.0 (Figure 2d). It is important to note that at pH = 6.0 the SSC almost reached the level of Au NP **1**•Zn^{2+}, which clearly indicates the effectiveness of protonated TACN-head group as binding sites. On the other hand, the same study performed on Au NP **1**•Zn^{2+} showed a nearly constant surface saturation concentration of 2.3 ± 0.2 μM over the entire pH interval (Figure 2c). This is interesting, because it implies that the regulatory effect of Zn^{2+} is pH dependent.

2.2.2 Reversible catch & release of A

Since the addition of Zn^{2+} to Au NP **1** results in the capture of **A**, we reasoned that removal of Zn^{2+} from Au NP **1**•Zn^{2+} would cause the opposite effect, *i.e.* the release of **A** from the surface. For that reason the fluorescence intensity at 370 nm was measured upon the addition of N,N,N',N'-tetrakis(2-pyridylmethyl) ethylenediamine (TPEN), which is a ligand with a much higher affinity for Zn^{2+} compared to TACN (log $K_{TACN•Zn2+}$ = 11.5 *vs* log $K_{TPEN•Zn2+}$ = 15.4).[20] We were pleased to observe that the addition of 1 equivalent of TPEN (compared to Zn^{2+}) resulted indeed in a full

recovery of the initial fluorescence intensity indicating a complete reversibility of the process (Figure 2.3a).

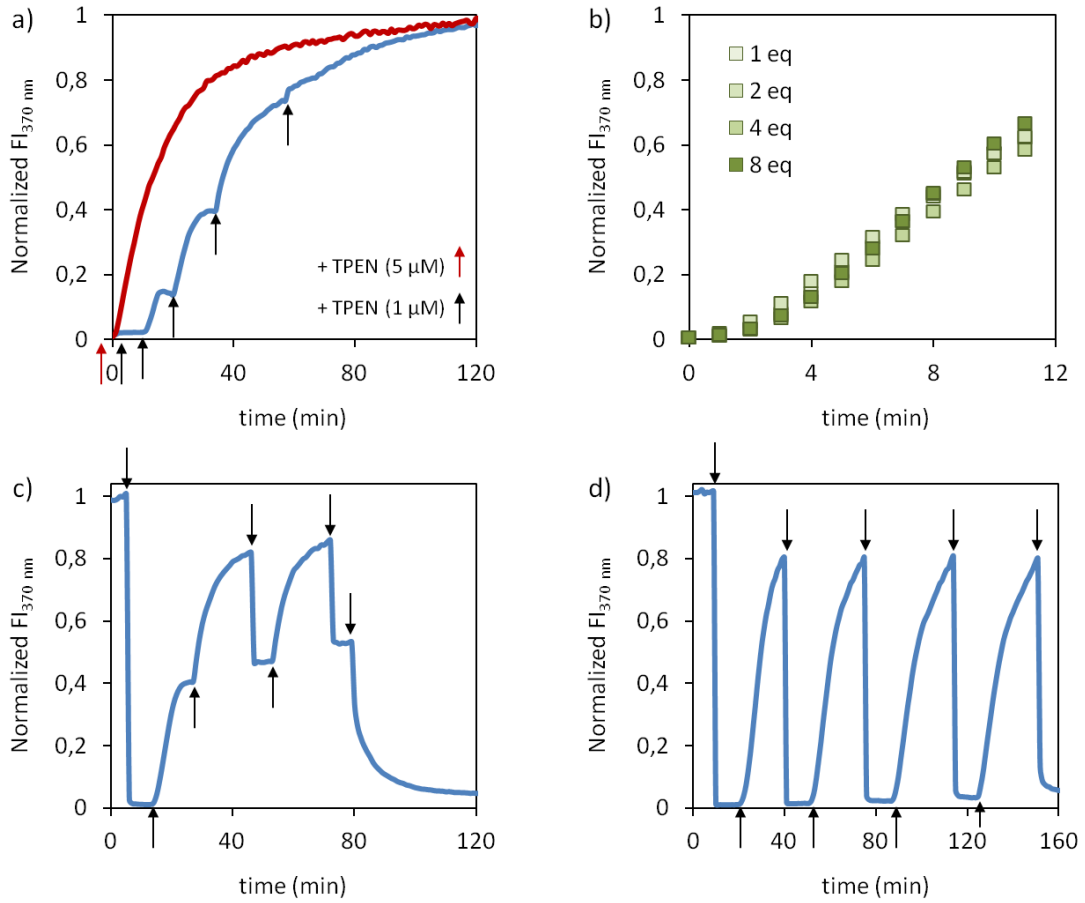

Figure 2.3. (a) Normalized fluorescence intensity at 370 nm as a function of the addition of aliquots of TPEN to a solution of Au NP **1**•Zn^{2+} and **A** at pH = 7.0 (b) Normalized fluorescence intensity at 370 nm as a function of the of time after the addition of 1, 2, 4 and 8 equivalents of TPEN. (c) Normalized fluorescence intensity at 370 upon alternating additions of aliquots of Zn^{2+} (downward arrows; 5, 1, 1, 3 µM, respectively) and TPEN (upward arrows; 3, 1, 1 µM, respectively). (d) Normalized fluorescence intensity at 370 upon alternating additions of aliquots of Zn^{2+} (downward arrows; 5 µM) and TPEN (upward arrows; 5 µM). Experimental conditions: [TACN] = 10 ± 1 µM, [**A**] = 2.0 µM [HEPES] = 10 mM, pH = 7.0, 37°C.

Contrary to the capture of **A**, the release process is relatively slow with a full release of **A** (1.2 µM) requiring nearly 2 hours. Since previous studies had shown that **A** exchange on the surface of Au NP **1**•Zn^{2+} is fast, we postulate that the release rate is determined by the dissociation rate of Zn^{2+} from the TACN•Zn^{2+} complex. This is supported by the observation that the release rate of **A** was independent of the concentration of TPEN added (1, 2, or 4 equivalents, figure 2.3b), but dependent on

the pH and type of metal ion used (see final paragraph). As before, the valency of the nanostructure could be controlled by the stepwise addition of TPEN. This experiment showed that the addition of small amounts of TPEN (1-2 μM) hardly induced the release of **A** from the surface which is in line with the previously discussed Zn^{2+} titrations. The full control over the valency of the system was demonstrated by alternating additions of small aliquots of TPEN and Zn^{2+} (Figure 2.3c). Finally, the full reversibility of the process was demonstrated by performing four repetitive 'capture-and-release' cycles through alternate additions of 5 μM of Zn^{2+} and TPEN (Figure 2.3d). In order to accelerate this experiment, Zn^{2+} was added after an **A** release equal to 80% of the maximum value. In four cycles, no changes were observed apart from a slight decrease in the release rate of **A**.

2.2.3 Release rate as a function of the pH

The nonlinear response of the system towards the addition of either Zn^{2+} or TPEN confirms the role of protonated TACN in the surface binding of **A** and reflects the fact that electrostatic interactions play an important role in complex formation. In addition, considering the pH-dependent profile of the SSC in the absence of Zn^{2+}, the change in valency of the system should be more pronounced at higher pH, due to a reduced surface capacity of Au NP **1** for **A**. This was indeed confirmed by performing 'catch-and-release' cycles in the pH range 6.5 - 8.0 (Figure 2.4a). The increase in initial fluorescence intensity at higher pHs for the same concentrations of **A** (2 μM) and Au NP **1** ([TACN] = 10 μM) reflects the presence of larger amounts of unbound **A**. In all cases the addition of Zn^{2+} (5 μM) resulted in a rapid quantitative quenching of fluorescence indicative of a quantitative capture of **A** by Au NP **1**•Zn^{2+}. For all pH values, the successive addition of TPEN (5 μM) caused a complete release of **A** restoring the initial values, but with reduced rates at higher pH values. A detailed analysis shows that the **A** released from the surface at each pH is described by (at least) two different kinetic components which were quantified by fitting the release curves to a kinetic model (Figure 2.4b). A plot of the obtained first order rate constants as a function of pH illustrates that at pH 7.0 the release rate of **A** is dominated by a single (intermediate) value ($k_{obs,\ major} = 36 \times 10^{-3}$ min^{-1}). At lower pH an additional second (faster) component is observed (170 min^{-1}), whereas at higher pH

values the second component to the rate is slower ($3.1x10^{-3}$ min^{-1}) (Figure 2.4c). These observations indicate that different binding modes exist for **A** on the surface, the relative ratios of which presumably originating from the different protonation states of the probe, TACN, and/or the TACN•Zn^{2+} complex. In summary, these data show that the pH can indeed be used not only to modulate the amplitude of the **A** 'catch-and-release' cycles, but also the rate at which the probe molecules are released.

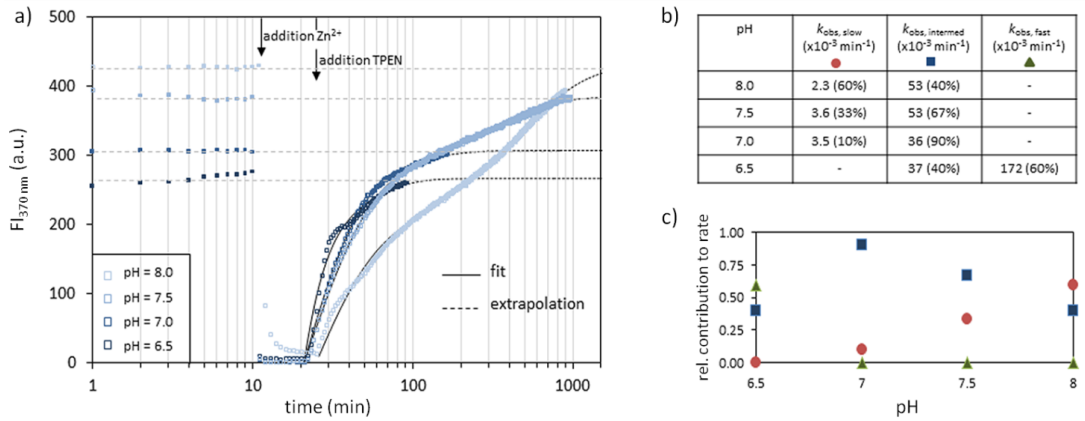

Figure 2.4. (a) Fluorescence intensity at 370 nm as a function of time upon the respective additions of Zn^{2+} and TPEN to a solution of Au NP **1** and **A**. The solid lines were generated by fitting the experimental data for the release of **A** to a kinetic model taking into account two first-order rate constants. (b) First-order rate constants determined at each pH. (c) Relative contributions to the overall rate by the slow (red), intermediate (blue), and fast (green) processes at each pH. Experimental conditions: [TACN] = 10 µM, [$Zn(NO_3)_2$] = 5 µM, [HEPES] = 10 mM (for pH 7.0-8.0), [MES] = 10 mM (for pH 6.0 and 6.5), 37 °C.

2.2.4 Release rate from a heterometalated surface

As the TACN-ligand is well known to complex several metals with different affinities, the controlled formation of a heterometalated surface (i.e. a surface metalated with different metal ions simultaneously) would in principle allow a regulation of the release rate of **A** from the surface by varying the ratio of metal ions in the monolayer. In order to test this hypothesis, we verified that the addition of 5 µM of $Cu(NO_3)_2$ to a solution of **A** (2 µM) and Au NP **1** ([TACN] = 10 µM) resulted in the quantitative capture of **A** (log $K_{TACN•Cu2+}$ = 15.4). An independent titration indeed confirmed a surface saturation concentration of 2.2 ± 0.1 µM of **A** on Au NP **1**•Cu^{2+}. Interestingly, the addition of TPEN (log $K_{TPEN•Cu2+}$ = 20.2) resulted in release of **A** as

before, but at a roughly 20-fold lower rate compared to that observed for Au NP **1**•Zn^{2+} with a complete release of **A** requiring more than 24 hours (Figure 5, light blue trace). The difference between Zn^{2+} and Cu^{2+} confirms that dissociation of the metal ion from the TACN-complex is indeed the rate-determining step for **A**-release. Finally, a study of the release rate of **A** from Au NP **1**•M^{2+} (with M = Zn^{2+}/Cu^{2+}) as a function of the ratio of Zn^{2+} and Cu^{2+} metal ions revealed that the release rate can be controlled rationally (Figure 2.5a).

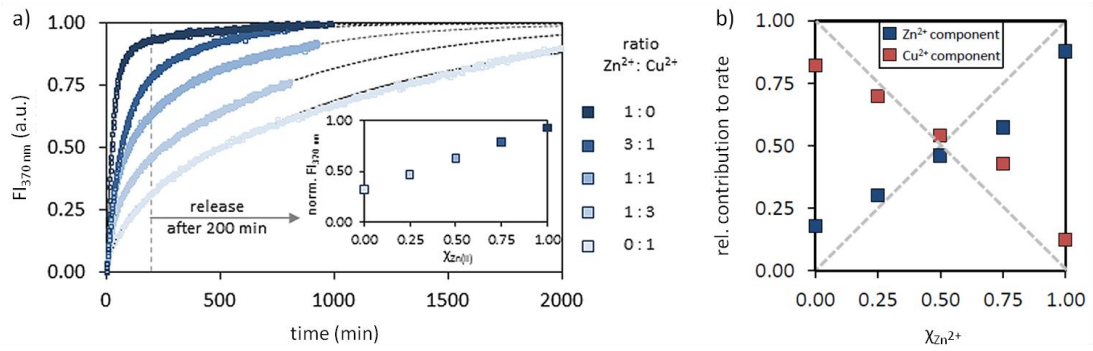

Figure 2.5. (a) Normalized fluorescence intensity at 370 nm as a function of time upon the addition of TPEN (5 µM) to a solution of Au NP **1**·M^{2+} (M = Zn^{2+}/Cu^{2+} as indicated at the right; [M^{2+}] = 5 µM). The inset shows the normalized FI after 200 min as a function of the mole fraction of Zn^{2+} in the monolayer. (b) Relative contributions to the release rates of the two kinetic terms as a function of the mole fraction of Zn^{2+} on the surface.

In fact, a plot of the normalized fluorescence intensity at 200 minutes as a function of the ratio Zn^{2+}/Cu^{2+} on the surface is nearly linear (insert Figure 2.4). The control over the release rate is further reflected by the fact the release rate of **A** is composed of two (major) kinetic terms the ratio of which corresponds nicely to the ratio of metal ions on the surface (Figure 2.5b). The deviation from the expected straight lines originates from the presence of additional kinetic components to the release rate due to the different binding modes of **A** as discussed above.

2.3 Conclusions

In conclusion, these studies show that metal ions can be used as regulatory elements to reversibly control the valency of a supramolecular system composed of a monolayer protected gold nanoparticle and small molecules. The pH of the solution plays an important role in determining the amplitude, but also in

determining the release rate of the small molecules from the monolayer surface. At a single pH, the release rate can be precisely tuned by using ratios of different metal ions. The current system offers the perspectives of regulating multivalent interaction between nanoparticles and biotargets and controlling the release of small molecules from the nanoparticle surface into bulk solution for sensing or signalling purposes or small molecule delivery. Finally, the linear signal response as a function of the ratio of two metal ions illustrates the possibility of developing sensing systems able to detect combinations of metals.

2.4 Experimental section

2.4.1 Instrumentation

NMR Analysis

^{1}H-NMR spectra were recorded using a Bruker AV300 spectrometer operating 300 MHz for ^{1}H, respectively. Chemical shifts (δ) are reported in ppm using D_2O residual solvent value as internal reference.[21] Diffusion-ordered ^{1}H NMR spectra were recorded using the "longitudinal-eddy-current-delay" (LED) pulse sequence.[22]

TEM Analysis

TEM images were recorded on a Jeol 300 PX electron microscope. One drop of sample was placed on the sample grid and the solvent was allowed to evaporate.
TEM images were elaborated using the freeware software ImageJ (http://rsb.info.nih.gov/ij/).

DLS Analysis

Dynamic light scattering measurements were recorded on a Zetasizer Nano-S (Malvern, Malvern, Worcestershire, UK) equipped with a thermostatted cell holder and an Ar laser operating at 633 nm.

TGA Analysis

Thermogravimetric analysis (TGA) was run on 1 2 mg nanoparticle samples using a Q5000 IR model TA instrument from 30 to 1000 °C under a continuous air flow.

pH measurements

The pH of buffer solutions was determined at room temperature using a pH-meter Metrohm-632 equipped with a Ag/AgCl/KCl reference electrode.

UV-Vis and Fluorescence spectroscopy

UV-Vis measurements were recorded on a Varian Cary50 spectrophotometer, while Fluorescence measurements were recorded on a Varian Cary Eclipse Fluorescence spectrophotometer. Both the spectrophotometers were equipped with thermostatted cell holders.

2.4.2 Materials

$Zn(NO_3)_2$ and $Cu(NO_3)_2$ were analytical grade products. 2-aminopurine riboside-5'-O-triphosphate (**A**) was obtained from Biolog Life Science Institute and used as received. 4-(2-hydroxyethyl)-1-piperazineethanesulfonic acid (HEPES) and 1,4-Piperazinediethanesulfonic acid (PIPES) were purchased from Sigma Aldrich and used without further purification. In all cases, stock solutions were prepared using deionized water filtered with a MilliQ-water-purifier (Millipore) and stored at 4 °C.

2.4.3 Synthesis and characterization of Au NP 1

$HAuCl_4 \cdot 3H_2O$ (36.5 mg, 0.093 mmol), weighed in a dry-box, was dissolved in H_2O (mQ; 10 mL). Separately, a solution of TOABr (0.5 g, 0.914 mmol) in degassed toluene (90 mL) was prepared (sonication for 1 h). The aqueous solution of Au(III) was extracted with the TOABr-solution (4×15 mL) causing the transfer of $[AuCl_4]^-$ ions into the organic phase (red-orange color). The organic phase was brought together with the remaining amount of the TOABr solution in a 250-mL round bottom flask and di-n-octylamine (1.2 mL, 4.471 mmol) was added (with a plastic syringe). The solution was vigorously stirred for 30 min under N_2, resulting in a progressive decoloration (red, yellow, green; few minutes). Subsequently, $NaBH_4$ (17 mg, 0.494 mmol) dissolved in H_2O (mQ; 2 mL) was added under vigorous stirring, resulting in the formation of the Au nanoparticles (brown coloring). The solution was stirred for an additional 3 h under N_2, after which the aqueous phase was removed with a separating funnel. Then, HS-C9-TACN (previously deprotected

from Ac-C9-TACNdiBoc[17] 0.071 mmol) solubilized in a minimum quantity of DMF (1 mL) was added quickly: the solution became colorless and after several minutes a brown precipitate was formed. The obtained suspension were stored under an inert atmosphere overnight. Then, H_2O (mQ; 5 mL) was added and the solutions were stirred for further 30 minutes under N_2. Finally, the aqueous phase was separated and washed with diethyl ether (2×15 mL), toluene (2x15 mL), ethylacetate (2x15 mL), and again diethyl ether (2x15 mL). The resulting dark brown aqueous phase was concentrated and passed through a Sephadex G-25 (mQ water). Finally, the collected brown fraction was concentrated and passed through a Sephadex LH-20 using MeOH.

Au NP **1** were characterized by ^{1}H-NMR, TEM, DLS and TGA analysis. In general, by carrying out ^{1}H-NMR experiments using a "longitudinal-eddy-current-delay" (LED) pulse sequence it is possible to differentiate molecules based on their diffusion coefficients. This provide an unequivocal proof that thiols are bound to the Au NP surface (broad signals) as well as a way to assess the purity of the samples. The obtained NMR spectra with (c) and without (b) the diffusion filter showed that only minimal amounts of unbound additives were present in the final sample (Figure 2.6).

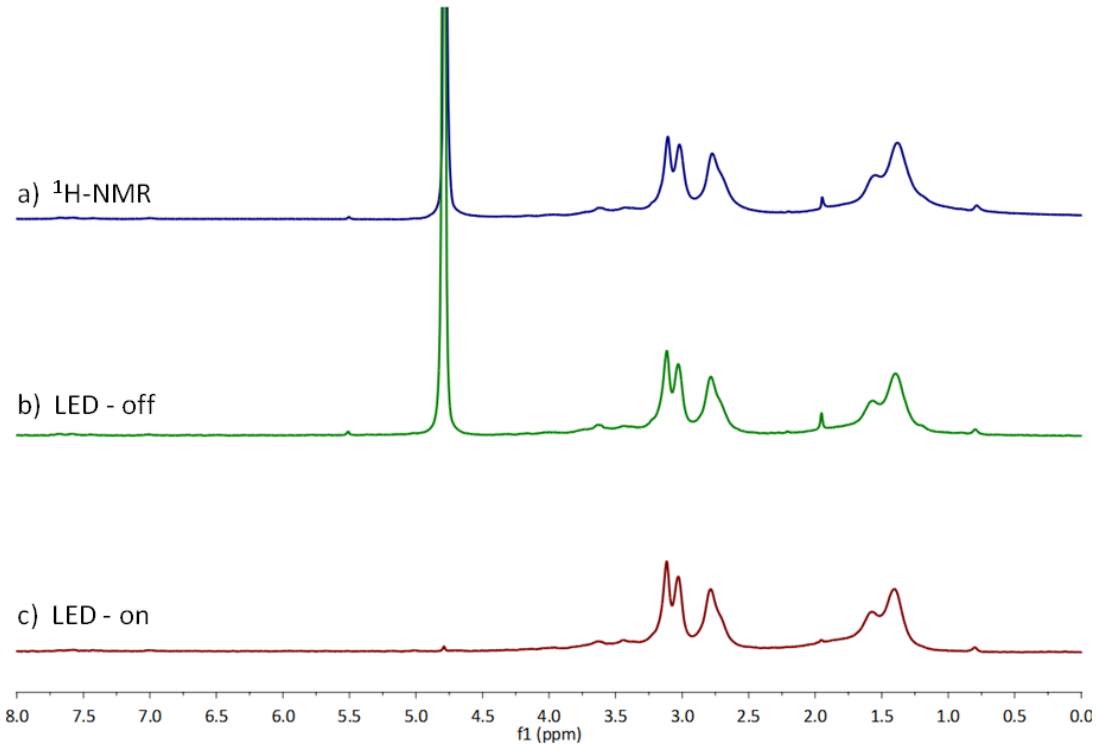

Figure 2.6. ^{1}H-NMR spectra of a solution of Au NP **1** in D_2O.

TEM, DLS and TGA analyses provide information about the size and morphology of functionalized gold nanoparticles. TEM analysis proved that the synthesized nanoparticles were nicely mono-dispersed, with a gold core diameter = 1.66 nm (sigma = ± 0.28 nm) (Figure 2.7c). The hydrodynamic radius observed by DLS was 5.1 ± 1.2 nm (Figure 2.7b), which is in agreement with the thiol length (ca. 1.7 nm). Finally, the weight loss measured by TGA was 47.2% (Figure 2.7d).

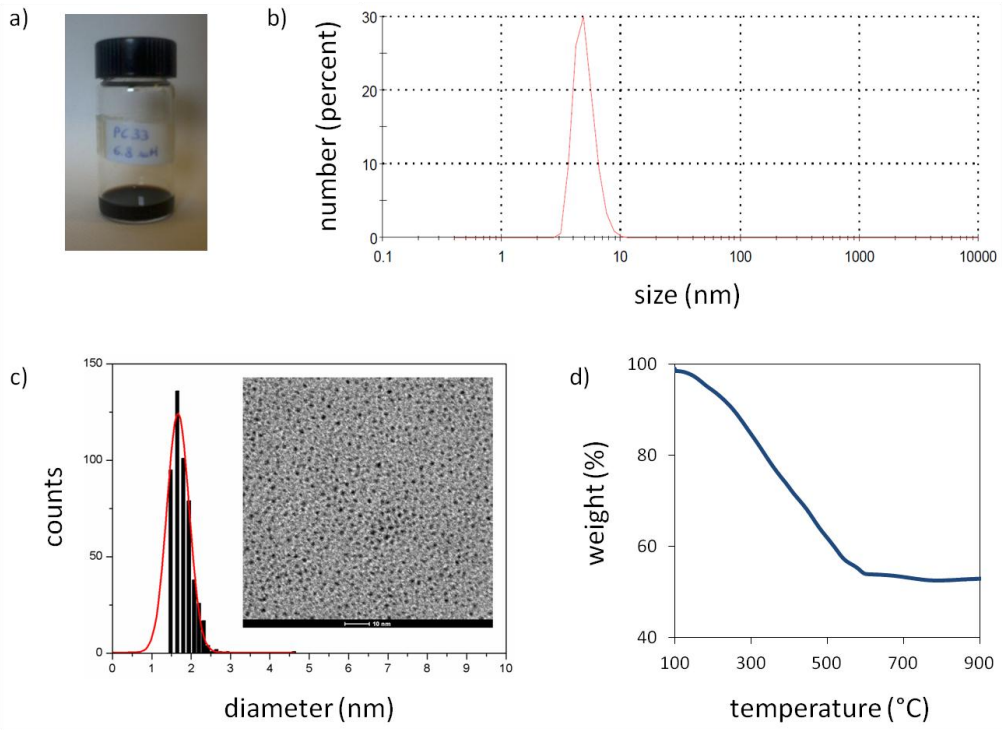

Figure 2.7. (a) picture of a batch of Au NP **1**. (b) DLS analysis. (c) TEM image (scale bar = 10 nm) together with the corresponding ImageJ elaboration. (d) TGA analysis.

Considering the Au core of the nanoparticle as a sphere, the diameter obtained from TEM analysis can be used to calculate the volume of the core (i.e. V_{Au}). The density of bulk Au (i.e. ρ_{Au} = 19.3 g/cm^3) can be easily converted into atoms/nm^3 by taking into account the Avogadro constant (6.02·10^{23} atoms/mol) and the atomic mass (196.97 u). Consequently, the numbers of Au atoms (x) in the core can be estimated using the following equation:

$$x = V_{Au\,core} \cdot \rho_{Au} = \frac{4}{3}\pi\left(\frac{\emptyset_{TEM}}{2}\right)^3 \rho_{Au} = 2.57\,nm^3 \cdot 59\,atoms/nm^3 = 141$$

The mass of the organic monolayer (i.e. m_{org}) can be determined considering the relative weights percentages observed by TGA: the weight loss belongs the organic part (i.e. w_{loss}), which decomposed during the analysis while the weight residue is associated to the gold core (i.e. w_{Au}), which is thermally stable. The mass of Au core can be calculated by multiplying the number of atoms by the atomic mass. Consequently, the number of thiols (y) present in the monolayer can be calculated by dividing the mass of the organic monolayer to the corresponding molecular weight (i.e. FW_{thiol}):

$$y = \frac{m_{org}}{FW_{thiol}} = \frac{m_{Au} \cdot \frac{w_{loss}}{w_{Au}}}{FW_{thiol}} = \frac{141 \cdot 196.97 \cdot \frac{47.2}{52.8}}{323} = 77$$

The thiol was deprotected in acidic conditions (HCl/MeOH) immediately before use. The pK_a of the two nitrogens of TACN are 10.4 and 6.8,[20] thus, since the obtained nanoparticles were soluble in water, FW_{thiol} corresponds to the mono-hydrochloridate form (i.e. 323 g/mol).[23] As a results, the average formula for this batch of Au NP **1** was $Au_{141}S_{77}$, which is nicely in agreement with previously reported characterizations.[18]

2.4.4 Determination of the stock solution concentrations

The concentration of metal ions stock solution ($Zn(NO_3)_2$ and $Cu(NO_3)_2$) solutions were determined by atomic absorption spectroscopy. The concentration of TACN-headgroups was determined by kinetic titration using either $Zn(NO_3)_2$ or $Cu(NO_3)_2$ as reported previously.[24] Similarly, the concentration of N,N,N',N'-tetrakis(2-pyridylmethyl) ethylenediamine (TPEN) was determined by a spectrophotometric titration using $Cu(NO_3)_2$, following the complexation of Cu^{2+} at 691 nm, the maximum of the absorption band of TPEN-Cu^{2+} complex. The concentration of **A** in the stock solution were determined by UV spectroscopy at pH 7.0 ($\varepsilon_{243\ (ATPf)}$ = 8000 $M^{-1}cm^{-1}$).

2.4.5 Determination of the Surface Saturation Concentration (SSC)

Fluorescence titrations were carried out by adding consecutive amount of a stock solution of **A** (200 µM) to a 3-mL aqueous solution ([HEPES] or [PIPES] = 10 mM) containing Au NP **1** (or Au NP **1**•M^{2+}). The additions were followed kinetically, in order to ensure the equilibration of the fluorophore molecules on the nanoparticles surface. The optical parameters used for **A** were λ_{ex} = 305 nm, λ_{em} = 370 nm, slits = 5/5 nm. Surface saturation concentration (SSC) were determined either by extrapolation of the linear part of the curve (a) or by fitting the experimental data to a 1:1 binding model (b). The two methods are illustrated using the following curve, obtained for **A** in the presence of Au **1**•Zn^{2+} (10 µM) at pH 7.0 (Figure 2.8).

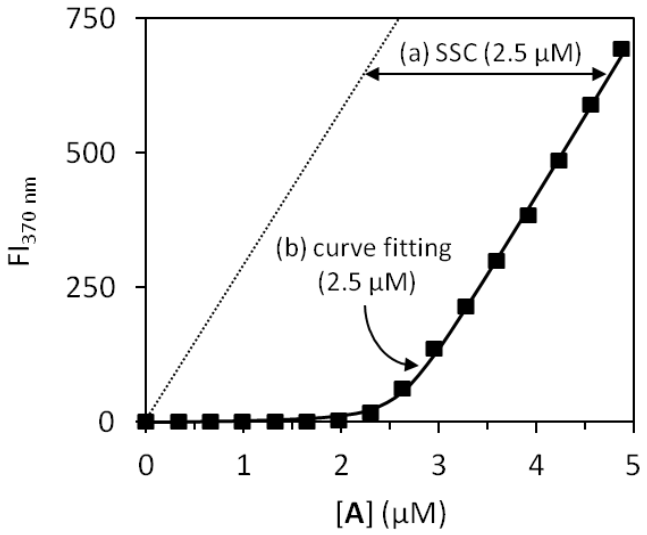

Figure 2.8. Determination of the SSC via extrapolation (a) or curve fitting (b).

a) extrapolation

After having reached the SSC, the additional amounts of **A** remains free in solution. Consequently, the fluorescence intensity increases linearly as a function of the amount of **A** ($y = mx + q$). Since in the absence of binding the hypothetical increase in fluorescence would be $y = mx$, it follows that the amount of **A** bound to the surface corresponds to $x = -q/m$ (in this case 2.5 µM).

b) curve fitting

The experimental points were fitted to a 1:1 binding model using Micromath Scientist for Windows, version 2.01:

```
// MicroMath Scientist Model File
IndVars: A
DepVars:  FI, A, NP, NPA
Params: x, K, NP0
NPA=K*NP*A
A=A0-NPA
NP=NP0-NPA
FI=x*A
// constraints
0<A<A0
0<NP<NP0
0<NPA<NP0
***
```

The model assumes a 1:1 complex formation between **A** and a fictitious binding site NP. NP0 gives the maximum number of binding sites for **A** (*i.e.* the SSC).

2.4.6 Release kinetics

After 10 minutes of equilibration at 37 °C, $Zn(NO_3)_2$ (15 µL, 1mM) was added to a 3-mL aqueous solution ([PIPES] or [HEPES] = 10 mM at the given pH) containing Au NP **1** ([TACN] = 10 µM) and probe **A** (30 µL, 200 µM). After the complete capture of **A**, TPEN (15 µL, 1mM) was added and the fluorescence intensity (λ_{ex} = 305 nm, λ_{em} = 370 nm, slits = 5/5 nm) was recorded until the complete release of the **A**. The obtained release curves reported in Figure 4 and Figure 5 were fitted using a kinetic model based on two first-order terms. The experimental points were fitted using the following model implemented in Micromath Scientist for Windows, version 2.01:

```
// MicroMath Scientist Model File
IndVars: T
DepVars: P, HP1, HP2
Params: x, k1, k2, HP0
HP10=x*HP0
HP20=(1-x)*HP0
HP1'=-k1*HP1
HP2'=-k2*HP2
P'=k1*HP1+k2*HP2
//
T=0
HP1=HP10
HP2=HP20
P=0
***
```

in which HP0 is total amount of **A** that is released during the kinetic course (fixed and normalized on 1), X is the relative ratio of the two kinetic components having K1 and K2 as the respective first order rate constants. Fitting was limited to a model based on 2 kinetic terms, since this generally well-described the release rate.

2.5 References

(1) Kiessling, L. L.; Gestwicki, J. E.; Strong, L. E. *Curr. Opin. Chem. Biol.* **2000**, *4*, 696.
(2) Dahan, A.; Portnoy, M. *J. Polym. Sci. Pol. Chem.* **2005**, *43*, 235.
(3) Badjic, J. D.; Nelson, A.; Cantrill, S. J.; Turnbull, W. B.; Stoddart, J. F. *Acc. Chem. Res.* **2005**, *38*, 723.
(4) Mulder, A.; Huskens, J.; Reinhoudt, D. N. *Org. Biomol. Chem.* **2004**, *2*, 3409.
(5) Rybtchinski, B. *ACS Nano* **2011**, *5*, 6791.
(6) Gestwicki, J. E.; Cairo, C. W.; Strong, L. E.; Oetjen, K. A.; Kiessling, L. L. *J. Am. Chem. Soc.* **2002**, *124*, 14922.
(7) Gillies, E. R.; Frechet, J. M. J. *Drug. Discov. Today* **2005**, *10*, 35.
(8) Daniel, M. C.; Astruc, D. *Chem. Rev.* **2004**, *104*, 293.
(9) Giljohann, D. A.; Seferos, D. S.; Daniel, W. L.; Massich, M. D.; Patel, P. C.; Mirkin, C. A. *Angew. Chem. Int. Ed.* **2010**, *49*, 3280.
(10) Saha, K.; Agasti, S. S.; Kim, C.; Li, X. N.; Rotello, V. M. *Chem. Rev.* **2012**, *112*, 2739.
(11) Palmer, L. C.; Stupp, S. I. *Acc. Chem. Res.* **2008**, *41*, 1674.
(12) Lim, Y. B.; Moon, K. S.; Lee, M. *Chem. Soc. Rev.* **2009**, *38*, 925.
(13) Uhlenheuer, D. A.; Petkau, K.; Brunsveld, L. *Chem. Soc. Rev.* **2010**, *39*, 2817.
(14) Fitzmaurice, D.; Rao, S. N.; Preece, J. A.; Stoddart, J. F.; Wenger, S.; Zaccheroni, N. *Angew. Chem. Int. Ed.* **1999**, *38*, 1147.
(15) Ling, X. Y.; Reinhoudt, D. N.; Huskens, J. *Chem. Mater.* **2008**, *20*, 3574.
(16) Klajn, R.; Fang, L.; Coskun, A.; Olson, M. A.; Wesson, P. J.; Stoddart, J. F.; Grzybowski, B. A. *J. Am. Chem. Soc.* **2009**, *131*, 4233.
(17) McClure, W. R.; Scheit, K. H. *FEBS Lett* **1973**, *32*, 267.
(18) Pieters, G.; Cazzolaro, A.; Bonomi, R.; Prins, L. J. *Chem Commun (Camb)* **2012**, *48*, 1916.
(19) Dulkeith, E.; Mortcani, A. C.; Niedereichholz, T.; Klar, T. A.; Feldmann, J.; Levi, S. A.; Van Veggel, F. C. J. M.; Reinhoudt, D. N.; Möller, M.; Gittins, D. I. *Phys. Rev. Lett.* **2002**, *89*, 2030021.
(20) Smith, R. M.; Martell, A. E.; Motekaitis, R. J. NIST Critically Selected Stability Constant of Metal Complexes, version 8; NIST Standard Reference Database 46; National Institute of Standards and Technology: Gaithersburg, MD, 2004
(21) Gottlieb, H. E.; Kotlyar, V.; Nudelman, A. *J Org Chem* **1997**, *62*, 7512.
(22) Wu, D. H.; Chen, A. D.; Johnson, C. S. *J.Magn. Reson. Series A* **1995**, *115*, 260.
(23) Quite unstable hydrochloride adducts can lose their HCl molecules after 140 °C, see for example: Adv. Pharm. Bull. 2013, 3, 419.
(24) Bonomi, R.; Cazzolaro, A.; Sansone, A.; Scrimin, P.; Prins, L. J. *Angew. Chem. Int. Ed.* **2011**, *50*, 2307.

Chapter 3

Controlling supramolecular complex formation on the surface of a gold nanoparticle in water[†]

In this Chapter studies are described aimed at understanding the noncovalent interactions that cause the high affinity between small molecules and Au NP ***1***·Zn^{2+}***.*** *A patch of negative charges in the molecular structure is essential for binding, but , it will be shown that the presence of additional non-covalent interactions (e.g. hydrophobic) can significantly enhances the affinity. The hydrophobic interactions originate from the insertion of an aromatic unit in the hydrophobic part of the monolayer. This is evidenced by a shift in the emission wavelength of environment-sensitive fluorophores upon binding. The results shown here represent a step forward to a complete understanding of the supramolecular interactions that drive complex formation on the monolayer surface and provide a rationale for modulating the supramolecular chemistry occurring at interface.*

[†] Part of this Chapter was published in: G. Pieters, C. Pezzato, L. J. Prins *Langmuir* **2013**, *29*, 7180-7185.

3.1 Introduction

The self-assembly of large supramolecular structures in water is an attractive approach towards systems able to interact with biotargets such as proteins, oligonucleotides, or even cells.[1] Self-assembly permits a straightforward access towards complex nanosized objects with a minimal synthetic effort.[2] Additional advantages include error-correction during self-assembly and adaptive behavior of the resulting structure towards the target or external stimuli (pH, temperature, metal ions, etc). Various supramolecular aggregates, such as micelles, rods, peptide amphiphiles, supramolecular polymers, etc. have shown to be excellent building blocks for the recognition and sensing of biotargets.[3-5] The self-assembly of small molecules on the surface of Au NPs represent an alternative approach toward the development of multivalent supramolecular systems. For example, a heteromeric multivalent surface can be simply generated by adding different small molecules to a single Au NPs scaffold.[6] Compared to the formation of mixed monolayers on Au NPs, this avoids the synthesis, purification and characterization of each separate Au NPs, which is not always straightforward. Importantly, the use of noncovalent interactions for assembling the small molecules on the monolayer surface permits in principle a spontaneous adaptability towards a target. A critical issue in this approach is a high affinity of the small molecules for the monolayer surface, since complex formation should occur under saturation conditions even at low micromolar concentrations in water. In this context, to ensure binding to Au NP **1**•Zn^{2+}, small molecules have to be selected with the prerequisite of having a patch of negative charges in their structures. Nonetheless, previous studies provided clues that the binding affinity of the probes for the monolayer surface was not just caused by electrostatic interactions, but also by interactions with the hydrophobic part of the monolayer.[7,8] Similar observations have been reported also elsewhere.[9-12] In general, many example of supramolecular complex formation in water driven by a combination of hydrophobic and electrostatic interactions have been reported.[1,13-15] Here, compelling evidence that hydrophobic interactions play an important additional role in the binding of small molecules to Au NP **1**•Zn^{2+} will be provided. The presence of a strong hydrophobic interaction permits a reduction of the number of negative charges present in the charge without comprising the

formation of the multivalent structure under saturation conditions. It is shown that the possibility of regulating the binding strength of the probes gives an element of control over the supramolecular chemistry that takes place on the monolayer surface (selective exchange or 'catch-and-release' of surface bound probes).

3.2 Result and discussion

3.2.1 Electrostatic and hydrophobic interaction drive the complex formation

In order to see whether hydrophobic interactions may play an additional role in the binding of small molecule to Au NP **1**•Zn^{2+}, we decided to study the self-assembly of a series of commercially available fluorescent nucleotides (**B**, **C** and **D**, Figure 3.1).

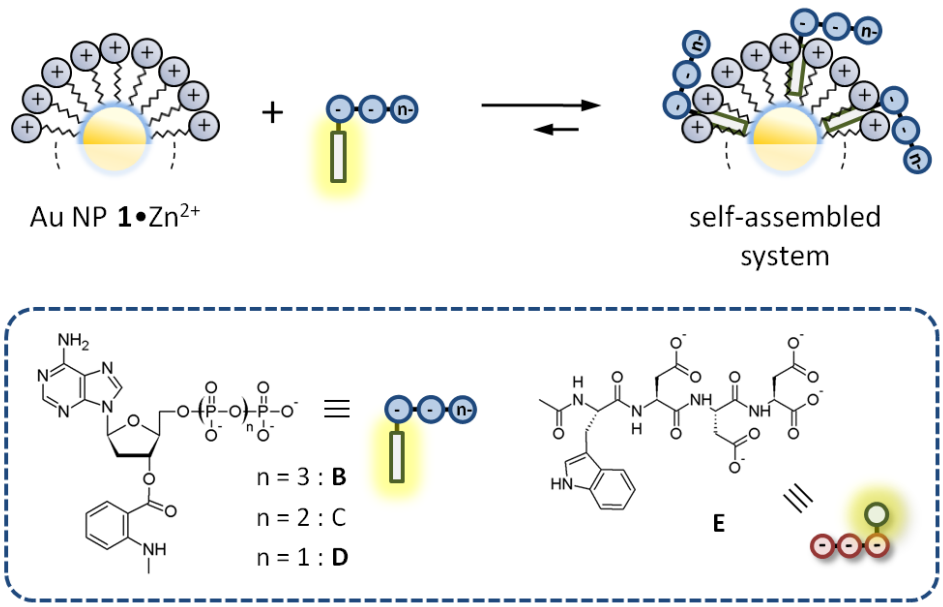

Figure 3.1. Schematic representation of the formation of a multivalent supramolecular system. On the bottom are reported the molecular structures of the components used in this chapter.

The fluorescent anions has been chosen for several reason. First, they have an apolar aromatic unit attached to the deoxyribose ring which seemed perfectly placed to penetrate into the monolayer. Second, The *N*-methylamino anthranilic ester (MANT) unit is fluorescent (λ_{ex} = 355 nm, λ_{em} = 448 nm) which is essential for studying the binding to Au NP **1**•Zn^{2+}. Third, the MANT-fluorophore is sensitive to its environment[16] and it is reported that the emission wavelength shifts 10-20 nm to shorter wavelengths in apolar environments.[17]

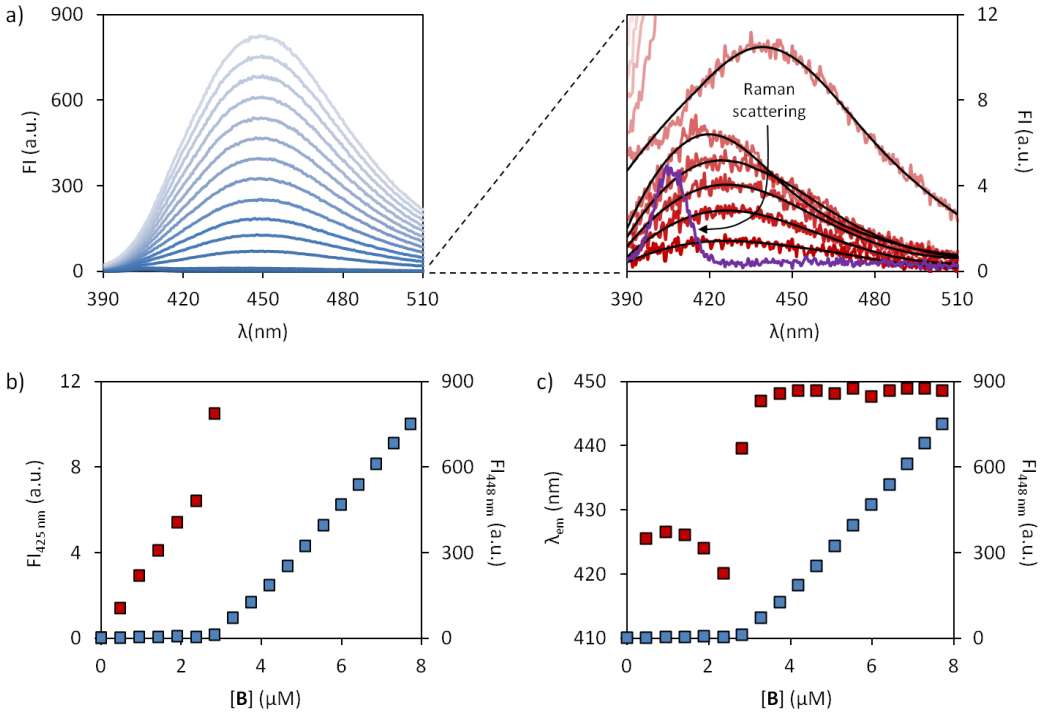

Figure 3.2. (a) Fluorescence emission spectra upon the addition of increasing amount of **B** to a buffered aqueous solution of Au NP **1**·Zn^{2+} (pH 7.0). The corrected spectra obtained after the first addition are reported on the right. Each of the solid black lines represent the corresponding smoothed spectrum. (b) Fluorescence intensities at 425 nm (red) and 448 nm (blue) as a function of the concentration of **B**. (c) Maximum in the MANT emission as a function of the concentration of **B** (red) superimposed on the fluorescence intensity at 448 nm (blue) as a function of the concentration of **B**. Experimental conditions: [TACN•Zn^{2+}] = 10 ± 1 μM, [HEPES] = 10 mM, pH = 7.0, 25 °C.

Having in mind the very high affinity of ATP and its fluorescent analogue **A** for Au NP **1**•Zn^{2+} (see previous chapter), we started to study the interaction between **B** and Au NP **1**•Zn^{2+} by means of a fluorescence titration (Figure 3.2a). A detailed analysis of the obtained spectra gave an interesting insight in the nature of the complex formation. The first additions of **B** resulted only in a minor fluorescence emission with a maximum at around 425 nm. For these concentrations, the emission spectra were corrected subtracting the contribution from the signal at 407 nm owing to Raman scattering of water. The corrected spectra were then smoothed two times with the Savitzky-Golay method in order to evaluate the corresponding emission maximum and intensity accurately (see zoom in figure 3.2a). Up to a concentration of around 2.5 μM of **B** a linear increase in the (weak) emission intensity at 425 nm was observed. Importantly, the observed maximum is blue-shifted (23 nm below the expected wavelength), suggesting that the MANT-fluorophore is inserted in the apolar monolayer (figure 3.2b). In fact, further additions of **B** resulted in a strong

increase in fluorescence emission with a maximum at 448 nm corresponding to the (expected) emission of free **B**. From a plot of the fluorescence intensity at 448 nm as a function of the concentration of **B** a SSC of 3.2 µM was determined. In confirm of the change in environment of the MANT-fluorophore, the change in maximum emission wavelength neatly occurs upon reaching the SSC (figure 3.2c). It is interesting to notice that just before reaching the SSC a further small blue shift in the emission maximum is observed to 420 nm, which may point at an organizational process for permitting the accommodation a major number of probe molecule on the surface.

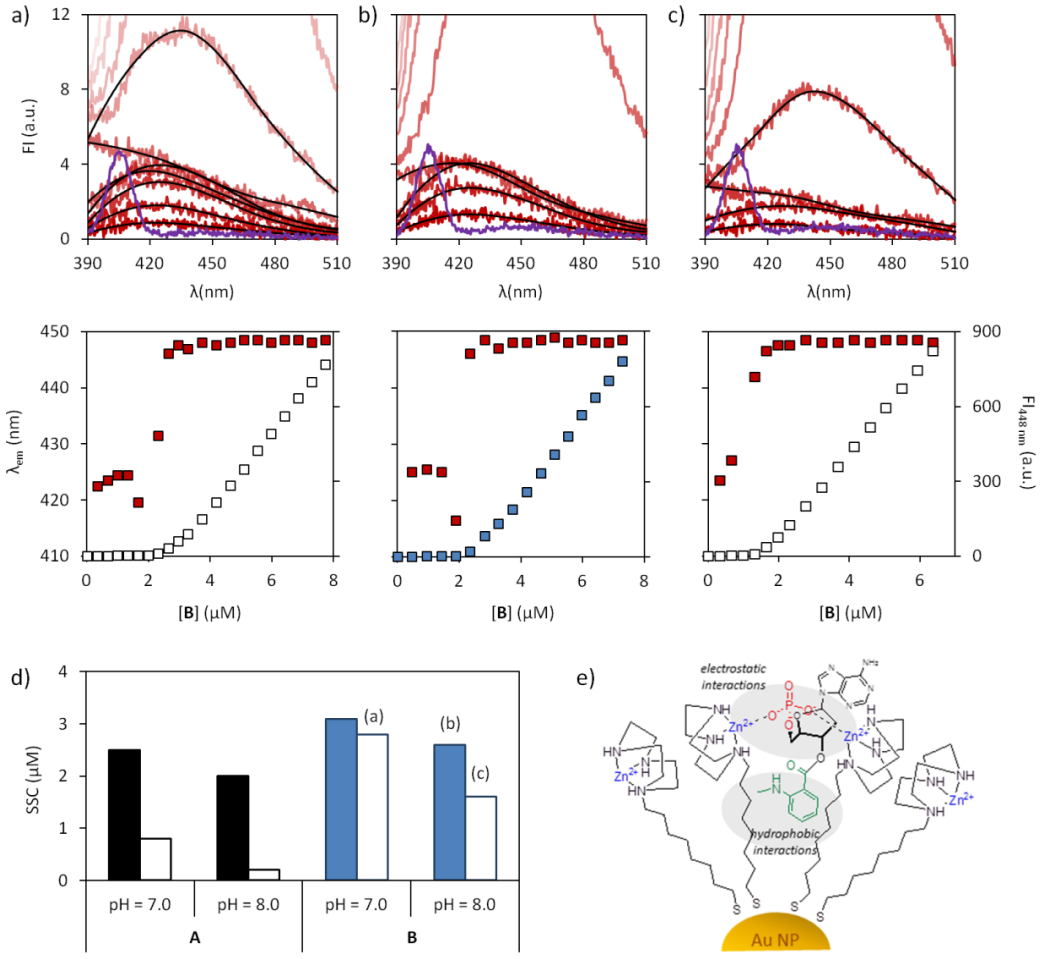

Figure 3.3. Corrected fluorescence spectra upon the addition of increasing amount of **B** to a buffered aqueous solution of Au NP **1** (pH 7.0) (a), Au NP **1**·Zn^{2+} (pH 8.0) (b) and Au NP **1** (pH 8.0) (c). Each of the solid black lines represent the corresponding smoothed spectrum. The maximum in the MANT emission as a function of the concentration of **B** (red) superimposed on the fluorescence intensity at 448 nm (blue) as a function of the concentration of **B** is reported on the bottom of each of the three different conditions. Experimental conditions: [TACN•Zn^{2+}] = 10 ± 1 µM, [HEPES] = 10 mM, pH = 7.0 or 8.0, 25 °C; λ_{ex} = 355 nm, slits = 10/5 nm. (d) Comparison between the SSC values obtained for **A** and **B** in different conditions. (e) Schematic illustration of the proposed binding mode.

These first results indicate that the MANT-fluorophore is inserted in the monolayer. To obtain more information we analyzed the interaction between **B** and Au NP **1**•Zn^{2+} under conditions where no binding was observed for **A**. **A** is structurally very similar to **B** but lacks the MANT-fluorophore. As shown in the previous chapter, in the absence of Zn^{2+} the SSC of **A** dropped from 2.5 µM to 0.8 µM at pH 7.0, while at pH 8.0 a very low SSC-value of 0.2 µM was measured for **A** on Au NP **1**. On the contrary, **B** showed nearly no decrease in SSC at pH 7.0 (from 3.2 to 2.8 µM) and still a significant value at pH = 8.0 (1.8 µM) in the absence of Zn^{2+}. As for **A** the presence of Zn^{2+} hardly affect the SSC at pH 8.0 (from 3.2 to 2.6 µM). The recorded spectra were elaborated as describe above and, remarkably, in all cases a blue-shift in the emission wavelength was observed during the first additions (figure 3.3a-c). So, whereas for the **A** the presence of Zn^{2+} (or a high degree of protonation of TACN-head groups) in the monolayer is essential for obtaining a significant SSC, these experiments show that this is much less relevant for **B** and reflect a substantial difference in binding mode between **A** and **B** (figure 3.3d-e).

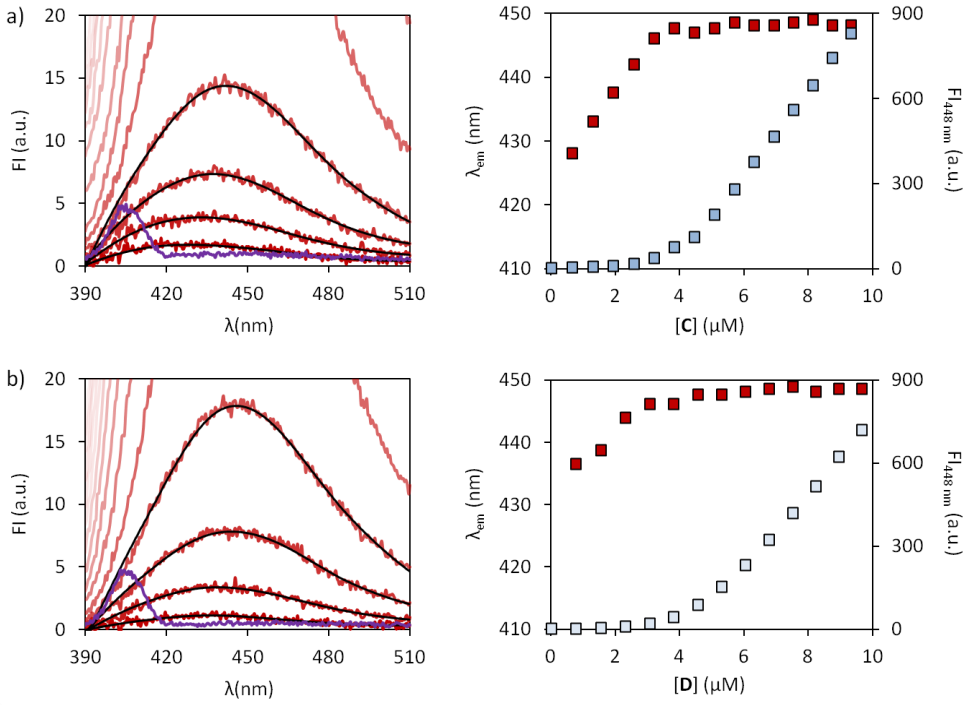

Figure 3.4. Corrected fluorescence spectra upon the addition of increasing amount of **C** (a) or **C** (b) to a buffered aqueous solution of Au NP **1**·Zn^{2+} (pH 7.0). Each of the solid black lines represent the corresponding smoothed spectrum. The corresponding behaviour of the MANT emission (red) superimposed on the fluorescence intensity at 448 nm as a function of the concentration of the fluorescent probe is reported on the right. Experimental conditions: [TACN•Zn^{2+}] = 10 ± 1 µM, [HEPES] = 10 mM, pH = 7.0 or 8.0, 25 °C.

In order to confirm these first evidences, we moved to study **C** and **D**. Notwithstanding the reduced negative charge, both compounds still bound to Au NP **1**•Zn^{2+} under saturation conditions (Figure 3.4a-b). In particular for **D**, having just 1 phosphate group, this is impressive, especially considering the relatively low affinity of the analogous compound AMP. Also for **C** and **D** a blue-shift in the emission wavelength was observed during the fluorescence titrations (figure 3.4a-b). It is interesting to observe that, within the MANT-series, the difference in emission wavelength progressively decreased (23 nm for **B**; 20 nm for **C**; 11 nm for **D**). This is tentatively ascribed to a different position of the MANT-fluorophore in the hydrophobic part of the monolayer. Furthermore, it is important to note that a reduced size of the probe is accompanied by an increase in SSC (3.2 µM for **B**; 4.2 µM for **C**; and 4.8 µM for **D**). For **D** this means a binding stoichiometry of 1 probe for each 2 TACN•Zn^{2+} complexes. With an estimated 70 thiols covering the gold nanoparticle this implies that at saturation around 35 **D** probes are localized on the surface.

3.2.2 Competition experiments with ATP

The SSC in itself does not provide information on the strength of the interaction. Information on the relative affinity of the probes for the monolayer surface was obtained from a series of competition experiments between ATP and the MANT-probes. In these experiments increasing amounts of the competitor ATP were added to a MANT-probe bound to the surface of Au NP **1**•Zn^{2+} and the fluorescence emission from the released MANT-probe was measured at 448 nm (figure 3.5b). These displacement experiments provide information on the relative affinity between ATP and the respective MANT-probe. The displacement of 50 % of **D** (1.75 µM) required approximately 4.0 µM of ATP corresponding to a relative binding affinity of around 2 in favour of **D**. The very similar binding affinity is remarkable considering the presence of just 2 negative charges in **D** against 4 for ATP. Another remarkable observation is that the addition of up to 1 mM of ATP just replaced 0.75 µM of **B** (ca. 25 %) from the surface. A control experiment in which ATP and **B** were added in a reversed order excluded that these distributions were the result of kinetically slow exchange processes (figure 3.5c).

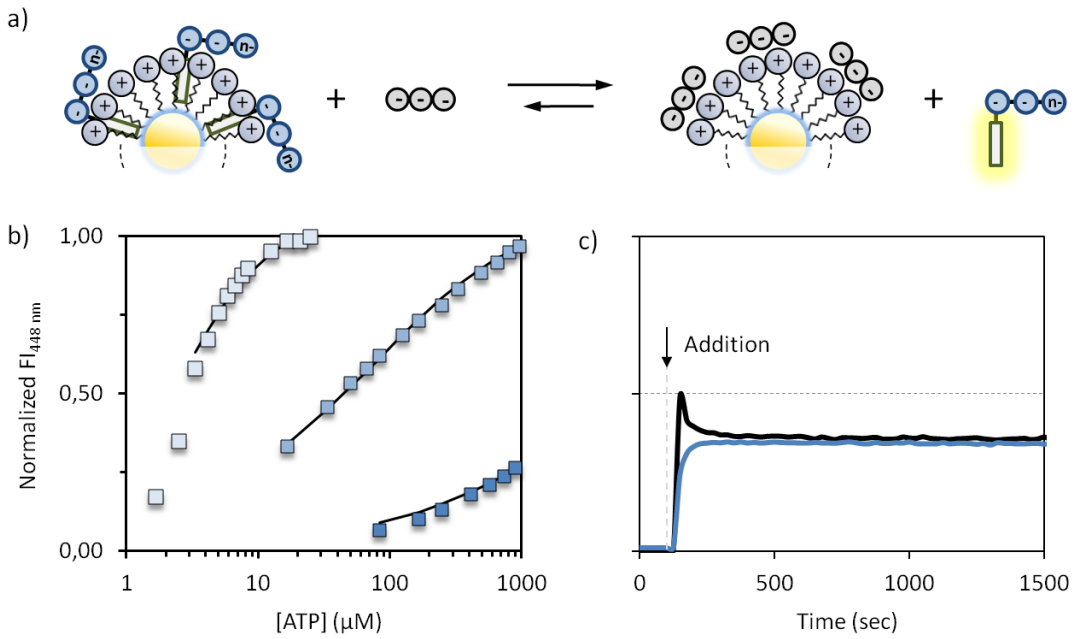

Figure 3.5. (a) Schematic representation of the displacement experiment. (b) Normalized fluorescence intensities at 448 nm as a function of ATP added to a solution of Au NP **1**·Zn^{2+} loaded with either **B** (dark blue), **C** (blue) or **D** (light blue). The solid lines were obtained from fitting the data to an appropriate model (see the experimental section). Normalized fluorescence intensities at 448 nm as a function of time upon the addition (at the arrow) of **B** (3.0 μM) to a solution of Au NP **1**•Zn^{2+} (10 μM) and ATP (1 mM) (black line) *and* the addition of ATP (1 mM) to a solution of Au NP **1**•Zn^{2+} (10 μM) and **B** (3.0 μM) (dark blue line). Experimental conditions: [TACN•Zn^{2+}] = 10 ± 1 μM, [**B**] = 3.0, [**C**] = [**D**] = 3.5 μM, [HEPES] = 10 mM, pH = 7.0, 25 °C; λ_{ex} = 355 nm, λ_{em} = 448 nm.

3.2.3 Controlling the properties of a dynamic heteromeric surface

The ability to regulate the binding affinity of small molecules to the monolayer surface is a key element for the application of these supramolecular structures as responsive systems. The peculiar high affinity of the MANT-probes offers some important possibilities which will be illustrated by two examples. The first is the possibility to exclusively exchange one component from a heteromeric surface. For this purpose, the carboxylate probe **E** was chosen as a second unit because it has a much lower affinity compared to **B** and because the fluorescence emission from tryptophan (λ_{ex} = 280 nm, λ_{em} = 360 nm) can be monitored independently from the MANT-fluorophore. As before, the interaction between **E** and Au NP **1** (with and without Zn^{2+}) were studied by means of fluorescence titration, but in the presence of increasing amount of **B** pre-assembled on the monolayer surface (figure 3.6).

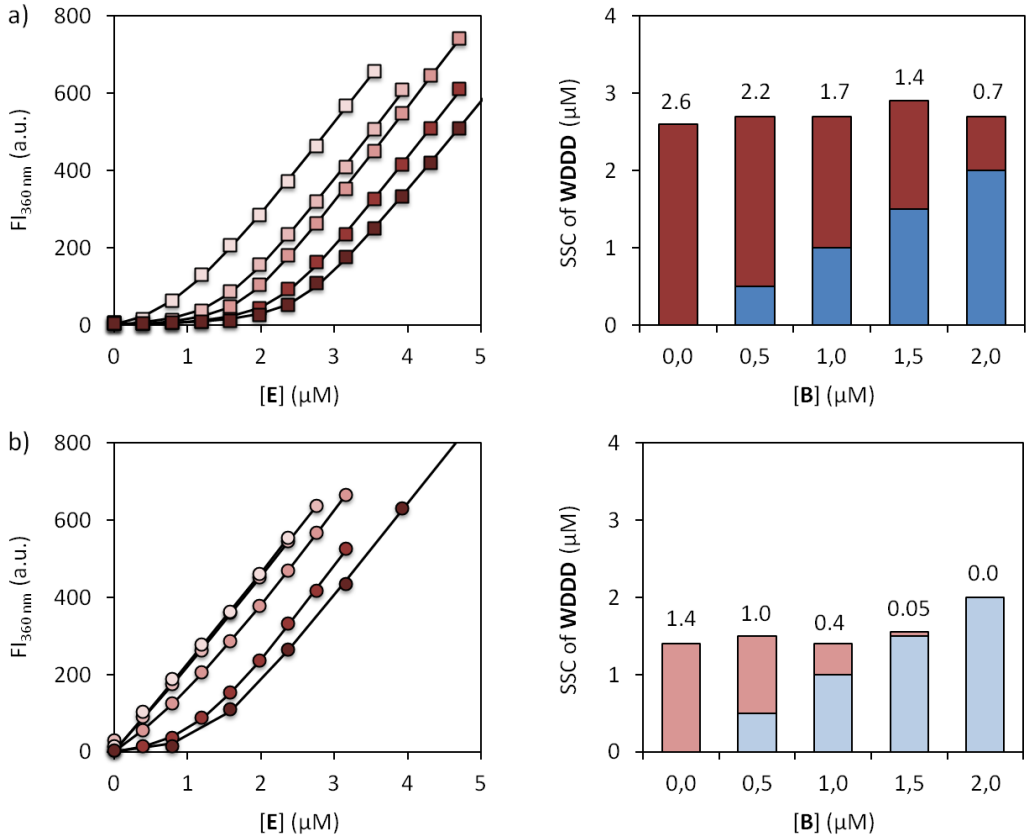

Figure 3.6. Fluorescence intensity at 360 nm as a function of the amount of **E** added to either Au NP **1**•Zn^{2+} (a) or Au NP **1** (b) in the presence of different amounts of **B** loaded on the surface. The corresponding surface compositions as a function of the amount of **B** present are reported on the right. Experimental conditions: [TACN•Zn^{2+}] = 10 ± 1 μM, [HEPES] = 10 mM, pH = 7.0, 25 °C; λ_{ex} = 280 nm, λ_{em} = 360 nm, slits = 10/10.

An heteromeric surface can be simply generated by adding **B** (1.0 μM) and **E** (1.4 μM) to Au NP **1**•Zn^{2+}. These concentration are enough to saturate the 80% of the monolayer surface. Indeed, the absence of fluorescence emission upon excitation of either MANT or tryptophan confirms that both probes are quantitatively bound to the monolayer surface. The addition of **ADP** as a competitor results in the exclusive displacement of **E** from the surface as witnessed by the full recovery of the expected fluorescence of **E** and the complete absence of fluorescence emission from **B** (Figure 3.7a). This is a significant progress compared to our previous studies in which a selectivity factor of just 7 between two different probes was achieved.[6]

The second example exploits the high affinity of **B** for Au NP **1** even in the absence of Zn^{2+}. By taking advantage of the protocol reported in the previous chapter this generates the possibility to exclusively 'catch-and-release' the **E** probe from a heteromeric composed by **B** (2.0 μM) and **E** (1.0 μM). In this case the surface

composition was regulated such that a significant amount of **E** is bound only when Zn^{2+} is present (figure 3.7b).

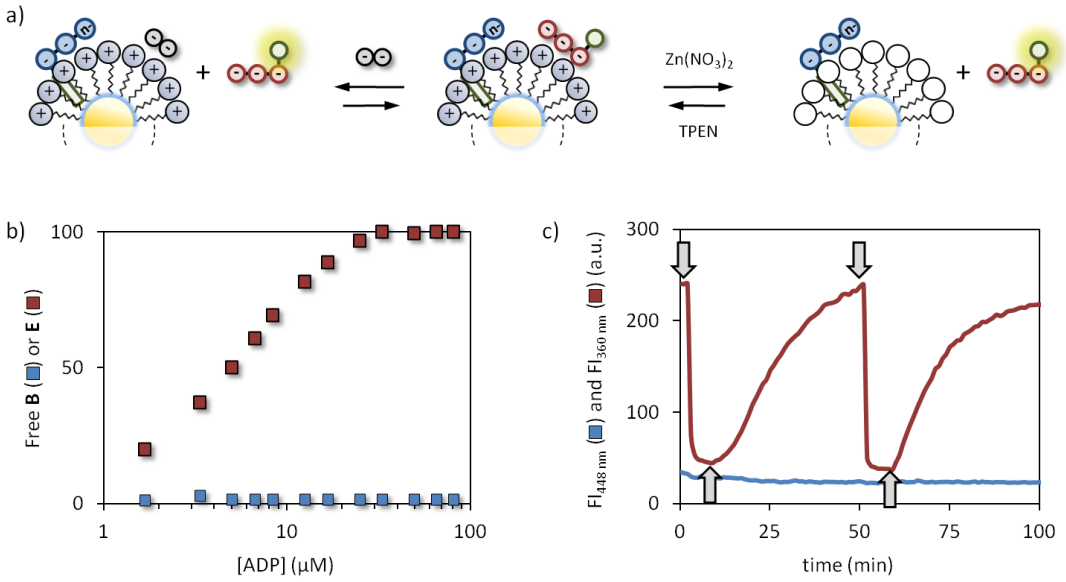

Figure 3.7. (a) Schematic representation of the selective exchange of **E** from a heteromeric surface composed of **E** and **B** (from right to left) or the selective the selective catch and release of **E** from a heteromeric surface composed of **E** and **B** upon the removal and addition of Zn^{2+} from the monolayer. (b) free **E** and **B** upon the addition of increasing amount of ADP. Experimental conditions: [TACN•Zn^{2+}] = 10 ± 1 μM, [**B**] = 1.0 μM, [**E**] = 1.4 μM, [HEPES] = 10 mM, pH 7.0, T = 25 °C. (c) Fluorescence intensities as a function of time upon the addition of $Zn(NO_3)_2$ (5 μM, downward arrow) or TPEN (5 μM, upward arrow) to a heteromeric surface composed of **E** and **B**. Experimental conditions: [TACN] = 10 μM, [**B**] = 2.0 μM, [**E**] = 1.0 μM, [HEPES] = 10 mM, pH 7.0, T = 37 °C.

So, the addition of TPEN to Au NP **1**•Zn^{2+} resulted in the removal of Zn^{2+} from the monolayer surface. In the absence of Zn^{2+} the **E** probe loses its affinity for the surface and is released in solution with a consequent increase in fluorescence intensity. On the other hand, the SSC of **B** is hardly affected by the removal of Zn^{2+} (see above) and no release of **B** was observed at all. After a complete release of **E** from the surface, $Zn(NO_3)_2$ was added which re-metalated the TACN head groups resulting in the 'capture' of the **E**-probe. Two full 'catch-and-release' cycles of **E** were performed and at no moment any fluorescence emission of **B** was observed.

3.3 Conclusions

In conclusion, these data show that hydrophobic interactions play an important role in determining the affinity of small molecules for the surface of a cationic monolayer. The insertion of the MANT-unit into the monolayer was evidenced by a

blue-shift in the emission wavelength. The presence of the hydrophobic unit permitted a reduction of the number of negative charges required for forming complexes under saturation conditions. The use of smaller molecules causes an increase in the SSC and, thus, the valency of the obtained supramolecular nanostructure. This is of importance for future applications of these supramolecular systems in the field of (bio)recognition. Further, the ability to diversify the binding interactions of small molecules with the monolayer service is important for the development of dynamic and responsive surfaces.

3.4 Experimental section

3.4.1 Instrumentation

See chapter 2.

3.4.2 Materials

For Au NP **1**, $Zn(NO_3)_2$, TPEN, probe **A**, and buffers see previous chapter. 2'-deoxy-3'-O-(N'-methylanthraniloyl)adenosine-5'-O-triphosphate (**B**), 2'-deoxy-3'-O-(N'-methylanthraniloyl)adenosine-5'-O-diphosphate (**C**) and 2'- Deoxy-3'-O-(N'-methylanthraniloyl)adenosine-5'-O-monophosphate (**D**) were obtained from Biolog Life Science Institute and used as received. Probe **E** was already present in the laboratories of prof. Prins. ATP and ADP were purchased from Sigma Aldrich and used as received.

3.4.3 Determination of the stock solution concentrations

The concentration of **B**, **C** **D** and ATP in their respective stock solution were determined by UV spectroscopy at pH 7.0 ($\varepsilon_{355\ (ATPf)}$ = 5800 $M^{-1}cm^{-1}$ $\varepsilon_{259\ (ATP,\ ADP)}$ = 15400 $M^{-1}cm^{-1}$)

3.4.4 Determination of the SSCs

Fluorescence titrations were carried out by adding consecutive amount of a stock solution of **B**, **C**, **D** or **E** to a 3-mL aqueous solution ([HEPES] = 10 mM, pH 7.0) containing Au NP **1** (with or without Zn^{2+}, 10 μM). In the case of **B**, **C** and **D** emission spectra were collected 10 min after each addition (λ_{ex} = 355 nm, slits = 10/5 nm;

cyclic mode). In the case of **E**, the additions were followed with a simple kinetic (λ_{ex} = 280 nm, λ_{em} = 360 nm, slits = 10/10 nm). SSCs value were determined as described in the first chapter.

3.3.5 Displacement experiments

The displacement experiments were performed by adding consecutive amounts of a stock solution of ATP (25 mM) to a 3-mL aqueous solution ([HEPES] = 10 mM, pH = 7.0) containing Au NP **1**•Zn^{2+} (10 µM) coated with the fluorescent probes (**B**: 3.0 µM, **C**: 3.5 µM, **D**: 3.5 µM) at 25°C. The time course of the fluorescence intensity after each addition was monitored at the emission maximum of the MANT-probe (λ_{ex} = 355 nm, λ_{ex} = 448 nm, slits = 10/5 nm). The displacement curves were fitted to a simple model:

$$NP{\bullet}A + B \underset{}{\overset{K}{\rightleftharpoons}} NP{\bullet}B + A$$

in which the nanoparticle complex is reduced to a single species. Since complex formation occurs under saturation conditions it is assumed that [NP•B] equal [A]. It was noted that the model fits the initial points of the displacement curves poorly, which originates from the fact that the probes are present at a concentration below the SSC. Consequently, initial additions of ATP may result in surface binding without displacement. This is particularly evident in the **D**-curve. The model was implemented in Micromath Scientist for Windows, version 2.01:

```
// MicroMath Scientist Model File
IndVars: B0
DepVars: FI, A, NPA, B
Params: K, X, NPA0
A=SQRT(K*NPA*B)
NPA=NPA0-A
B=B0-A
FI=X*A
//
0<NPA<NPA0
0<A<NPA0
0<B<B0
***
```

3.3.6 Selective displacement

This displacement experiment were performed by adding consecutive amounts of a stock solution of (2.5 mM) to a 3-mL aqueous solution ([HEPES] = 10 mM, pH = 7.0) containing Au NP **1**•Zn^{2+} (10 μM) coated with the fluorescent probes ([**B**] = 1.0 μM, [**E**] = 1.4 μM) at 25°C. The time courses of the two fluorescence intensity after each addition were monitored at 448 nm and 360 nm (multi-wavelength kinetic at fixed slits = 10/10 nm).

3.3.7 Selective catch and release

B (30 μL, 200 μM) and **E** (15 μM, 200 μM) were added to a 3-mL aqueous solution ([HEPES] = 10 mM, pH = 7.0) containing Au NP **1**•Zn^{2+} (10 μM) and after 5 minutes of equilibration at 37 °C the time courses of the two fluorescence intensity were monitored at 448 nm and 360 nm (multi-wavelength kinetic at fixed slits = 10/10 nm). Aliquots of $Zn(NO_3)_2$ (15 μL, 1.0 mM) were added during the kinetic after 2 and 51 minutes. Aliquots of TPEN (15 μL, 1.0 mM) were added 8 min after the additions of $Zn(NO_3)_2$.

3.5 References

(1) Oshovsky, G. V.; Reinhoudt, D. N.; Verboom, W. *Angew Chem Int Ed Engl* **2007**, *46*, 2366.
(2) Lehn, J. M. *Angew. Chem.-Int. Edit. Engl.* **1988**, *27*, 89.
(3) Palmer, L. C.; Stupp, S. I. *Acc. Chem. Res.* **2008**, *41*, 1674.
(4) Lim, Y. B.; Moon, K. S.; Lee, M. *Chem. Soc. Rev.* **2009**, *38*, 925.
(5) Uhlenheuer, D. A.; Petkau, K.; Brunsveld, L. *Chem. Soc. Rev.* **2010**, *39*, 2817.
(6) Pieters, G.; Cazzolaro, A.; Bonomi, R.; Prins, L. J. *Chem Commun (Camb)* **2012**, *48*, 1916.
(7) Bonomi, R.; Cazzolaro, A.; Sansone, A.; Scrimin, P.; Prins, L. J. *Angew. Chem. Int. Ed.* **2011**, *50*, 2307.
(8) Zaramella, D.; Scrimin, P.; Prins, L. J. *J. Am. Chem. Soc.* **2012**, *134*, 8396.
(9) Ellis, A. V.; Vjayamohanan, K.; Goswaimi, R.; Chakrapani, N.; Ramanathan, L. S.; Ajayan, P. M.; Ramanath, G. *Nano Lett.* **2003**, *3*, 279.
(10) Bonomi, R.; Selvestrel, F.; Lombardo, V.; Sissi, C.; Polizzi, S.; Mancin, F.; Tonellato, U.; Scrimin, P. *J. Am. Chem. Soc.* **2008**, *130*, 15744.
(11) Phillips, R. L.; Miranda, O. R.; Mortenson, D. E.; Subramani, C.; Rotello, V. M.; Bunz, U. H. F. *Soft Matter* **2009**, *5*, 607.
(12) Liu, X.; Hu, Y.; Stellacci, F. *Small* **2011**, *7*, 1961.
(13) Davis, J. T.; Spada, G. P. *Chem Soc Rev* **2007**, *36*, 296.

(14) Kubik, S.; Reyheller, C.; Stüwe, S. *Journal of Inclusion Phenomena* **2005**, *52*, 137.
(15) Liu, L.; Guo, Q. X. *Journal of Inclusion Phenomena* **2002**, *42*, 1.
(16) Hiratsuka, T. *Biochim Biophys Acta* **1983**, *742*, 496.
(17) Jameson, D. M.; Ecclestone, J. F. In Fluorescence Spectroscopy; Brand, L., Johnson, K. L., Eds; Academic Press: San Diego, 1997; Vol. 278, pp 363-390.

Chapter 4

Zn^{2+}-regulated self-sorting and mixing of phosphates and carboxylates on the surface of functionalized gold nanoparticles[‡]

This Chapter deals with the spontaneous organisation in a complex mixture of small molecules and different nanoparticles. It will be shown that a mixture of phosphate- and carboxylate-containing molecules self-sorts on the monolayer surface of two differently functionalized gold nanoparticles. Self-sorting is driven by the selective interactions between the phosphate probe and Zn^{2+}-complexes in one monolayer, which drives the carboxylate probe to the other nanoparticle. The clustering of small molecules on the monolayer surface under saturation conditions can be envisioned as a form of compartmentalization, since the self-assembly process effectively localizes the probe molecules in a well-defined constricted space surrounding the nanoparticles. A fundamental role in the system is played by Zn^{2+} metal ions in the monolayer, which act as regulatory elements that control the concentration and contents of the compartment. The removal/addition of Zn^{2+} metal ions from the system is used to revert the system from an ordered to a disordered state and vice versa, which give the possibility to control the organization of populations of molecules in a complex mixture.

[‡] Part of this Chapter has been published in: C. Pezzato, P. Scrimin, L. J. Prins *Angew. Chem. Int. Ed.* **2014**, *53*, 2104-2109.

4.1 Introduction

Nature strictly relies on self-assembly for the formation of functional molecular structures.[1] In the hierarchy from the self-assembly of small molecules up to the level of the entire cell, compartmentalization plays an essential role. Compartmentalization provides control over the chemical contents of a local environment in terms of concentration and composition, which, in turn, gives control over recognition process and chemical reactions occurring within the compartment. Typically, the chemical contents of compartments is modulated by transmembrane and transporter proteins that are activated or deactivated by regulatory molecules or ions. Inspired by nature, chemists have learned over the past decades to master the process of self-assembly up to the level that highly complex molecular structures are now readily accessible.[2] Nonetheless, compartmentalization in synthetic self-assembled systems is still very hard to achieve.[3,4] Most effort has been dedicated to micellar systems in which the bilayer membrane acts as a physical barrier that separates the compartment from the surrounding bulk. Nonetheless, the self-assembly of coexisting different micelles is very challenging and requires the use of nonmiscible amphiphiles.[5,6] Strategies on how to overcome this limitation can be obtained from studying self-sorting processes in the self-assembly of well-defined molecular architectures.[7,8] Here, building blocks are instructed with chemical information leading to the specific recognition of either themselves (narcissistic self-sorting) or complementary partners (social self-sorting). It has recently been shown that narcissistic self-sorting can indeed drive the spontaneous formation of homodomains in micellar aggregates hinting towards the possibility of creating chemical systems with the complexity of natural systems.[9] Alternative approaches towards compartmentalization in self-assembled synthetic systems rely on polymer self-assembly,[10,11] layer-by-layer deposition of polyelectrolytes on microspheres[12,13] and macromolecule induced phase segregation in water.[14-16] Compartmentalization is considered to have played an important role in the early stages of life and many of the above examples have been developed to serve as new protocell models.[17,18] Also the self-sorting of small molecules on solid 2D surfaces is drawing a lot of attention as it provides an attractive way towards surface patterning for

applications in the field of nanotechnology.[19,20] Here, we describe the self-sorting of small molecules on the surface of monolayer protected gold nanoparticles (Au NPs). It will be shown that the addition of two different Au NPs to a mixture of carboxylate- and phosphate probes results in the spontaneous self-sorting of the probes on the two available surfaces. The clustering of the small molecules on the surfaces can be considered a form of compartmentalization because of three fundamental characteristics: increase of local concentration, regulation of the concentration and differentiation between compartments. It will be shown that these features are all regulated by the Zn^{2+} metal ions present in the monolayer. In addition, it will be shown that Zn^{2+} is a regulatory element for the transfer of molecules between the different compartments. This permits the system to cycle between a self-sorted state in which the two types of molecules reside in different compartments and a 'mixed state' in which the molecules are randomly distributed.

4.2 Results and discussion

4.2.1 Preliminary binding and displacement studies

In the first chapter, we have seen that, the presence of the Zn^{2+}-metal ion in the monolayer of Au NP **1**•Zn^{2+} caused an increase in the SSC of the probes on the surface compared to the analogous system Au NP **1** without Zn^{2+}. In addition, Zn^{2+} caused a higher affinity of phosphate-probes compared to carboxylate-probes. Here, we focus the attention to see whether the metal ion would be able to induce the selective assembly of a phosphate-probe on the surface of Au NP **1**•Zn^{2+} in the presence of a carboxylate probe. A second aselective nanosystem (*e.g.* Au NP **2**[21-23] having quaternary ammonium head groups) could then act as a scavenger of the carboxylate probe, resulting in the self-sorting of two probes on two different surfaces (Figure 4.1). In order to explore this possibility we selected the probes **C** and **F**, which have three negative charges in the form of phosphates or carboxylates, respectively. Both probes are equipped with a fluorogenic moiety (a N-methylamino anthranilic ester in **C**, coumarin 343 in **F**). The distinct excitation and emission wavelengths for **C** (λ_{ex} = 355 nm, λ_{em} = 448 nm) and **F** (λ_{ex} = 450 nm, λ_{em} = 493 nm) allow for a simultaneous study of both probes in a mixture. Importantly, both probes bind to the surface of either Au NP **1**•Zn^{2+} or Au NP **2** under saturation

conditions even at low micromolar concentrations in water, implying that it is possible to operate at probe concentrations at which effectively all probe molecules are bound.

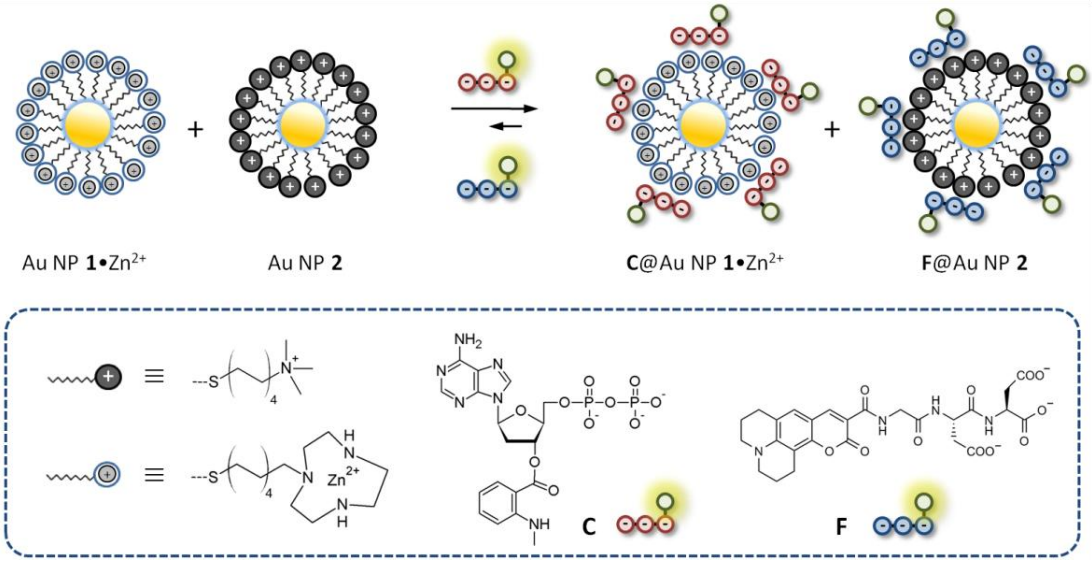

Figure 4.1. (a) Schematic representation of the self-sorting of probes **C** and **F** on Au NPs **1**•Zn^{2+} and **2**.

As usual, the SSCs of both probes on the surfaces of Au NP **1**•$Zn^{2+}$and Au NP **2** were determined by means of fluorescence titrations (see the experimental section). The respective concentrations of Au NP **1**•$Zn^{2+}$and Au NP **2** were regulated such that both nanosystems would be able to bind approximately the same amount of probes (3.4 µM for **C** and 2.7 µM for **F**).

In order for self-sorting to occur, two requirements must be fulfilled. The first one is that Au NP **1**•Zn^{2+} must have a higher affinity for probe **C** with respect to probe **F** and, second, Au NP **1**•Zn^{2+} must in general have a higher affinity for either probe compared to Au NP **2**. Only in that case, the distribution of the probes on the two available surfaces will be determined by the preference imposed by Au NP **1**•Zn^{2+}. Both prerequisites were studied by a series of competition experiments. Initially, competition experiments between **C** and **F** were performed to determine their relative affinities for Au NP **1**•Zn^{2+} and Au NP **2**, respectively. In these experiments, increasing amounts of probe **C** were added to a solution of either Au NP **1**•Zn^{2+} or Au NP **2** containing probe **F** at a fixed concentration of 2.7 µM. After each addition the fluorescence emission of both **C** and **F** was measured. The strong difference

between Au NP **1**•Zn^{2+} and Au NP **2** becomes immediately evident from a glance at the corresponding displacement curves (Figure 4.2a *vs* 4.2b).

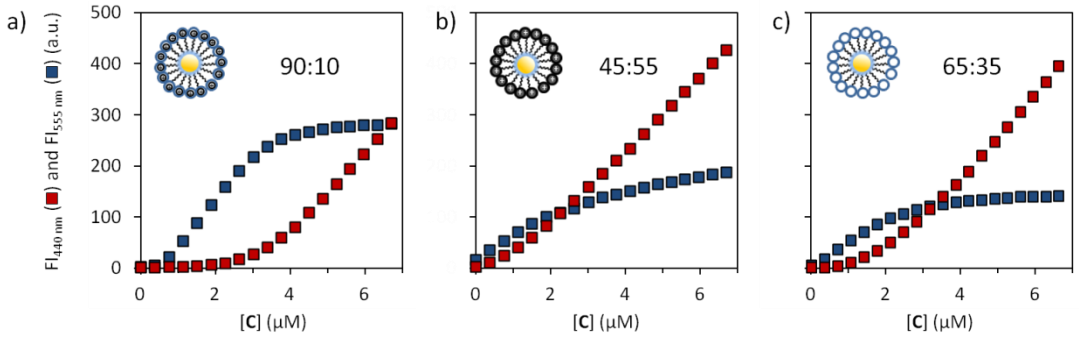

Figure 4.2. Fluorescence intensities of probes **C** (red squares) and **F** (blue squares) as a function of the amount of **C** added to either **F**@Au NP **1**•Zn^{2+} (a), **F**@Au NP **2** (b) or **F**@Au NP **1** (c). For each situation the **C**:**F** surface ration is reported (see the experimental section for more details. Experimental conditions: [Au NP **1**•Zn^{2+}] = [Au NP **1**] = 8 μM, [Au NP **2**] ≈ 20 μM, [**F**] = 2.7 (or 1.3 μM in the case of Au NP **1**), [HEPES] = 10 mM, pH = 7.0, 37 °C.

The initial additions of **C** to **F**@Au NP **1**•Zn^{2+} resulted in a quantitative displacement of **F** by **C** indicated by the linear increase in fluorescence intensity of **F** and the complete quenching of **C** (Figure 4.2a). On the other hand, addition of **C** to **F**@Au NP **2** gave only a partial displacement of **F** (Figure 4.2b). A quantitative analysis revealed the surface composition of each nanosystem after the addition of **C** (3.4 μM): **C**:**F** = 90:10 for Au NP **1**•Zn^{2+} and 45:55 for Au NP **2** (see the experimental section). These results show that Au NP **1**•Zn^{2+} binds **C** with a much higher affinity compared to **F**, whereas Au NP **2** does not have a marked preference.

Proof that Au NP **1**•Zn^{2+} has a higher affinity surface compared to Au NP **2** was obtained by studying the affinities of probes **C** and **F** for either surface in the presence of increasing amounts of tetraethylammonium chloride (TEACl). The increase in ionic strength in the solution weakens the interaction of the two anionic probes and the monolayer surfaces. The displacement of surface-bound probes **C** and **F** was studied independently for each nanosystem (Figure 4.3a-b). The obtained curves demonstrated that both probes **C** and **F** are quantitatively displaced from Au NP **2** upon the addition of 80 mM of TEACl (Figure 4.3b). The nearly superimposable curves obtained for probes **C** and **F** indicate that the chemical nature of the anionic group is irrelevant for binding, which explains the lack of selectivity for probe binding to Au NP **2**. On the other hand, the same experiment performed using Au

NP **1**•Zn^{2+} resulted in a displacement of just 15% of **C** and 50% of **F** (Figure 4.3a). These experiments illustrate three important features: 1) the much lower displacement levels demonstrate that Au NP **1**•Zn^{2+} binds either probe stronger than Au NP **2**; 2) it confirms the selectivity of Au NP **1**•Zn^{2+} for **C** over **F** and 3) it shows that the interaction between **C** and Au NP **1**•Zn^{2+} is the only one that is hardly affected by an increase in ionic strength.

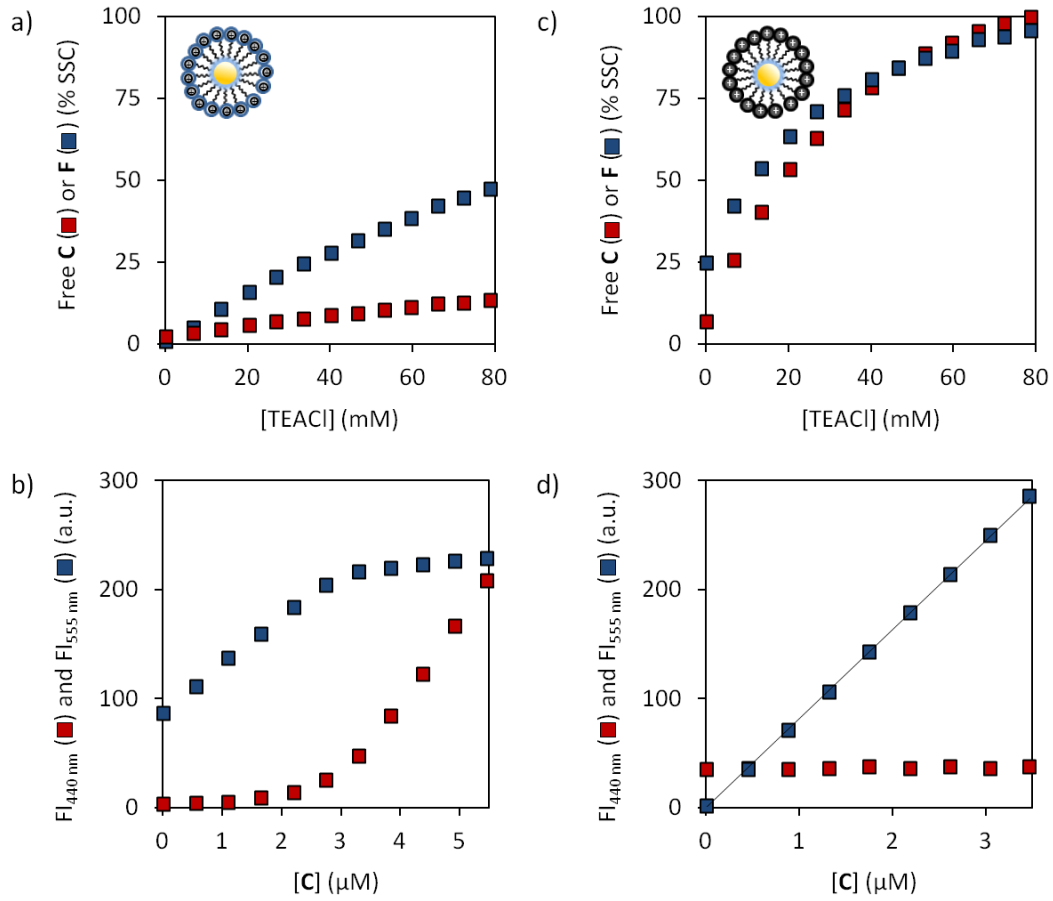

Figure 4.3. (a-b) Amount of displaced **C** (red squares) and **F** (blue squares) as a function of the amount of TEACl added to (a) either **C**@Au NP **1**•Zn^{2+} or **F**@Au NP **1**•Zn^{2+}, and (b) either **C**@Au NP **2** or **F**@Au NP **2**. (c-d) Fluorescence intensities as a function of (c) the amount of **C** added to a solution of **F**, Au MPC **1**•Zn^{2+}, Au MPC **2**, and TEACl and (d) the amount of **F** added to a solution of **C**, Au MPC **1**•Zn^{2+}, Au MPC **2**, and TEACl. Experimental conditions: [Au MPC **1**•Zn^{2+}] = 8 μM, [Au MPC **2**] ≈ 20 μM, [HEPES] = 10 mM, pH 7.0, 37 °C; where present: [TEACl] = 80 mM, [**F**] = 2.7 μM, [**C**] = 3.4 μM.

Two control experiments confirmed that the observed probe selectivities and affinities are maintained also in a complex system composed of both nanosystems and probes (Figure 4.3c-d). In the first one, a solution containing both nanosystems Au NP **1**•Zn^{2+}, Au NP **2**, probe **F** and 80 mM of TEACl was titrated with probe **C** (Figure 4.3c). In the absence of **C**, a lower amount of **F** was bound (1.1 μM), in

agreement with the SSC of **F** on Au NP **1**·Zn^{2+} under these conditions. The addition of **C** up to around 2.8 µM resulted in binding of **C** and a complete displacement of **F**. This amount of **C** is in line with the SSC of **C** on Au NP **1**·Zn^{2+} and confirms that the selectivity of Au NP **1**•Zn^{2+} for **C** is maintained in the full-component mixture. Alternatively, titration of **F** to a solution of Au NP **1**•Zn^{2+}, Au NP **2**, probe **C** and 80 mM of TEACl showed no binding of **F** at all, confirming the higher affinity of **C** also in the full-component mixture.

4.2.2 Self-sorting experiments

Having established that Au NP **1**•Zn^{2+} binds **C** selectively over **F** and that Au NP **1**•Zn^{2+} binds both probes **C** and **F** with a higher affinity compared to Au NP **2**, we then proceeded with the self-sorting experiment by adding Au NP **1**•Zn^{2+} and Au NP **2** stepwise to a solution of probes **C** and **F** (Figure 4.4a). At each step the fluorescence intensity of either probe was measured and used to calculate the amount of free probe in solution for each of the consecutive situations. The addition of Au NP **1**•Zn^{2+} resulted in a near quantitative capture of **C**, whilst only a marginal amount of **F** was captured. The respective amounts of captured probe (88% for **C** and 12% for **F**) correspond exactly to those found in the displacement studies (Figure 4.2a). The successive addition of Au NP **2** caused the complete capture of all remaining probes **C** and **F** that were still free in solution, resulting in a situation where effectively all probes are surface bound. Based on the experiments described before, this represents a situation in which **C** resides predominantly on Au NP **1**•Zn^{2+}, whereas **F** is localized on Au NP **2**. This was confirmed by the observation that the addition of 80 mM of TEACl to the self-sorted system caused only a very minor release of **C** (17 %) consistent with the amount localized on Au NP **1**•Zn^{2+}. On the other hand, probe **F** was nearly quantitatively (96 %) released at the same time which is consistent with its localization on Au NP **2**. Additional evidence for the localization of **C** on Au NP **1**•Zn^{2+} came from the final addition of the N,N,N',N'-tetrakis(2-pyridylmethyl) ethylenediamine (TPEN)-ligand, which is as a scavenger for the Zn^{2+}-ions present in the monolayer of Au NP **1**•Zn^{2+}. Indeed, the addition of TPEN to the nanoparticle mixture caused a partial release of probe **C** to a final value of around 60%. The remaining 40 % corresponds to 1.1 µM of probe **C**

still bound to the surface of on Au NP **1** and is consistent with the SSC of probe **C** under these conditions (Figure 4.3e). Importantly, the probe displacement curves observed after the sequential additions of TEACl and TPEN are identical to those of a control experiment in which the displacement experiments using TEACl and TPEN were performed separately on **C**@Au NP **1**•Zn^{2+} and **F**@Au NP **2** (Figure 4.4b and c, respectively).

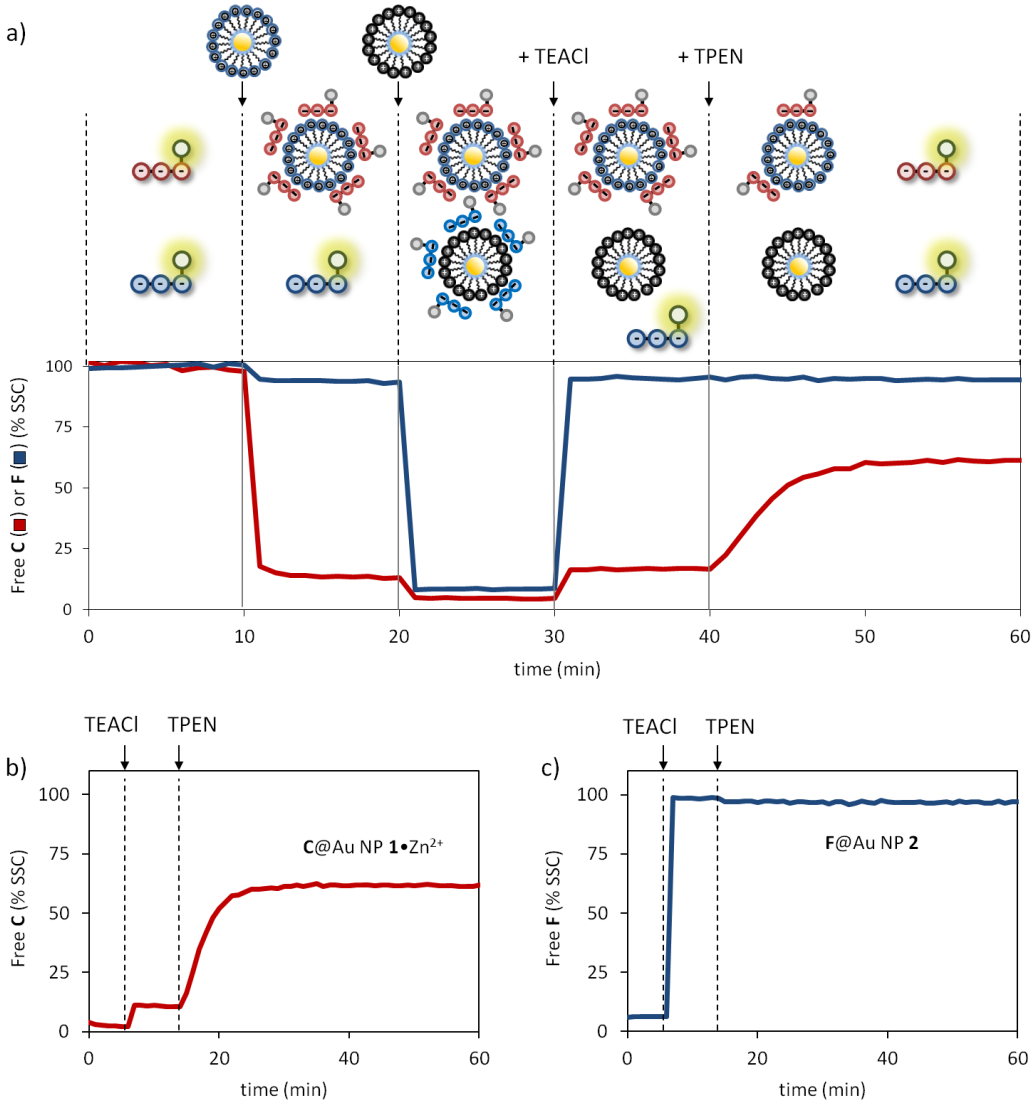

Figure 4.4. (a) Self-sorting experiment. (b-c) Sequential addition of TEACl and TPEN to a (b) **C**@Au NP **1**•Zn^{2+} or (c) **F**@Au NP **2**. Experimental conditions: [Au NP **1**•Zn^{2+}] = 8 µM, [Au NP **2**] ≈ 20 µM, [TEACl] = 80 mM, [TPEN] = 20 µM, [**C**] = 3.4 µM, [**F**] = 2.7 µM, [HEPES] = 10 mM, pH 7.0, 37 °C.

4.2.3 The role of the Zn^{2+}-metal ion

The importance of Zn^{2+} in inducing self-sorting was investigated by performing analogous studies as described before, but using Au NP **1** instead of Au NP **1**•Zn^{2+}. At the same concentration of TACN head groups a drop of the SSC for both probes **C**

and **F** was observed in the absence of Zn^{2+} (see experimental part). Importantly, though, the absence of Zn^{2+} also reduces significantly the selectivity of the monolayer surface. This emerged in a clear manner from a displacement study performed by adding increasing amounts of **C** to **F**@Au NP **1** (Figure 4.2c). The resulting curves are more similar to those obtained for Au NP **2**. In particular, after adding 1.7 µM of **C** (equal to its SSC) the ratio of surface-bound probes **C** and **F** amounts to 65:35, against 90:10 for Au NP **1**•Zn^{2+} and 45:55 for Au NP **2**, respectively. The fact that Au NP **1** still maintains some of its preference for **C** presumably results from the formation of H-bonds between the TACN-units and the phosphate groups which is not possible for Au NP **2**.[24]

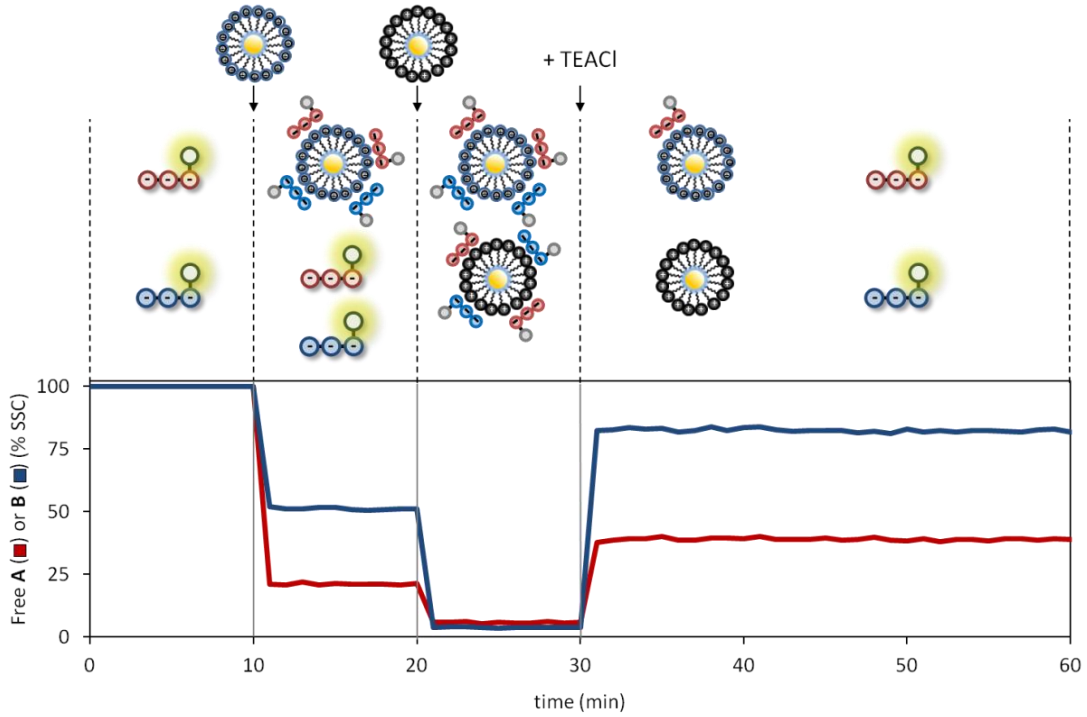

Figure 4.5. Self-sorting experiment in the absence of Zn^{2+}. Experimental conditions: [Au NP **1**] = 8 µM, [Au NP **2**] ≈ 20 µM, [TEACl] = 80 mM, [TPEN] = 20 µM, [**C**] = 1.7 µM, [**F**] = 1.3 µM, [HEPES] = 10 mM, pH 7.0, 37 °C.

A repetition of the self-sorting experiment using Au NP **1** and Au NP **2** gave a much different result (Figure 4.5). The addition of Au NP **1** to a solution of **C** and **F** resulted in the partial capture of either one of them with a 60:40 ratio of **C**:**F** which corresponds to that of the displacement studies. The subsequent addition of Au NP **2** resulted in a near quantitative quenching of the fluorescence of both probes indicating that after the addition all probes are bound to a surface. Nonetheless, the

absence of selective probe capture indicates that self-sorting does not occur in the absence of Zn^{2+}. Indeed, the similarity between both surfaces was further confirmed by the observation that in this case the addition of TEACl (80 mM) resulted in the immediate release of both probes **C** and **F**, and not just probe **F**. The extent of probe release is in agreement with the respective SSCs of **C** and **F** for Au NP **1** and Au NP **2** in the presence of 80 mM TEACl. It is noted that the difference in end values compared to the self-sorting experiment described in Figure 4 results from the different concentrations of **C** and **F**.

4.2.4 Zn^{2+}-mediated cycling between a 'self-sorted' and 'mixed' state

Considering the essential role of Zn^{2+} in the self-sorting process, we then argued that removal of Zn^{2+} from the self-sorted situation **C**@Au NP **1**•Zn^{2+}/**F**@Au NP **2** would drive the system to a less ordered state in which the probe **C** and **F** are randomly mixed on the surfaces (Figure 4.6, top). The addition of TPEN resulted in the gradual release of **C** from Au NP **1**•Zn^{2+} owing to the lower SSC of **C** on Au NP **1** (Figure 4.6, bottom). The rate of this process is determined by the dissociation rate of Zn^{2+} from the TACN•Zn^{2+} complex.[25] Here, it takes around 20 minutes for free **C** to reach a constant value of 0.7 µM, which corresponds to a release of around 20% of surface bound **C**. However, based on the difference in the SSC between **C**@Au NP **1**•Zn^{2+} and **C**@Au NP **1** a much higher amount (1.7 µM) was expected, which implies that part of the released **C** translates to the surface of Au NP **2**. Since the surface of Au NP **2** is saturated with **F**, this translation must induce a displacement of **F** from Au NP **2**. Indeed, simultaneous to the release of **C** also the appearance of free probe **F** is observed. The identical kinetic profile indicates that **C** and **F** exchange rapidly on the surface, which is in agreement with previous studies. The removal of Zn^{2+} from Au NP **1**•Zn^{2+} causes also a loss of selectivity for that the monolayer and the results is a situation where both probes are randomly distributed on either nanoparticle. The system can be reverted back to the sorted state by adding Zn^{2+}, which regenerates the TACN•Zn^{2+} complexes in Au NP **1**. This process is very fast and again illustrates the rapid probe exchange kinetics in the system. A second cycle demonstrated that it is possible to reversibly switch between the self-sorted and mixed state.

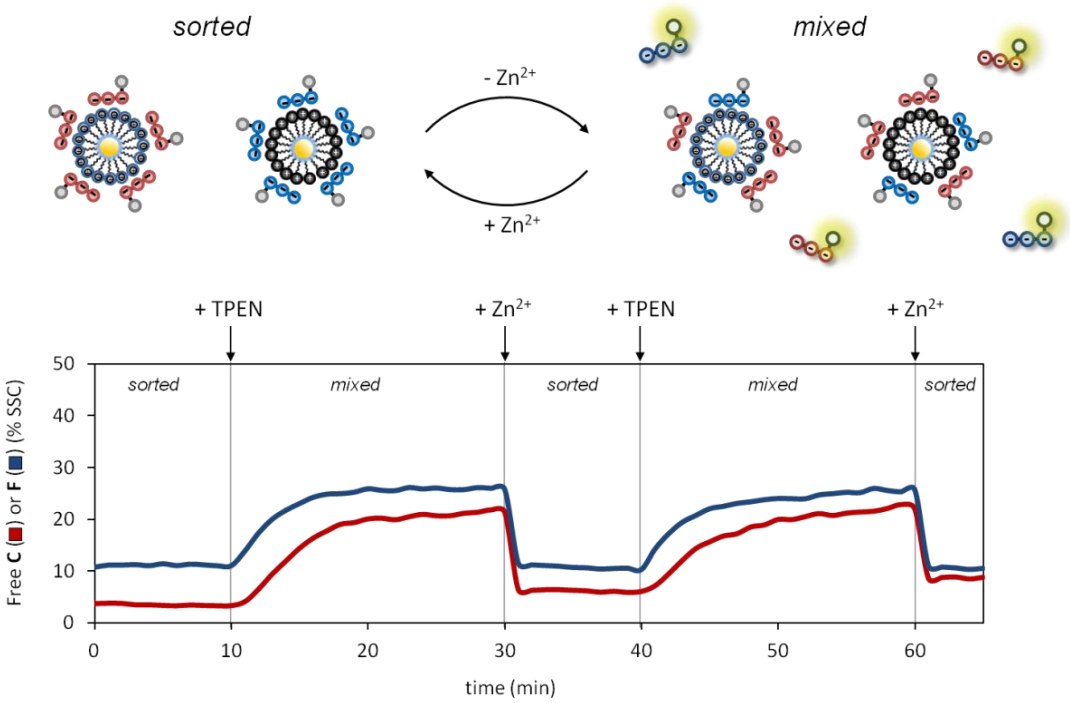

Figure 4.6. Zn^{2+}-regulated switching between a 'self-sorted' and 'mixed' state. Experimental conditions: : [Au NP **1**•Zn^{2+}] = 8 μM, [Au NP **2**] ≈ 20 μM, [**C**] = 3.4 μM, [**F**] = 2.7 μM, $[TPEN/Zn^{2+}]_{cycled}$ = 20 μM, [HEPES] = 10 mM, pH 7.0, 37 °C.

The importance of this experiment is that it shows that it is possible to control the distribution of the two probes in the system. The removal/addition of Zn^{2+} in one compartment sets of a cascade of events affecting also the second compartment ultimately leading towards a completely different state of the system (self-sorted or mixed). This points to an additional role of Zn^{2+} as regulator of mass transport between the compartments.

4.3 Conclusions

In summary, the concept of self-sorting can be used to spontaneously introduce order in a homogeneous system composed of nanoparticles and small molecules. Whereas self-sorting is most frequently associated to the formation of well-defined supramolecular architectures, in our case it regards the topological location of populations of molecules on the surface of different nanoparticles. The clustering of small molecules on the monolayer surface under saturation conditions is a form of compartmentalization, since the self-assembly process effectively localizes the probe molecules in a well-defined constricted space surrounding the nanoparticles.

At difference with membrane-enclosed compartments, there is no physical separation between bulk and the compartment and molecules can exchange rapidly between compartment and bulk.[23] Despite the 'open-space' nature of the compartment, though, it bears all the important characteristics typically associated with compartmentalization: increase of local concentration, regulation of the concentration and differentiation between compartments. A fundamental role in the system is played by the Zn^{2+} metal ion, which act as regulator of all these features. The removal/addition of Zn^{2+} metal ions from the system can also be used to switch between an ordered and disordered state.

4.4 Experimental section

4.4.1 Instrumentation

NMR-Analysis

^{1}H, ^{13}C spectra were recorded using a Bruker AV300 spectrometer operating at 75 and 300 MHz for ^{13}C and ^{1}H, respectively. Chemical shifts (δ) are reported in ppm using ACN-d_6 and D_2O residual solvent values as internal reference. The coupling constants (*J*) are listed in Hertz (Hz), while the multiplicity of the signals are shown as follow: s: singlet, d: doublet, t: triplet, q: quartet, sp: septet, m: multiplet.

ESI-MS Analysis

ESI-MS measurements were performed on an Agilent Technologies 1100 Series LC/MSD Trap-SL spectrometer equipped with an ESI source, hexapole filter and ionic trap.

HPLC

HPLC purifications were performed on a preparative HPLC Shimazu LC-8A equipped with a Shimazu SPD-20A UV detector. The column used for separation was a Jupiter Proteo 4u 90A 250 x 21.20 mm, 4 µm. All the runs were carried out using a flow of 17 mL/min. Eluents: H_2O (A) and ACN (B) + 0.1% TFA.

pH measurements and UV-Vis Spectrometry

see chapter 2.

4.4.2 Materials

Au NP **1** and **2** were synthesized as described in the chapter 1 (see next section). For $Zn(NO_3)_2$, TPEN, probe **B**, and HEPES see previous chapters. Tetraethylammonium chloride (TEACl) was obtained from Sigma Aldrich and used without further purification.

4.4.3 Synthesis and characterization of Au NP 1 and 2.

Au NP **1** and **2** were synthesized following the protocol reported in experimental section of the first chapter: the solution of DOA-stabilized nanoparticles was split into portions, to which the respective thiol was added. After purification the two batches of Au NPs were characterized as described earlier. Data were in accordance with the literature.[23]

4.4.4 Synthesis and characterization of C343-GDD-OH (F)

The fluorescent tripeptide C343-GDD-OH was synthesized on solid support using a Fmoc-based peptide chemistry standard procedure. After the cleavage of the Fmoc group of the Gly residue, coupling reaction with commercially available C343-COOH was performed, leaving the suspension shaked overnight. After the washing procedure the resin was cleaved with a TFA/H_2O/TIPS : 96/2/2 mixture (2 hours). The suspension was filtered and the final solution was evaporated under reduced pressure. The resulting solid residue was purified by preparative HPLC to give the desired peptide as a dark yellow solid (10 mg).

HPLC (Column: Phenomenex RP Jupiter 4U Proteo 90 Å. Gradient : from 90:10 to 10:90 H_2O:ACN (0.1% TFA) in 35 minutes, 450 nm): 18.55 min.

^{1}H-NMR (D_2O/ACN-d_3) δ ppm: 8.43 (s, 1H), 7.09 (s, 1H), 4.71 (t, *J* = 6.4 Hz, 1H), 4.61 (t, *J* = 6.0 Hz, 1H), 4.02 (d, *J* = 3.7 Hz, 2H), 3.40 – 3.20 (m, 4H), 2.92 – 2.58 (m, 8H), 1.92 – 1.76 (m, 4H).

^{13}C-NMR (D_2O/ACN-d_3) δ ppm: 174.1, 173.9, 171.6, 171.0, 165.7, 163.7, 153.2, 149.6, 149.0, 148.9, 127.9, 121.1, 108.4, 106.8, 105.9, 96.0, 95.9, 50.4, 50.1, 49.9, 43.4, 36.5, 36.0, 27.4, 21.0, 20.0.

MS (ESI+, ACN+0.1% HCOOH) *m/z*: 573.1 ([M+H^+], 100, calcd 573.5), 595.0 ([M+Na^+], 33, Calcd 595.5).

4.4.5 Determination of the SSCs

Fluorescence titrations were carried out by adding consecutive amount of a stock solution of **C** or **F** to a 3-mL aqueous solution ([HEPES] = 10 mM, pH 7.0) containing Au NP **1** (with or without Zn^{2+}, 8 μM) or Au NP **2** (20 μM). The optical parameters used for **C** were λ_{ex} = 355 nm, λ_{em} = 450 nm, slits =10/5 nm, while the ones used for **F** were λ_{ex} = 450 nm, λ_{em} = 493 nm, slits =2.5/5 nm. The same experiments were repeated in the presence of TEACl (80 mM). SSCs value were determined as described in the first chapter and are listed in the following table.

Table 4.1 List of the SSCs values

Nanosystem	TEACl	SSC of probe **C** (μM)	SSC of probe **F** (μM)
Au NP **1**•Zn^{2+}	no	3.4 ± 0.2	2.7 ± 0.2
Au NP **2**	no	2.7 ± 0.2	2.4 ± 0.2
Au NP **1**	no	1.7 ± 0.2	1.3 ± 0.2
Au NP **1**•Zn^{2+}	yes	2.8 ± 0.2	1.0 ± 0.2
Au NP **2**	yes	no binding	no binding
Au NP **1**	yes	1.1 ± 0.1	0.2 ± 0.2

4.4.6 Competition experiments

In order to follow the simultaneous emission of both probes, the instrument settings were slightly modified compared to the previous titrations in order to account for the different fluorescence properties of probes **C** and **F** the following parameters were used:

C : λ_{ex} = 340 nm, λ_{em} = 440 nm, slits = 10/5 nm;
F : λ_{ex} = 385 nm, λ_{em} = 555 nm, slits = 10/5 nm.

Competition experiments between **C** and **F** were performed by adding consecutive amounts of a stock solution of **C** (286 μM in mQ-water) to a buffered acqueous solution (HEPES 10 mM, pH = 7.0) containing Au NP **1**, **1**•Zn^{2+} (8 μM) or **2** (20 μM) saturated with probe **F** (1.3, 2.7 and 2.7 μM respectively). Conversion of the FIs into concentrations was performed using the final points of each titration. The slope of

the linear part of the red curves (probe **C**, Figure 2a) corresponds to $\Delta FI/\Delta[A]_{free}$, whereas the final part of the blue curves (probe **F**) gives the FI for the amount of **F** present in the system. Since displacement is not complete for Au MPC **2** the blue curve was extrapolated using a model. The following table lists the concentrations of all species for the concentrations used.

Table 4.2 Free and surface bound probe concentrations and surface ratio of **C** and **F**

Nanosystem	$\mathbf{C}_{total}$ (μM)	$\mathbf{C}_{free}$ (μM)	$\mathbf{C}_{bound}$ (μM)	$\mathbf{F}_{total}$ (μM)	$\mathbf{F}_{free}$ (μM)	$\mathbf{F}_{bound}$ (μM)	**C:F** surface ratio
Au NP **1**•Zn^{2+}	**3.4**	0.5	2.9	**2.7**	2.3	0.4	**90:10**
Au NP **2**	**3.4**	2.0	1.4	**2.7**	0.9	1.8	**45:55**
Au NP **1**	**1.7**	0.4	1.3	**1.3**	0.6	0.7	**65:35**

4.4.7 Displacement experiment with TEACl

The displacement experiments were performed by measuring the fluorescent intensities after adding consecutive amounts of a stock solution of TEACl (2.05 M) in mQ-water) to a 3-mL buffered acqueous solution ([HEPES] = 10 mM, pH = 7.0) containing either Au NP **1**•Zn^{2+} or **2** coated with probe **C** (3.4 μM) or probe **F** (2.7 μM). For this experiment the optical settings were the classic ones. The maximum FIs expected for a full release were obtained by adding small additional amounts of **C** to Au MPC **1**•Zn^{2+} and Au MPC **2** (providing $\Delta FI/\Delta[\mathbf{C}]_{free}$) at the end of the TEACl titrations involving probe **C** or by adding an excess of ATP (150 μM) to Au NP **1**•Zn^{2+} and Au NP **2** to cause a full displacement of probe **F**. The intrinsic fluorescent properties of probe **C** are slightly affected (10%) by the presence of TEACl – a correction was performed to account for this. The fluorescence intensity of probe **F** is not affected by the addition of 80 mM TEACl.

4.4.8 Control titrations

In order to prove that the observed surface selectivities and affinities are maintained also in a complex system, titrations were performed by adding consecutive amounts of either **C** or **F** to a buffered solution ([HEPES] 10 mM, pH = 7.0) containing Au NP **1**•Zn^{2+}, Au NP **2**, and TEACl (80 mM) in the presence of either

C or **F**, respectively. The FIs of both probes were measured after each addition. The optical settings were the same used in the competition experiments (see above).

4.4.9 Self-sorting experiments

Self-sorting experiments were carried by sequentially adding to a 3-mL buffered aqueous solution ([HEPES] = 10 mM, pH = 7.0) containing probes **A** (3.4 μM) and **B** (2.7 μM):

a) Au NP **1**•Zn^{2+} (or Au NP **1**, final concentration = 8 μM)

b) Au NP **2** (final concentration = 20 μM)

c) TEACl (final concentration = 80 mM)

d) TPEN (final concentration = 20 μM)

The FIs of both probes were simultaneously followed as a function of time analogously as the competition experiements. Conversion of the measured FIs into concentrations of free **C** and **F** were performed by comparing the measured FIs to the expected values for free **C** and **F** in solution. These were determined as follows:

a) The expected values correspond to those from the competition experiments;

b) The expected values were obtained from the control titrations described in the previous section (with the notion that the emission of **C** was corrected for the absence of TEACl);

c) The expected values were obtained from the experiments described in the previous section;

d) See c). The presence of TPEN does not affect the fluorescence properties of **C** and **F**.

4.4.10 Control displacements

This displacement experiments were performed by measuring the fluorescent intensities after adding TEACl (80 mM) and TPEN (20 μM) to a 3-mL buffered aqueous solution ([HEPES] = 10 mM, pH = 7.0) containing Au NP **1**•Zn^{2+} (8 μM) saturated with probe **C** (3.4 μM) or Au NP **2** (20 μM) saturated with probe **F** (2.7 μM).

4.5 References

(1) Alberts, B. J., A.; Lewis, J.; Raff, M.; Roberts, K.; Waiter, P. *Molecular Biology of the Cell*; 5th ed.; Garland Science: New York, 2007.

(2) *Supramolecular Chemistry: From Molecules to Nanomaterials*; John Wiley & Sons Ltd: Chichester, UK, 2012; Vol. 5.

(3) Safont-Sempere, M. M.; Fernandez, G.; Wurthner, F. *Chem. Rev.* **2011**, *111*, 5784.

(4) Rest, C.; Mayoral, M. J.; Fernandez, G. *Int. J. Mol. Sci.* **2013**, *14*, 1541.

(5) Asakawa, T.; Ishino, S.; Hansson, P.; Almgren, M.; Ohta, A.; Miyagishi, S. *Langmuir* **2004**, *20*, 6998.

(6) Dong, S. L.; Xu, G. Y.; Hoffmann, H. *J. Phys. Chem. B* **2008**, *112*, 9371.

(7) Wu, A. X.; Isaacs, L. *J. Am. Chem. Soc.* **2003**, *125*, 4831.

(8) Mukhopadhyay, P.; Zavalij, P. Y.; Isaacs, L. *J. Am. Chem. Soc.* **2006**, *128*, 14093.

(9) Pal, A.; Karthikeyan, S.; Sijbesma, R. P. *J. Am. Chem. Soc.* **2010**, *132*, 7842.

(10) Choi, H. J.; Montemagno, C. D. *Nano Lett.* **2005**, *5*, 2538.

(11) Peters, R.; Louzao, I.; van Hest, J. C. M. *Chem. Sci.* **2012**, *3*, 335.

(12) Stadler, B.; Price, A. D.; Chandrawati, R.; Hosta-Rigau, L.; Zelikin, A. N.; Caruso, F. *Nanoscale* **2009**, *1*, 68.

(13) Richardson, J. J.; Ejima, H.; Lorcher, S. L.; Liang, K.; Senn, P.; Cui, J. W.; Caruso, F. *Angew. Chem. Int. Ed.* **2013**, *52*, 6455.

(14) Long, M. S.; Jones, C. D.; Helfrich, M. R.; Mangeney-Slavin, L. K.; Keating, C. D. *Proc. Natl. Acad. Sci. U.S.A.* **2005**, *102*, 5920.

(15) Koga, S.; Williams, D. S.; Perriman, A. W.; Mann, S. *Nat. Chem.* **2011**, *3*, 720.

(16) Strulson, C. A.; Molden, R. C.; Keating, C. D.; Bevilacqua, P. C. *Nature Chem.* **2012**, *4*, 941.

(17) Mann, S. *Acc. Chem. Res.* **2012**, *45*, 2131.

(18) Mann, S. *Angew. Chem. Int. Ed.* **2013**, *52*, 155.

(19) Elemans, J.; Lei, S. B.; De Feyter, S. *Angew. Chem. Int. Ed.* **2009**, *48*, 7298.

(20) Orentas, E.; Lista, M.; Lin, N. T.; Sakai, N.; Matile, S. *Nat. Chem.* **2012**, *4*, 746.

(21) You, C. C.; Miranda, O. R.; Gider, B.; Ghosh, P. S.; Kim, I. B.; Erdogan, B.; Krovi, S. A.; Bunz, U. H. F.; Rotello, V. M. *Nat. Nano.* **2007**, *2*, 318.

(22) De, M.; Rana, S.; Akpinar, H.; Miranda, O. R.; Arvizo, R. R.; Bunz, U. H. F.; Rotello, V. M. *Nature Chem.* **2009**, *1*, 461.

(23) Pieters, G.; Cazzolaro, A.; Bonomi, R.; Prins, L. J. *Chem. Commun.* **2012**, *48*, 1916.

(24) Bazzicalupi, C.; Bencini, A.; Lippolis, V. *Chem Soc Rev* **2010**, *39*, 3709.

(25) Pieters, G.; Pezzato, C.; Prins, L. J. *J. Am. Chem. Soc.* **2012**, *134*, 15289.

Chapter 5

Pattern-based sensing of nucleotides with functionalized gold nanoparticles[§]

In this Chapter the complexity of non-covalent interactions that govern the interactions between small molecules and Au NP 1·Zn^{2+} is exploited for developing a multi-indicator displacement assay. A sensing system is obtained by self-assembling multiple fluorescent indicators with different binding affinity for Au NP 1·Zn^{2+}. The system is able to generate a characteristic output signal for each of the eight nucleotides XDP and XTP (X = A, T, G, C) that is also concentration dependent.

[§] Part of this Chapter has been published in: C. Pezzato, B. Lee, K. Severin, L. J. Prins *Chem. Commun.* **2013**, *49*, 469-471.

5.1 Introduction

Monolayer protected gold clusters (Au NPs) have emerged as key components of innovative bioassays.[1,2] The utility of Au NPs originates from a combination of several attractive features related to their preparation and intrinsic optoelectronic properties.[3] Au NPs are stable self-assembled multivalent systems obtained through reproducible synthetic protocols and can be functionalized with a large variety of ligands involved in (bio)recognition. The optoelectronic properties of the gold nucleus, such as plasmon resonance absorption, conductivity, or redox behavior, can be used for signal generation as these are typically sensitive to recognition processes occurring at the monolayer surface. A key role is played by the surface functionalities of the monolayer which confer selectivity to the sensing system. This point was illustrated in an impressive manner by Rotello and co-workers who developed nanoparticle-based systems for protein sensing relying on a pattern-based analysis.[4-6] Among others, a sensor array ('nose') was used consisting of six different cationic nanoparticles in combination with an anionic PPE polymer as a fluorescent indicator. Proteins interacted differently with the six types of nanoparticles resulting in a variable amount of displaced fluorescent polymer, and thus a characteristic signal pattern.

As we have seen earlier, our nanoparticles are able to interact with small anionic molecules such as peptides and nucleotides due to their multivalent cationic nature. In particular, the binding affinity of a given oligoanion for Au NP **1**•Zn^{2+} depends on: 1) the number of negative charges of the oligoanion,[7] 2) the chemical nature of the anionic group (phosphate *vs.* carboxylate),[8] and 3) the presence of hydrophobic moieties able to penetrate into the monolayer.[9] These structural factors indicated that the role of the monolayer appeared to be more complex than just providing a positively charged surface. In fact, here we show that the apparent nonspecific surface of Au NP **1**•Zn^{2+} (because not equipped with selective ligands) is able to discriminate between structurally very closely related molecules. From an applicative point of view this is important as it simplifies the use of gold nanoparticles in sensing applications, because just one type of functionalized nanoparticle is used rather than an array. In addition, the obtained results are also

important from a more fundamental point of view as they provide new insights in molecular recognition events occurring at surfaces.

5.2 Results and discussion

5.2.1 Set up a multi-indicator displacement assay

An indicator-displacement-assay (IDA)[10] was set up to monitor the different response of Au NP **1**•Zn^{2+} to various analytes (Figure 5.1). In contrast to the work of Rotello, variety is not generated by using different nanoparticles in an array format, but by attachment of multiple fluorescent indicators to one type of Au NP. An intrinsic advantage of such a multicomponent IDA is its flexibility, because the amount and the nature of the dyes can be changed easily.[11]

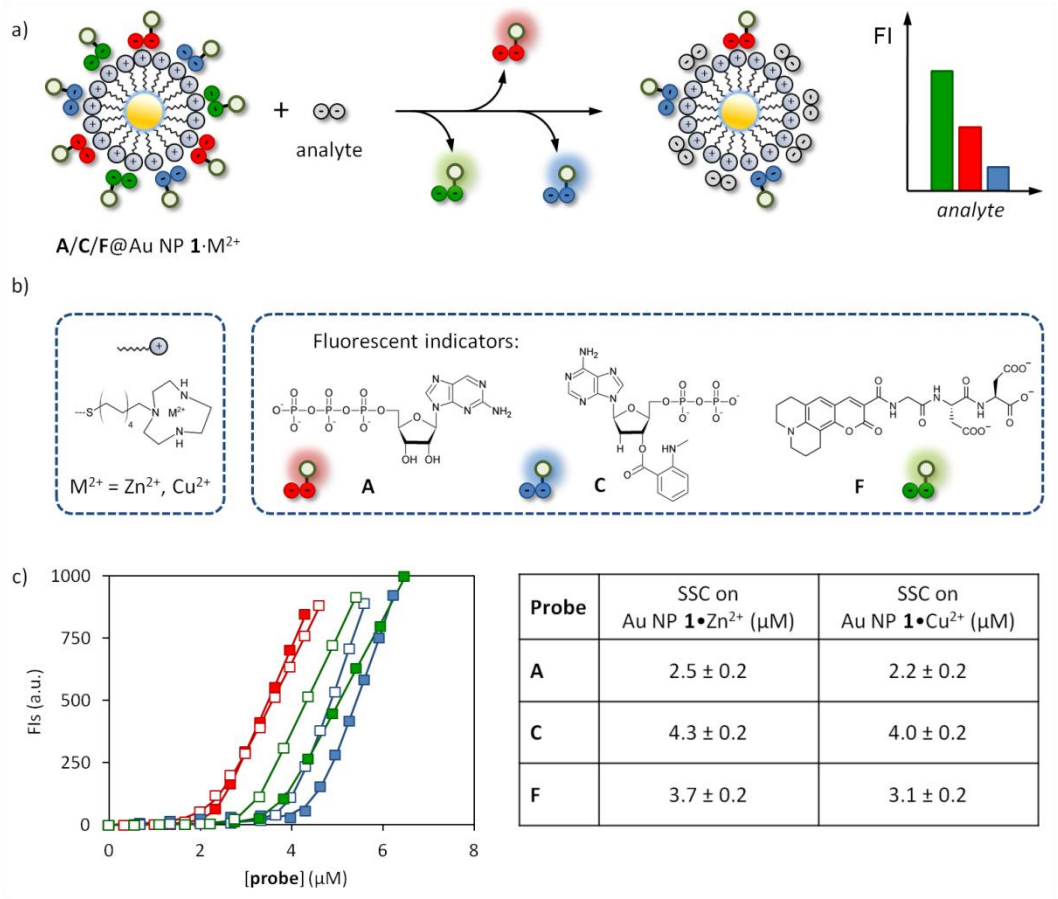

Probe	SSC on Au NP **1**•Zn^{2+} (μM)	SSC on Au NP **1**•Cu^{2+} (μM)
A	2.5 ± 0.2	2.2 ± 0.2
C	4.3 ± 0.2	4.0 ± 0.2
F	3.7 ± 0.2	3.1 ± 0.2

Figure 5.1. (a) Schematic representation of the displacement of multiple indicators from the surface of Au NP **1**•M^{2+} upon the addition of an analyte. (b) Molecular structures of the monolayer and fluorescence indicators used in this part. (c) Fluorescence intensity as a function of **A** (red, 370 nm), **C** (blue, 448 nm) or **F** (green, 493 nm) added to either Au NP **1**•Zn^{2+} (filled squares) or Au NP **1**•Zn^{2+} (empty squares). The corresponding SSCs values are reported on the right. Experimental conditions: [Au NP **1**•Zn^{2+}] = [Au NP **1**•Cu^{2+}] = 10 μM, [HEPES] = 10 mM, pH = 7.0, 25 °C.

In order to generate a specific response pattern, anionic fluorescent indicator probes were selected based on the following criteria: (1) the ability to bind Au NP **1**•Zn^{2+} under saturation conditions at low micromolar concentrations in aqueous buffer, but (2) with different relative binding affinities for Au NP **1**•Zn^{2+} in order to install a dynamic range as large as possible, and (3) different excitation and emission wavelengths. The fluorescent probes **A** (λ_{ex} = 305 nm, λ_{em} = 370 nm), **C** (λ_{ex} = 355 nm, λ_{em} = 450 nm), and **F** (λ_{ex} = 445 nm, λ_{em} = 493 nm) met these criteria. Probe **A** has a high affinity for Au NP **1**•Zn^{2+}, while the N-methylamino anthranilic ester (MANT) moiety in **C** penetrates into the monolayer thus adding a significant hydrophobic component to binding. Probe **F** is a tri-peptide with three carboxylates and it would enlarge the dynamic range to include analytes with a lower affinity. Fluorescence titrations confirmed the high affinity of all probes for Au NP **1**•Zn^{2+} and were used to determine the SSC for each of them (Figure 5.1c). Subsequently, a multi-indicator surface was generated by loading the different probes contemporarily onto the surface of Au NP **1**•Zn^{2+} at an individual concentration equal to (0.7×SSC)/3. In the absence of any competitor, the fluorescence intensities of either probe were less than 3% of the respective maximum fluorescence intensities (Figure 5.2a). This efficient fluorescence quenching indicates that all probes were quantitatively bound to the surface.

5.2.2 Responsiveness of the multi-indicator surface

The 8 nucleotides XDP and XTP (N = A, T, G, C) were chosen as targets, because the subtle chemical differences between these analytes make detection and differentiation challenging.[12,13-16] Consequently, these analytes comprise an excellent test case for the assessment of the differentiation potential of Au NP **1**•Zn^{2+}. The response of the multi-indicator surface to the presence of analytes was initially verified by adding increasing amounts of ATP and ADP to a buffered aqueous solution (HEPES, pH = 7.0) of the dye-loaded Au NP **1**•Zn^{2+} while measuring the fluorescence emission from the three indicators as a function of time. It was found that attainment of the thermodynamic equilibrium required around 30 minutes, after which stable fluorescence signals were observed (see for example

the time course of the three fluorescence intensities upon the addition of ADP, Figure 5.2b).

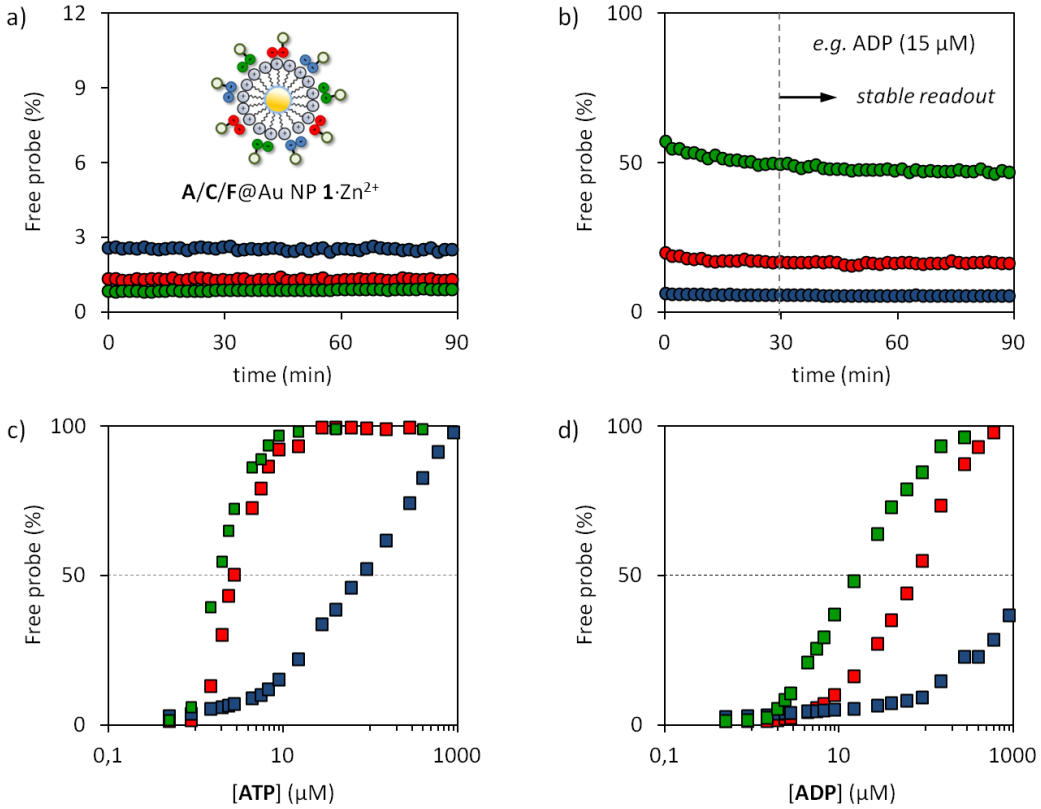

Figure 5.2. (a) Time course of the fluorescence emission at 370 nm (red), 448 nm (blue) and 493 nm (green) as a function of time emerging from the dye-loaded Au NP **1**•Zn^{2+}. (b) Time course of the three fluorescence upon the addition of ADP (15 µM). An equilibration time of around 30 min is required to obtain a stable readout. (c-d) Relative displacement of **A** (red), **C** (blue) and **C** (green) from the surface of Au NP **1**•Zn^{2+} as a function of analytes ATP (c) or ADP (d). Experimental conditions: [indicators] = 0.7 × SSC/3, [TACN•Zn^{2+}] = 10 ± 1 µM, [HEPES] = 10 mM, pH = 7.0, 25 °C.

Inspection of the whole displacement curves immediately reveals the different response of the system towards the addition of ATP and ADP. As expected based on the number of negative charges, much larger amounts of ADP are required to obtain the same level of indicator displacement compared to ATP (Figure 5.2c vs. 5.2d). The displacement curves induced by ADP confirm the anticipated relative binding affinities of the three probes for Au NP **1**•Zn^{2+} (Figure 5.2c). The indicator **F** has the lowest affinity because of the presence of just three negative charges present in the form of carboxylates. The affinity of **C** is higher compared to that of **A** confirming that the reduction from four to three negative charges is more than

compensated for by the presence of the hydrophobic MANT moiety. The displacement curves also confirm that the indicators cover a significant range of affinity. The fluorescence intensity of samples with dye **C** changes gradually over a wide concentration range of ATP, contrary to what is observed for the indicators **A** and **F**, which are nearly completely displaced upon the addition of 20 µM of the analyte. On the other hand, indicator **C** is much less useful for the detection of ADP, because even high concentrations of ADP cause just a minor displacement of **C**. For this analyte, however, the indicators **A** and **F** are suitable for signal generation.

Having confirmed the conceptual validity of the sensing system, we next turned to a full analysis of all nucleotide di- and tri-phosphates XDP and XTP (X = A, T, G, C) at three different concentrations (5, 50 and 100 µM). All measurements were performed in 96 microwell plates with six repetitions for each sample. The fluorescence intensities of each of the three indicators were recorded using the respective excitation/emission wavelengths by performing multiple measurements as a function of time.

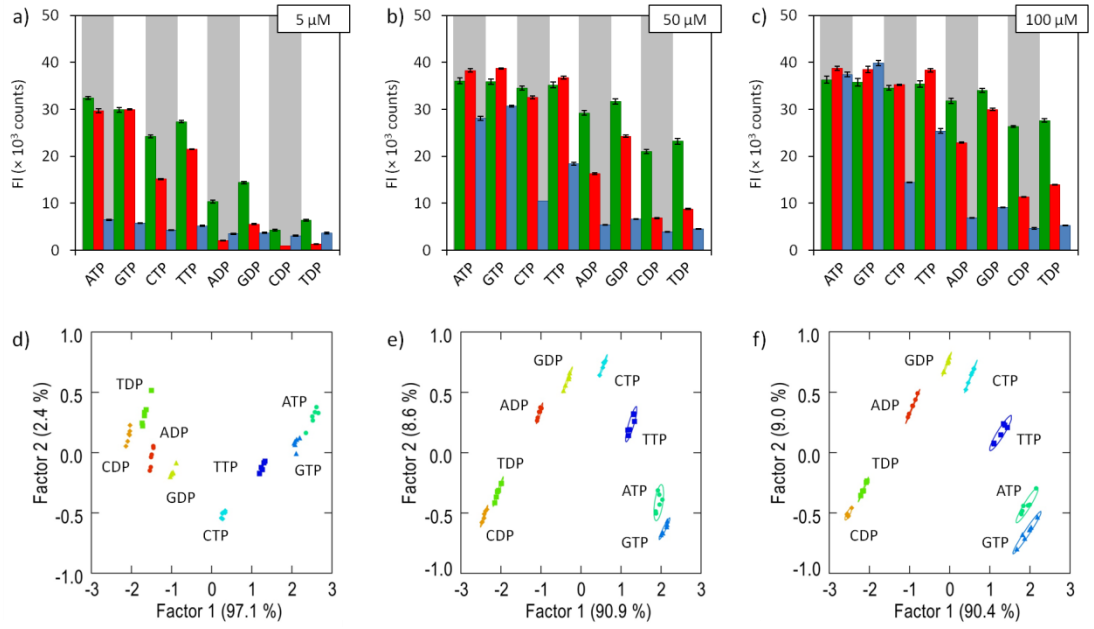

Figure 5.3. Response patterns at (a) 5, (b) 50 and (c) 100 µM analyte concentration (each barrel represent the average of six independent repetitions) and corresponding PCA score plots (from d to f, respectively). The data were obtained by displacement assays using Au NP **1**•Zn^{2+} and the indicators **A** (red), **C** (blue) and **F** (green).

As before, after an equilibration time of 30 minutes a stable fluorescence readout was observed. The fluorescence intensity of each indicator was then plotted for each analyte at each concentration. At a given concentration, each of the eight analytes generates a different response pattern, demonstrating the capacity of the system to detect small structural differences (Figure 5.3a-c). Principal component analyses (PCA)[17] of the three data sets allow visualizing the clustering of the data. Well separated data groups are observed at all three concentrations (Figure 5.3d-f). The first principal component ('Factor 1') correlates with the binding affinity of the analyte for Au NP **1**•Zn^{2+}: the highest scores are found for the strongly bound ATP and GTP, whereas the lowest scores are observed for CDP and TDP. Interesting differences are observed between the pyrimidine- and purine-based nucleotide couples (C/T vs. A/G). The purine-based nucleotides typically induce a stronger displacement of the indicators, which implies a hydrophobic interaction between the aromatic moiety and the monolayer, similar to that observed previously for the MANT-containing indicator **C**.

5.2.3 Toward a full discrimination of the all nucleotides

The performance of the sensing system can be further improved by using Cu^{2+} in addition to Zn^{2+}. As shown in the first chapter the metal ion in the monolayer can be used to regulate the release rate of small molecules from the monolayer.[18] In a similar manner, it changes the interaction of both the indicators and the analytes with the monolayer, and, consequently, the output signal. We have repeated the displacement assay in an identical manner using Cu^{2+} instead of Zn^{2+}. Compared to Au NP **1**•Zn^{2+}, the slightly lower surface capacity in the presence of Cu^{2+} (Figure 5.1c) causes a generally lower intensity of the output signal. Nonetheless, the addition of different concentrations of nucleotides still gave distinct response patterns (Figure 5.4a-c). The number of principal components in a PCA analysis can be less than or equal to the number of variables used. Importantly, by taking into account the third principal component in a PCA analysis performed on the combined Zn^{2+} and Cu^{2+} data sets, it is possible to differentiate all analytes at concentrations of 50 and 100 μM (Figure 5.4d-e).

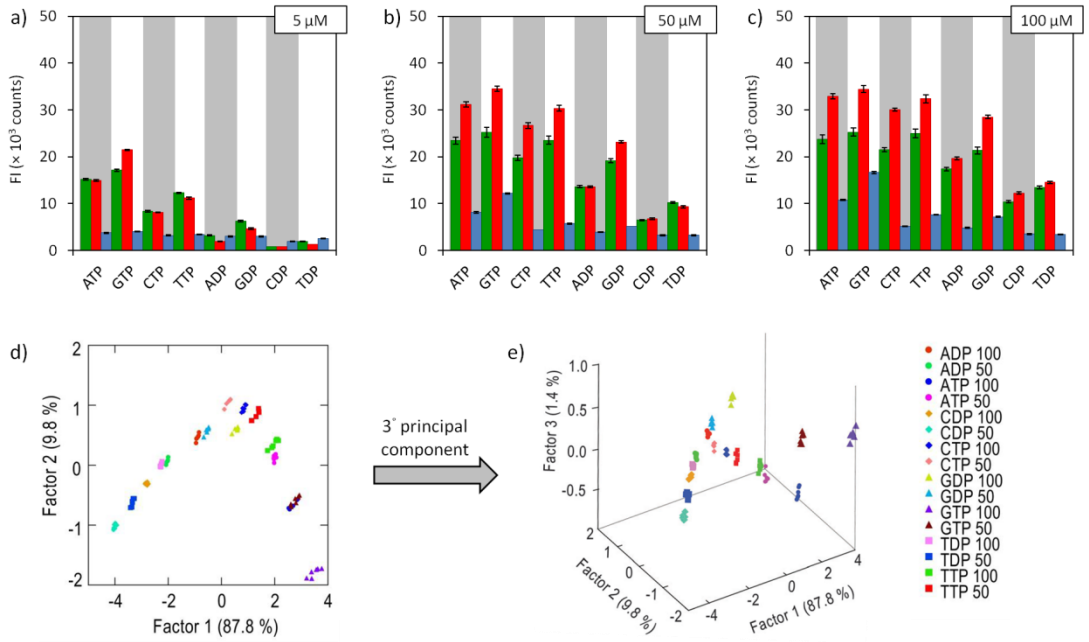

Figure 5.4. Response patterns at (a) 5, (b) 50 and (c) 100 µM analyte concentration (each barrel represent the average of six independent repetitions) and corresponding PCA score plots (from d to f, respectively). The data were obtained by displacement assays using Au NP **1**•Cu^{2+} and the indicators **A** (red), **C** (blue) and **F** (green). (d) PCA score plot for the analysis of eight nucleotides at two different concentration (50 and 100 µM) resulting from the combined Zn^{2+} and Cu^{2+} data sets: note that GTP50 and ATP100 are overlapped. (e) 3D-PCA score plot obtained from the same data sets used in (d). The third principal component is essential for discriminating all the analytes.

The discriminatory power of the system was substantiated by a linear discriminant analysis (LDA)[17] and a jack-knife validation procedure. Here, 20% of the data was randomly omitted, and the remaining data were used as a training set for the LDA. The omitted observations were then classified resulting in a correct classification in all cases (100%).

5.3 Conclusions

In conclusion, we have developed a gold nanoparticle-based sensing system that is able to discriminate eight nucleotides in a straightforward manner. An attractive feature of the system is that its preparation relies on self-assembly: the sensing ensemble is obtained by simply mixing multiple fluorescent indicators with a single type of Au NP. The resulting fluorescent sensor is able to generate an output signal which is dependent on the chemical nature of the analyte and its concentration. The system is highly modular and the output signal can be easily altered by

changing the fluorogenic indicators or the metal ion present in the monolayer. The ability of a rather nonspecific monolayer to discriminate chemically very similar analytes is a sign of the variety of noncovalent interactions that take place on the monolayer surface.

5.4 Experimental section

5.4.1 Instrumentation

UV-Vis and Fluorescence spectroscopy

UV-Vis measurements were recorded on a Varian Cary50 spectrophotometer, while Fluorescence measurements were recorded on a Varian Cary Eclipse Fluorescence spectrophotometer (SSCs) and on a on a TECAN M1000 PRO micro-plate reader using Greiner Bio-one microtiter plates (polystyrene 96-WELL*F) (assays).

5.4.2 Materials

For Au NP **1**, $Zn(NO_3)_2$, $Cu(NO_3)_2$, probe **A**, **C**, **F** and HEPES see previous chapters. The analytes (ATP, ADP, GTP, GDP, CTP, CDP, TTP, TDP) were purchased from Sigma Aldrich and used as received.

5.4.3 Determination of the stock solution concentrations

The concentration of **A**, **C** and **F** in the stock solution were determined by UV spectroscopy as described in the experimental part of chapter 2, 3 and 4, respectively. Similarly, all concentrations of the analytes in the stock solution were determined (at pH 7.0) using the following molar extinction coefficients: $\varepsilon_{259\ (ATP,\ ADP)} = 15400\ M^{-1}cm^{-1}$, $\varepsilon_{253\ (GTP,\ GDP)} = 13700\ M^{-1}cm^{-1}$, $\varepsilon_{272\ (CTP,\ CDP)} = 9100\ M^{-1}cm^{-1}$ and $\varepsilon_{268\ (TTP,\ TDP)} = 9600\ M^{-1}cm^{-1}$.

5.3.4 Determination of the Surface Saturation Concentration (SSC)

Fluorescence titrations were carried out by adding consecutive amount of a stock solution of probe **A**, **C** or **F** to a 3-mL aqueous solution ([HEPES] = 10 mM, pH = 7.0) containing Au NP **1**•M^{2+} (10 μM, M^{2+} = Zn^{2+}, Cu^{2+}). The additions were followed kinetically, in order to ensure the equilibration of the fluorophore molecules on the nanoparticles surface.

5.4.5 Indicator displacement assays

In order to load different probes contemporary on the surface of Au NP **1**•M^{2+} (M^{2+} = Zn^{2+}, Cu^{2+}) the obtained SSC values (Figure 1) were considered. The quantity of each probe was regulated such that the composition of the heteromeric surface in the plate well is 1:1:1 (final concentration equal to 0.70xSSC/3). The displacement experiments were performed Cy adding 40 µL of a fresh aqueous solution of 1:1:1 probes-coated Au NP **1**•Zn^{2+} (or Cu^{2+}) in HEPES buffer (10 mM, pH = 7.0) to the plate-wells, each of them containing 310 µL of a solution of analyte buffered in the same manner. All volumes added were calculate in order to obtain the right concentrations in the final volume (350 µL). The evolution of the three fluorescence intensities was measured using the following instrumental settings:

A: λ_{ex} = 305 nm, λ_{em} = 370 nm; slit 5/5; gain = 135; z-position = 23078 µm;

C: λ_{ex} = 355 nm, λ_{em} = 448 nm; slit 10/10; gain = 121; z-position = 23392 µm;

F: λ_{ex} = 450 nm, λ_{em} = 493 nm; slit 5/5; gain = 80; z-position = 23392 µm;

Shaking: double orbital for 40 s;[19]

Mode: top fluorescence reading;

Number of flashes = 50;

Integration time = 20 µs;

Lag time = 0 µs;

Settle time = 75 ms.

5.5 References

(1) Giljohann, D. A.; Seferos, D. S.; Daniel, W. L.; Massich, M. D.; Patel, P. C.; Mirkin, C. A. *Angew Chem Int Ed Engl* **2010**, *49*, 3280.

(2) Saha, K.; Agasti, S. S.; Kim, C.; Li, X.; Rotello, V. M. *Chem Rev* **2012**, *112*, 2739.

(3) Daniel, M. C.; Astruc, D. *Chem Rev* **2004**, *104*, 293.

(4) You, C. C.; Miranda, O. R.; Gider, B.; Ghosh, P. S.; Kim, I. B.; Erdogan, B.; Krovi, S. A.; Bunz, U. H.; Rotello, V. M. *Nat Nanotechnol* **2007**, *2*, 318.

(5) De, M.; Rana, S.; Akpinar, H.; Miranda, O. R.; Arvizo, R. R.; Bunz, U. H.; Rotello, V. M. *Nat Chem* **2009**, *1*, 461.

(6) Bunz, U. H.; Rotello, V. M. *Angew Chem Int Ed Engl* **2010**, *49*, 3268.

(7) Bonomi, R.; Cazzolaro, A.; Sansone, A.; Scrimin, P.; Prins, L. J. *Angewandte Chemie-International Edition* **2011**, *50*, 2307.

(8) Pieters, G.; Cazzolaro, A.; Bonomi, R.; Prins, L. J. *Chem Commun (Camb)* **2012**, *48*, 1916.
(9) Pieters, G.; Pezzato, C.; Prins, L. J. *Langmuir* **2013**, *29*, 7180.
(10) Nguyen, B. T.; Anslyn, E. V. *Coord. Chem. Rev.* **2006**, *250*, 3118.
(11) Severin, K. *Curr Opin Chem Biol* **2010**, *14*, 737.
(12) Adams, M. M.; Joyce, L. A.; Anslyn, E. V. in Supramolecular Chemistry From Molecules to Nanomaterials (Techniques); ed. Steed, J. W., Gale, P. A., John Wiley & Sons, Ltd, Vol. 2, 2012.
(13) Zhou, Y.; Xu, Z.; Yoon, J. *Chem Soc Rev* **2011**, *40*, 2222.
(14) McCleskey, S. C.; Griffin, M. J.; Schneider, S. E.; McDevitt, J. T.; Anslyn, E. V. *J Am Chem Soc* **2003**, *125*, 1114.
(15) Buryak, A.; Pozdnoukhov, A.; Severin, K. *Chem Commun (Camb)* **2007**, 2366.
(16) Yao, Z.; Feng, X.; Hong, W.; Li, C.; Shi, G. *Chem Commun (Camb)* **2009**, 4696.
(17) Jurs, P. C.; Bakken, G. A.; McClelland, H. E. *Chem Rev* **2000**, *100*, 2649.
(18) Pieters, G.; Pezzato, C.; Prins, L. J. *J. Am. Chem. Soc.* **2012**, *134*, 15289.
(19) It was observed that the meniscus of all wells had the same shape

Chapter 6

Label-free detection of protein kinase activity[**]

A straightforward indicator-displacement assay (IDA) has been developed for the quantitative analysis of the conversion of ATP into ADP. The IDA relies on the use of gold nanoparticles passivated with a monolayer of thiols terminating with a 1,4,7-triazacyclononane (TACN)•Zn^{2+} head group. The analytes ATP and ADP compete to a different extent with a fluorescent probe for binding to the monolayer surface. In the presence of ATP the fluorescent probe is free in solution, whereas in the presence of ADP the fluorescent probe is captured by the nanoparticles and its fluorescence is quenched. The linear response of the fluorescence signal towards different ratios of ATP:ADP permitted the detection of protein kinase activity simply by adding aliquots of the enzyme solution to the assay solution followed by measurement of the fluorescent intensity. The assay poses no restrictions on the target kinase nor does it require labeling of the kinase substrate. The assay was tested on the protein kinases PIM-1 and Src and validated through a direct comparison with the classical radiometric assay using [γ-^{32}P]-labeled ATP.

[**] Part of this Chapter has been published in: C. Pezzato, D. Zaramella, M. Martinelli, G. Pieters, M. Pagano, L. J. Prins *Org. Biomol. Chem.* **2015**, *13*, 1198.

6.1 Introduction

Protein kinases (PKs) are a class of enzymes that play critical roles in a variety of cellular functions including cell growth, development, differentiation, membrane transport, and cell death.[1] Their function is exerted by transferring the γ-phosphate group from ATP to a serine, threonine or tyrosine residue in specific substrate proteins. These phosphorylation events modulate the activity of a vast number of proteins, including ion channels, transcription factors and phosphatases.[2] PKs act primarily as components of signalling pathways in which extra- and intracellular stimuli are transduced by the cell into a series of phosphorylation events that ultimately bring about a cellular response, such as cell growth, development, differentation, membrane transport, and cell death.[3,4] Abnormalities in signalling pathways can lead to various pathological conditions including many forms of cancer. For this reason, PKs are highly important targets for both basic research and drug development.[5] Traditionally, PK assays rely on the use of ^{32}P-labeled ATP ensuring a high sensitivity.[6] However, the application of these assays is hampered by the generated radioactive waste and the short halflife of ^{32}P-labeled ATP. Besides, the laborious protocols are not compatible with high-throughput screening. Therefore non-radioactive methods are rapidly gaining interest.[7,8] In particular, various fluorescence techniques (fluorescence intensity endpoint measurement,[9] fluorescence resonance energy transfer (FRET),[10] fluorescence polarization (FP),[11] and fluorescence lifetime imaging (FLIM)[12] have emerged as alternatives. Nonetheless, for a large part these techniques rely on elaborate constructs involving fluorophores conjugated to enzymes or antibodies. Consequently, there is a strong drive to develop new kinase assays using simple and stable components.[13-17]

In the previous chapters, we have studied the interaction between small anionic molecules, such as nucleotides and peptides, and Au NP **1**•Zn^{2+}. It was found that such molecules bind to the monolayer surface under saturation conditions even at low micromolar concentrations in aqueous buffer. Detailed studies revealed that the interactions originate from a combination of electrostatic and hydrophobic interactions and coordination bonds, whose relative contribution depends on the structure of the molecules. In particular, we have seen how subtle changes in

binding affinity permitted a full discrimination of the eight di- and trinucleotides (*X*DP and *X*TP, with *X* = A, T, G, C) by Au NP **1**•Zn^{2+}.[18] Fluorescence output signals were generated by the displacement of fluorescent probe molecules from the surface of Au NP **1**•Zn^{2+} upon the addition of analytes, *i.e.* external competitors. The observed large difference in affinity between ATP and ADP, prompted us to investigate whether a similar approach would be able to serve as a PK assay by quantitatively reporting on the conversion of ATP into ADP (Figure 6.1).

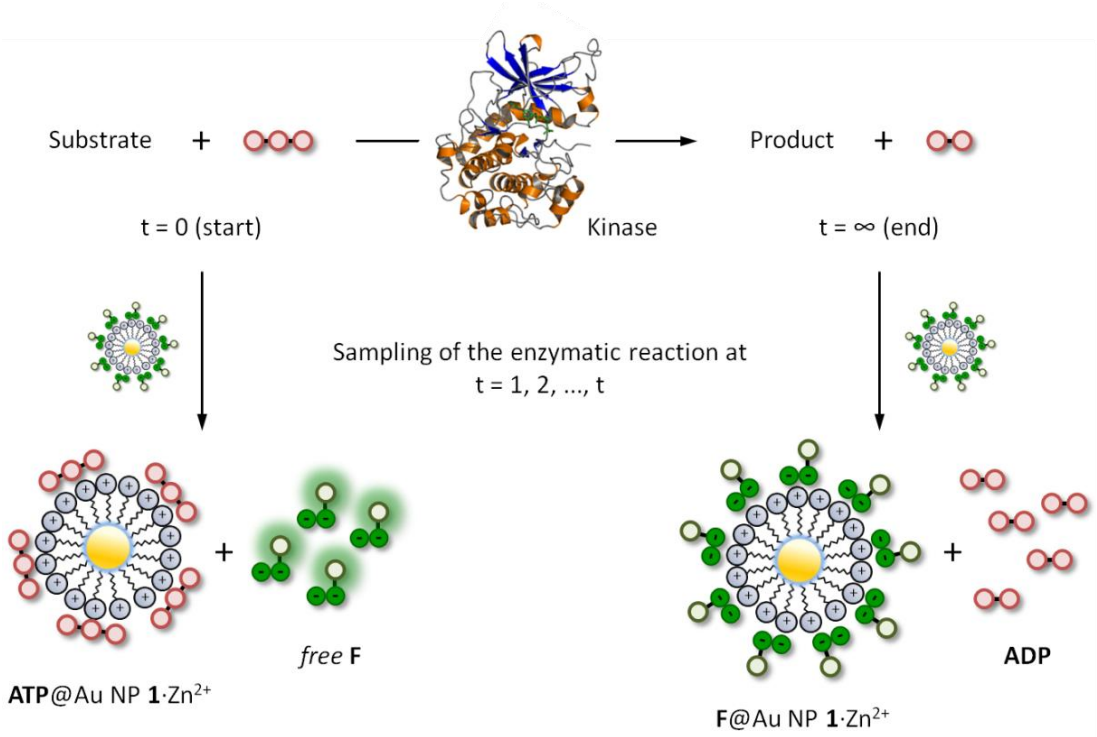

Figure 6.1. Working principle of the displacement assay. Protein kinase activity results in the transfer of a phosphate-group from ATP to the enzyme substrate yielding the product (phosphorylated substrate) and ADP. ATP and ADP have different affinities for Au NP **1**•Zn^{2+} because of their different charge. ATP is able to displace the (quenched) fluorescent probe **F** from the surface of Au NP **1**•Zn^{2+} resulting in a turn ON of fluorescence, but ADP is less competitive and does not display **F**. Sampling the reaction over time gives aliquots with different ATP:ADP ratios leading to different displacement levels of probe **F** and, thus, different fluorescence intensities.

6.2 Results and discussion

6.2.1 Set up of the indicator displacement assay

Compared to the previous sensing system, here we wanted to maximize the differences within one of the four nucleotide couples (*X*DP and *X*TP, with *X* = A) rather than obtaining a full discrimination between and within all of them. For this purpose, we decided to set up a simpler indicator-displacement assay (IDA)[19] based on Au NP **1**•Zn^{2+} and a proper fluorescent indicator. The fluorescent indicator was

selected based on the following criteria: 1) excitation and emission wavelengths far away from the (near-) UV region to avoid interference with natural chromophores/fluorophores (*e.g.* Trp- or Tyr-residues), 2) the ability to bind Au NP **1**•Zn^{2+} under saturation conditions at low micromolar concentrations in aqueous buffer, 3) the capability to respond in a very different manner to ATP and ADP in competition experiments. The fluorescent tripeptide **F**, equipped with coumarin 343, satisfied the first two points with λ_{ex} = 450 nm and λ_{em} = 493 nm and a SSC equal to 3.7 ± 0.2 µM at a head group concentration of 10 µM at pH 7.0.

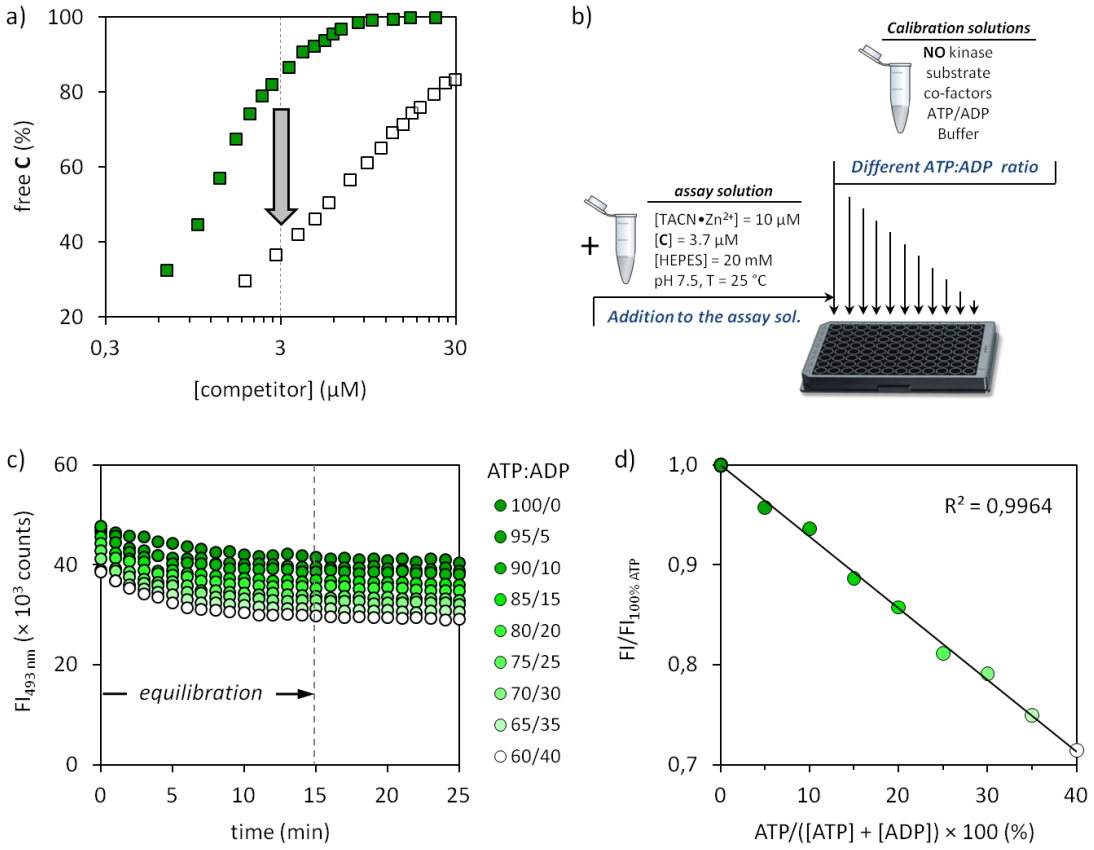

Figure 6.2. a) Displacement of **F** from the surface of Au NP **1**•Zn^{2+} upon the addition of ATP (dark green) or ADP (light green). The arrow indicates the maximum difference between the two profiles, which was found to be at 3.0 µM. b) practical set up for the calibration: aliquots of solutions containing different ATP/ADP ratio are diluted into the assay solution to reach a final concentration of [ATP]+[ADP] = 3.0 µM. c) Time course of the fluorescence intensity at 493 nm upon the addition of the different calibrating solutions; each point is the average of two independent repetitions. d) Normalized fluorescence intensity at 493 nm as a function of ATP conversion. ATP conversion was simulated by using different ratio of ATP:ADP at a constant concentration of 3.0 µM. Experimental conditions: [TACN•Zn^{2+}] = 10 µM, [**F**] = 3.7 µM, [HEPES] = 20 mM, pH = 7.5, T = 25 °C.

The third point was verified by performing two displacement experiments in which the fluorescence intensity of **F** was measured upon the addition of increasing amounts of ATP or ADP to a solution of **F**@Au NP 1•Zn^{2+} (Figure 6.2a). Initial

fluorescent intensities in these experiments started at around 9 % of the maximum signal expected for a full release of probe **F**, due to the presence of a small amount of free **F** in solution. Fully in line with previous results much larger concentrations of ADP were required to displace the same amount of **F** from Au NP **1**•Zn^{2+} resulting from the lower number of negative charges in ADP compared to ATP. The maximum difference in signal intensity was observed at an analyte concentration of 3.0 µM (see the arrow in Figure 6.2a).

6.2.2 Calibration

Having confirmed the ability of the system to discriminate in a straightforward manner between ATP and ADP, we next investigated whether the system could respond quantitatively to different ratios of ATP and ADP. As test case we chose Src, the namesake of the Src-family kinases (SFKs), a group of tyrosine kinases, physiologically involved in the early steps of signal transduction, the increased activity of which is associated with several types of cancer.[20,21] Binding of ATP to Src is characterized by a K_M value of 8.6 µM.[22] As a substrate, we used a specific peptide (renamed Src-tide, H-KVEKIGEGTYGVVYK-H, 250 µM) derived from the cyclin-dependent kinases cdc2 (residue 6 through 20) and used in vitro for testing the activity of SFKs in the presence of the cofactors Mn^{2+} and Mg^{2+} (5 mM).[23] In order to minimize possible interferences of enzyme, substrate and co-factors with the displacement assay we opted for a *discontinuous approach* in which the enzyme solution was sampled and diluted to the assay concentration for read out. Initially, we performed a calibration of the system by artificially simulating enzyme activity. Twelve independent solutions were prepared, each of them containing all the enzyme assay components except for the enzyme, but with different ratios of ATP:ADP at a constant overall concentration of 50 µM. Aliquots of these solutions were added to the IDA assay solution containing **F**@Au NP **1**•Zn^{2+} in 96 well plates to reach an overall concentration of ATP and ADP equal to 3.0 µM (Figure 6.2b). The fluorescence intensities originating from displaced **F** were measured after a signal stabilization time of 15 minutes (Figure 6.2c). Importantly, the fluorescence intensity decreased linearly as a function of the relative amount of ADP added (simulating up to 40% conversion) (Figure 6.2d). This illustrates that the ATP→ADP

conversion can be quantitatively assessed and that the enzyme assay components do not interfere with the displacement assay.

6.2.3 Validation

At this point we validated the system as a true protein kinase assay by following the Src induced conversion of ATP to ADP as a function of time. In order to demonstrate unambiguously the reliability of the new assay, enzyme activity was also measured in parallel using a conventional radiometric assay with [γ-^{32}P]-labeled ATP (Figure 6.3a). In order to assure a right comparison a common reaction medium was prepared containing all components (except for ATP) at the same concentrations used for the calibration, but this time with Src-kinase (30 µL of a stock solution with a specific activity of ≈ 2.5 pmol/min/µL). The mixture was split into two portions, to one of which a small amount of [γ-^{32}P]-ATP was added. The second portion was compensated for this addition by adding the same volume of mQ water. The resulting mixtures were incubated at 37 °C and the phosphorylation reaction was initiated by adding ATP (50 µM). Every 4 minutes samples were taken and quenched by pouring the aliquots in 0.1 % phosphoric acid (radiometric assay) or by freezing them in dry ice (displacement assay). After a time course of 35 minutes the aliquots were processed using conventional techniques (radiometric assay) or the protocol described above (IDA). Both assays gave a nearly superimposable result in terms of ATP conversion as a function of time indicating the reliability of the displacement assay (Figure 6.3b). Sampling of the enzyme solution and dilution of the aliquots in the assay buffer has the advantage that the initial experimental conditions for the enzyme (pH, buffer, substrate, cofactors, etc) hardly affect signal generation by the displacement assay. This, together with the fact that signal generation is a consequence of ATP→ADP conversion rather than substrate phosphorylation, makes it a universal assay for kinases. To demonstrate this, the protocol was repeated using PIM-1, the Proviral Integration site for Moloney murine leukemia virus kinase 1, a PK that is overexpressed in a number of tumors with a role in the resistance to apoptosis.[24] PIM-1 binds ATP with a lower affinity compared to Src (KM = 90 µM *vs* 8.6 µM).[25]

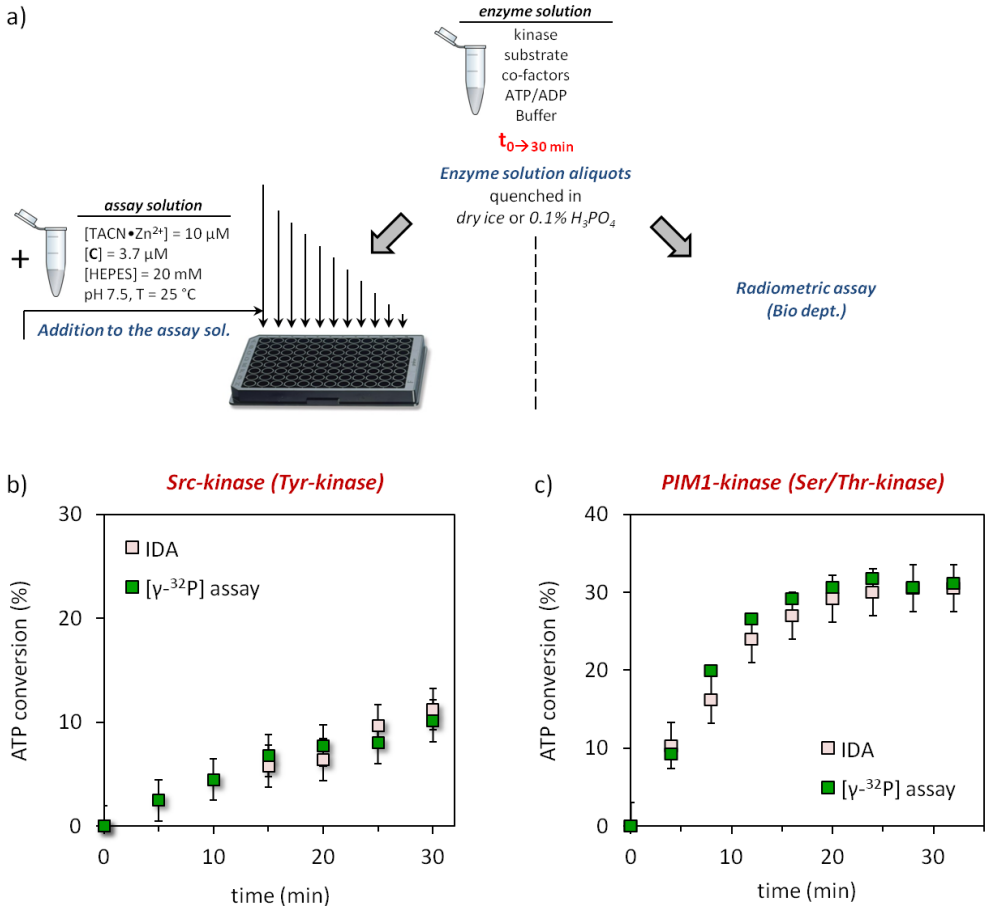

Figure 6.3. a) Practical set up of the IDA: aliquots from the enzyme solution taken at regular time intervals are diluted into the assay solution to reach a final concentration of [ATP]+[ADP] = 3.0 µM. b) Comparison of the results of the IDA and radiometric assay for Src-kinase. Experimental conditions for enzyme solution: Src-kinase (30 µL of a stock solution with a specific activity of ≈ 2.5 pmol/min/µL), [Src-tide] = 250 µM, [Mg^{2+}] = 5 mM, [Mn^{2+}] = 5 mM, [ATP] = 50 µM, [HEPES] = 20 mM, pH = 7.5, 37 °C. c) Comparison of the results of the IDA and radiometric assay for PIM1-kinase. Experimental conditions for enzyme solution: PIM1-kinase (50 uL of a stock solution with a specific activity of ≈ 10 pmol/min/µL), [PIM -tide] = 100 µM, [Mg^{2+}] = 10 mM, [ATP] = 100 µM, [HEPES] = 20 mM, pH = 7.5, 37 °C.

In contrast to Src, which requires one or more acidic amino acids in the vicinity of the phosphorylation site, PIM-1 targets serine or threonine residues surrounded by basic amino acids. The substrate used in the PIM-1 assay was synthesized according to Bullock *et al.* who had designed a highly specific substrate for PIM-1 (renamed Pim-tide = H-ARKRRRHPSGPPTA-NH2, 100 µM) using a positional scanning peptide library approach.[26] Also for this enzyme, both the radiometric assay and the displacement assay gave virtually identical results (Figure 6.3c). For this enzyme, the decrease in the rate of ATP consumption as a function of time observed in either assay is ascribed to enzyme degradation under the experimental conditions. With regard to the kinase detection limits, a 5% conversion of ATP in the enzyme solution

is required in order to create a change in fluorescence signal that can be accurately detected (see the calibration curve in Figure 6.2d). For the Src- and PIM1-kinase assays discussed here this implies a minimal ATP consumption of 2.5 and 5 μM, respectively, in the enzyme solution. In terms of enzyme activity these concentration changes imply a lower detection limit in the order of 0.1 pmole/min/μL (assuming a 30 minutes assay time).

6.3 Conclusions

A straightforward assay for the detection of kinase activity has been developed. The assay does not rely on antibodies, but instead, is based on easily accessible synthetic components. The assay is discontinuous: aliquots are taken from enzyme solutions and sampled on the ratio ATP:ADP by means of a fluorescence displacement assay. The assay was quantitatively validated by a comparison with the conventional radiometric assay based on [γ-^{32}P]-labeled ATP. It is noted that the assay-solution (composed of Au NP **1**•Zn^{2+} and **F**) gave the same response even after storage of 2 weeks at 4 °C. The fact that the assay relies on the detection of ATP→ADP makes it suitable for the detection of any kinase activity. We have shown that the new assay is fast, straightforward to use and gives reliable quantitative data. The ability to perform the assay in conventional microtiter plates allows for high-throughput screening. Indeed, our results point to a use of this assay in pharmaceutical studies aimed at discovering kinase inhibitors. Considering that the assay relies on the detection of ATP→ADP conversion and that signal generation results from a competition between negatively charged ATP/ADP with probe **F** for binding to Au NP **1**•Zn^{2+}, the application of the assay in its current form is less useful for in vivo measurements of kinase activity.

6.4 Experimental section

6.4.1 Instrumentation

UV-Vis and Fluorescence spectroscopy

UV-Vis measurements were recorded on a Varian Cary50 spectrophotometer, while Fluorescence measurements were recorded on a Varian Cary Eclipse Fluorescence

spectrophotometer (displacement experiment) and on a on a TECAN M1000 PRO micro-plate reader using Greiner Bio-one microtiter plates (polystyrene 96-WELL*F) (calibration and validation).

6.4.2 Materials

For Au NP **1**, probe **F**, ATP, ADP and buffers see previous chapters. The tyrosine kinase Src was a kind gift from Prof. A. M. Brunati at the University of Padova while PIM-1 was purchased from Sigma-Aldrich. The enzyme substrates Src-tide (H-KVEKIGEGTYGVVYK-H) and PIM-tide (HARKRRRHPSGPPTA-NH2) were synthesized by conventional Fmoc-based SPPS using a Zinsser Sophas automated peptide synthesizer.[27]

6.4.3 Preparation of the assay solution

The assay solution (50 mL) was prepared by adding the following volumes to a volumetric flask: 2 mL of HEPES buffer (pH 7.5, stock: 0.5 M, final concentration: 20 mM), 108 µL of Au NP **1**•Zn^{2+} (stock: 4.62 mM, final concentration: 10 µM – referring to [TACN•Zn^{2+}]), 0.5 mL of $Zn(NO_3)_2$ (stock: 1 mM, final concentration: 10 µM), 68.5 µL of **F** (final concentration: 3.7 µM). The solution was stored at 4 °C and could be used for at least 2 weeks without observing alteration of the signal.

6.4.4 Displacement studies

Displacement experiments were performed by adding consecutive amounts of a stock-solution of competitor ([ATP] = 1.0 mM, or [ADP] = 5.6 mM) in mQ water to 3 mL of assay solution. Each addition was followed kinetically, monitoring the emission of probe **A** at 493 nm.

6.4.5 Src-kinase assay

Calibration curve

Samples containing ATP and ADP in ratios varying from 1:0 to 0.6:0.4 were prepared at a constant concentration of 50 µM in HEPES buffer (pH = 7.5, 20 mM). Separate microtiter plate wells were loaded with 329 µL of assay solution and 21 µL of the calibration solution. Measurements were performed kinetically, monitoring the

emission of probe **A** at 493 nm for 30 min. All the signal became stable after at least 15 min. Repeating the calibration with samples containing ATP, ADP and, additionally, $MgCl_2$ (5 mM), $MnCl_2$ (5 mM), Src-tide (0.25 mM) and HEPES (pH = 7.5, 20 mM) gave identical results, indicating that all the components do not compromise the IDA efficiency.

Assay

The enzyme solution was prepared at 0 °C by mixing in the following order: mQ water (155 µL), $MgCl_2$ (300 mM, 5 µL), $MnCl_2$ (300 mM, 5 µL), HEPES (pH 7.5, 500 mM, 12 µL), Src-tide (967 µM, 78 µL) and Src (30 µL of a stock solution with a specific activity of ≈ 2.5 pmol/min/µL). After a rapid centrifugation a final volume of 300 µL was reached upon adding ATP (15 µL, 1 mM). After a second rapid centrifugation an aliquot of 30 µL was taken as "time zero point" maintaining the enzyme solution always at 0 °C. Afterwards, the enzyme soluton was put in an incubator at 37 °C. Every 5 min, 30 µL-aliquots of the reaction mixture were taken out and immediately frozen in dry ice to block the enzyme activity. The enzyme was then assayed in the same way used for calibration, adding 21 µL to a 329 µL of assay solution ($[ATP]_{well}$ = 3.0 µM). The radiometric assay was performed using an identical reaction mixture, but in the presence of ATP [γ-^{32}P] (3% v/v). In this case, the kinase reaction was quenched pouring the aliquots (5 µL) into 0.1 % phosphoric acid (25 µL), which in turn were spotted on a 2 cm2 piece of a Whatman P81 filtermat, washed three times for 4 minutes in 75 mM H_3PO_4, air dried, put in a vial with scintillation fluid, and assayed for 32P in a beta-counter (Packard).

6.4.6 PIM1-kinase assay

Calibration curve

Samples containing ATP and ADP in ratios varying from 1:0 to 0.6:0.4 were prepared at a constant concentration of 100 µM. Additionally, each sample contained $MgCl_2$ (10 mM), PIM-tide (0.1 mM), and HEPES (pH 7.5, 20 mM). Separate microtiter plate wells were loaded with 340 µL of assay solution and 10.5 µL of the calibration solution. Measurements were performed by monitoring the emission of probe **A** at 493 nm for 30 min. Also here, signals stabilised after around 15 min.

Assay

The enzyme solution was prepared at 0 °C by mixing in the following order: mQ water (195 µL), $MgCl_2$ (300 mM, 10 µL), HEPES (pH 7.5, 500 mM, 12 µL), PIM-tide (10 mM, 3 µL) and PIM-1 (50 µL of a stock solution with a specific activity of ≈ 10 pmol/min/µL). After a rapid centrifugation a final volume of 300 µL was reached upon adding ATP (30 µL, 1 mM). After a second rapid centrifugation an aliquot of 30 µL was taken as the time zero point maintaining the enzyme solution always at 0 °C. Afterwards, the enzyme solution was put in an incubator at 37 °C. Every 5 min, 25 µL aliquots of the reaction mixture were taken out and immediately frozen in dry-ice to turn off enzyme activity. The enzyme was then assayed in the same way as used for calibration by adding 10.5 µL to a 340 µL of assay solution ($[ATP]_{well}$ = 3.0 µM). For the assay on the 384-well plate format an identical procedure was followed but using different volumes (5 µL aliquots, 4x0.8 µL additions to 23.2 µL assay solution). The radiometric assay was performed using an identical reaction mixture, but in the presence of ATP [γ-^{32}P] (3% v/v). In this case, the kinase reaction was quenched pouring the aliquots (5 µL) into 0.1 % phosphoric acid (25 µL), which in turn were spotted on a 2 cm2 piece of a Whatman P81 filtermat, washed three times for 4 minutes in 75 mM H_3PO_4, air dried, put in a vial with scintillation fluid, and assayed for 32P in a beta-counter (Packard).

6.5 References

(1) Pinna, L. A. *Acc. Chem. Res.* **2003**, *36*, 378.
(2) Manning, G.; Whyte, D. B.; Martinez, R.; Hunter, T.; Sudarsanam, S. *Science* **2002**, *298*, 1912.
(3) van der Geer, P.; Hunter, T.; Lindberg, R. A. *Ann. Rev. Cell. Biol.* **1994**, *10*, 251.
(4) Hunter, T. *Cell* **2000**, *100*, 113.
(5) Cohen, P. *Nat. Rev. Drug Disc.* **2002**, *1*, 309.
(6) Hastie, C. J.; McLauchlan, H. J.; Cohen, P. *Nat. Protoc.* **2006**, *1*, 968.
(7) Ma, H.; Deacon, S.; Horiuchi, K. *Exp. Opin. on Drug Disc.* **2008**, *3*, 607.
(8) Li, Y.; Xie, W.; Fang, G. *Anal. Bioanal. Chem.* **2008**, *390*, 2049.
(9) Kupcho, K.; Somberg, R.; Bulleit, B.; Goueli, S. A. *Anal. Biochem.* **2003**, *317*, 210.
(10) Sato, M.; Umezawa, Y. *Methods* **2004**, *32*, 451.
(11) Gaudet, E. A.; Huang, K. S.; Zhang, Y.; Huang, W.; Mark, D.; Sportsman, J. R. *J. Biomol. Screen.* **2003**, *8*, 164.
(12) Wouters, F. S.; Bastiaens, P. I. *Curr. Biol.* **1999**, *9*, 1127.

(13) Zhang, T.; Edwards, N. Y.; Bonizzoni, M.; Anslyn, E. V. *J. Am. Chem. Soc.* **2009**, *131*, 11976.
(14) Hargrove, A. E.; Nieto, S.; Zhang, T.; Sessler, J. L.; Anslyn, E. V. *Chem. Rev.* **2011**, *111*, 6603.
(15) Ghale, G.; Ramalingam, V.; Urbach, A. R.; Nau, W. M. *J. Am. Chem. Soc.* **2011**, *133*, 7528.
(16) Bai, J.; Liu, C.; Yang, T.; Wang, F.; Li, Z. *Chem. Commun. (Camb)* **2013**, *49*, 3887.
(17) Martić, S.; Kraatz, H. B. *Chem. Sci.* **2013**, *4*, 42.
(18) Pezzato, C.; Lee, B.; Severin, K.; Prins, L. J. *Chem. Commun. (Camb)* **2013**, *49*, 469.
(19) Nguyen, B. T.; Anslyn, E. V. *Coord. Chem. Rev.* **2006**, *250*, 3118.
(20) Frame, M. C. *Biochimica et Biophysica Acta - Reviews on Cancer* **2002**, *1602*, 114.
(21) Wheeler, D. L.; Iida, M.; Dunn, E. F. *Oncologist* **2009**, *14*, 667.
(22) Karni, R.; Mizrachi, S.; Reiss-Sklan, E.; Gazit, A.; Livnah, O.; Levitzki, A. *FEBS Lett* **2003**, *537*, 47.
(23) Cheng, H. C.; Nishio, H.; Hatase, O.; Ralph, S.; Wang, J. H. *J. Biol. Chem.* **1992**, *267*, 9248.
(24) Magnuson, N. S.; Wang, Z.; Ding, G.; Reeves, R. *Future Oncol.* **2010**, *6*, 1461.
(25) Pagano, M. A.; Bain, J.; Kazimierczuk, Z.; Sarno, S.; Ruzzene, M.; Di Maira, G.; Elliott, M.; Orzeszko, A.; Cozza, G.; Meggio, F.; Pinna, L. A. *Biochem. J.* **2008**, *415*, 353.
(26) Bullock, A. N.; Debreczeni, J.; Amos, A. L.; Knapp, S.; Turk, B. E. *J. Biol. Chem.* **2005**, *280*, 41675.
(27) These substrates were synthesized and characterized by Davide Zaramella.

Chapter 7

ATP/ADP differentiation through catalytic signal amplification

In order to improve the sensitivity of the ATP-assay, the catalytic activity of Au NP 1·Zn^{2+} is exploited. Au NP 1·Zn^{2+} are able to catalyze the transphosphorylation reaction of 2-hydroxypropyl 4-nitrophenyl phosphate (HPNPP) yielding the chromophore 4-nitrophenol (PNP) as colored by-product. It will be shown that this feature can be used as a tool to detect ATP → ADP conversion by means of catalytic signal amplification. To that purpose, the structure of HPNPP was tailored in order to improve both Michaelis-Menten parameters, k_{cat} *and* K_m

7.1 Introduction

In general, the development of chemical-sensing methodologies alternative to biological assays is of strong current interest, because such methods involve simpler detection protocols and they can be adapted to a wide variety of targets through straightforward structural modifications.[1-4] A common feature of a broad range of assays, including the one described in the previous chapter, is that the extent of generated signal is proportional to the amount of the substrate converted by the target enzyme. The sensitivity of such assays would be greatly increased if the conversion of a single substrate molecule led to the formation of a multitude of reported molecules through a cascade of chemical events (e.g. catalytic). In this context, examples of chemical systems able to amplify originally weak input signals have been already reported.[5-9]

Despite the usefulness of Au NP **1**•Zn^{2+} as multivalent scaffold for anionic binding, similar gold nanoparticles terminating with 1,4,7-triazacyclononane (TACN)•Zn^{2+} complexes were originally conceived as synthetic models of phosphatases.[10] Phosphatases are enzymes able to catalyze the hydrolysis of phosphodiester bonds through the cooperation of Zn^{2+} metal ions. Likewise, Au NP **3** (see Figure 7.1 for the structure) were able to catalyze the transphosphorylation reaction of 2-hydroxypropyl 4-nitrophenyl phosphate (HPNPP), an activated phosphodiester commonly used as a model of RNA, through the cooperative action of two TACN•Zn^{2+} complexes localized on the monolayer surface.[11,12] These kinds of catalytic nanosystems have been referred to as nanozymes, for the fact that the reaction rate follows Michaelis-Menten reaction kinetics. This implies that catalysis is described by a binding event (defined by the dissociation constant K_M) followed by a chemical reaction (defined by the first-order rate constant k_{cat}). In particular, Au NP **3** displays an enzyme-like saturation behaviour with k_{cat} = 6.7x10^{-3} s^{-1} and K_m = 0.31 mM at pH 7.5 in water.[13] In addition, such catalytic activity can be easily switched off by adding oligoanions due to their highly charged nature compared to HPNPP. This, together with the extremely low background rate ($k_{uncat} \approx 10^{-7}$ s^{-1}) and the fact that the reaction can be monitored visibly by measuring the absorbance of 4-nitrophenate (PNP) product at 400 nm, have made this system very intriguing for the purpose given before. In fact, all these unique features have been used to set

up a very sensitive protocol for detecting protease activity (i.e. the cleavage of peptide bonds) with a catalytic amplification of the output signal: the incubation of negatively charged oligopeptides with a protease results in the formation of small peptides fragments, whose reduced anionic nature turns on the catalytic production of PNP molecules.[14]

Having in mind the system described in the last chapter, we were intrigued by the question of whether it is possible to develop an alternative protocol for detecting kinase activity with higher sensitivity. We reasoned that a differential catalytic production of reported molecules in response to ATP and ADP could be the answer to this question. The differentiation between ATP and ADP is challenging as they differ for just one negative charge, but it can be achieved by mastering the structures involved in the sensor system. In this chapter the catalytic activity of Au NP **1**•Zn^{2+} will be extensively studied within this aim. In particular, it will be shown how by tailoring the structure of HPNPP it is possible to gain control over k_{cat} and K_m and to differentiate ATP from ADP by means of a catalytic signal amplification.

7.2 Result and discussion

7.2.1 Catalytic activity of Au NP 1

Compared to Au NPs **3**, the organic monolayer of Au NPs **1** is constituted by a different thiol, which was designed for overcoming the long and expensive synthesis of the older one (Figure 7.1a). In this case the TACN ligand and the thiol moiety are simply linked by a shorter alkyl chain, which make the new thiol accessible in few steps from commercially available components. As we have seen before, TACN•Zn^{2+} complexes are formed instantaneously by adding a solution of $Zn(NO_3)_2$ *in situ*, thus, we started to investigate the reactivity of Au NP **1**•Zn^{2+} as a function of the concentration of Zn^{2+} metal ions (Figure 7.1b).

In line with previous studies, the obtained reactivity profile confirms that: 1) the more active system is the one fully loaded with Zn^{2+} and 2) the sigmoidal behaviour reflects the cooperative action between metal centres.[11] The catalytic nature of Au NP **1**•Zn^{2+} was quantified by varying the initial concentration of HPNPP (Figure 7.1c). By plotting the observed initial rate as a function of the concentration of HPNPP a clear saturation profile was obtained, indicating that also Au NP **1**•Zn^{2+} is

able to catalyse the transphosphorylation reaction of HPNPP with an enzyme-like behaviour. From these kinetics the apparent Michaelis-Menten paramenters k_{cat} = 1.4x10^{-3} and K_m = 0.25 mM were determined at pH 7.0. Compared to Au NPs **2**, the obtained value for k_{cat} is slightly lower, while the K_m is very similar. This is ascribed to the higher rigidity of the organic monolayer associated with the shorter length of the alkyl chains. Support in favor of this hypothesis can be found in a very recent study reported by Mancin and coworkers.[15]

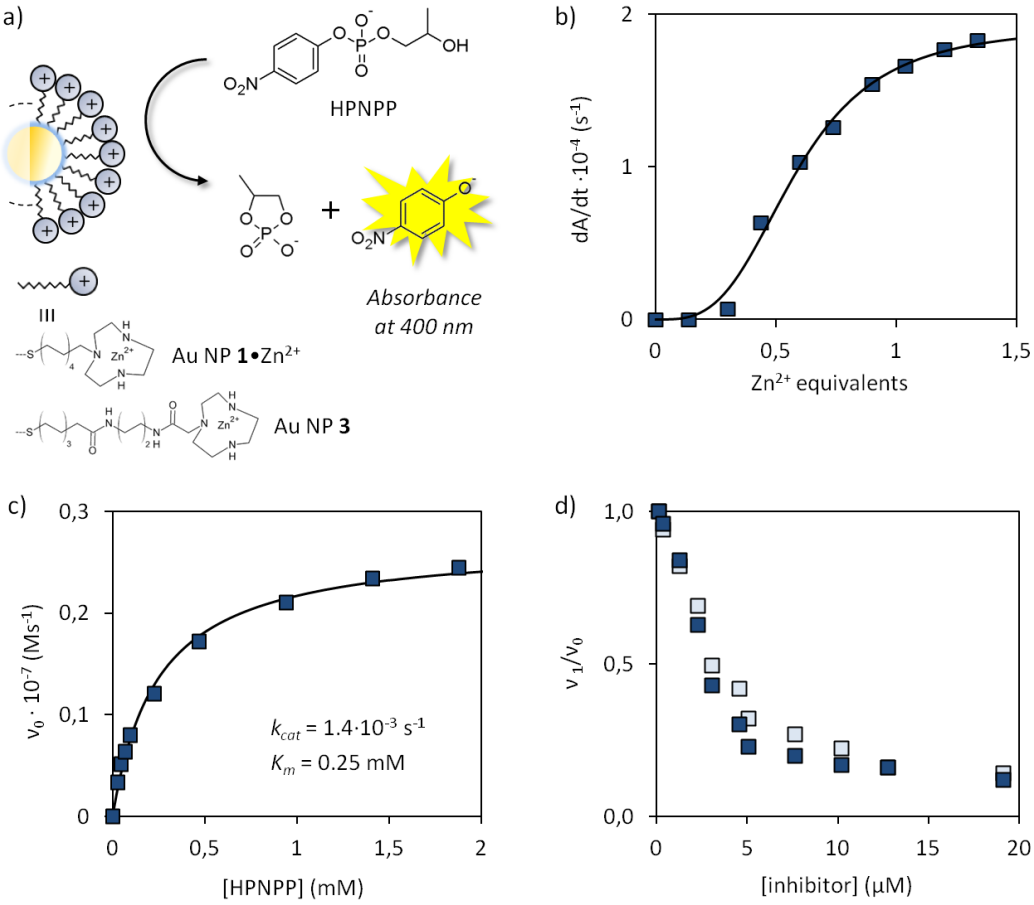

Figure 7.1. (a) Schematic representation of the transphosphorylation reaction of HPNPP promoted by either Au NP **1**•Zn^{2+} or Au NP **2**. (b) Initial rate for the cleavage of HPNPP as a function of the equivalents of Zn^{2+}. (c) Initial rate for the cleavage of HTFMP as function of the substrate concentration. (d) Inhibition curves of ATP (blue) and ADP (light blue). Experimental conditions: [TACN·Zn^{2+}] = 20 μM, [HPNPP] = 1 mM (b, d) or 0-2.0 mM (c), [HEPES] = 10 mM, pH = 7.0, 40 °C.

Having evaluated the catalytic production of PNP promoted by Au NP **1**•Zn^{2+} we turned on to study the inhibition in the presence highly charged oligoanions like ATP and ADP. Two independent inhibitions studies were performed by adding increasing amount of inhibitor (ATP or ADP) to a solution containing Au NP **1**•Zn^{2+} at

pH 7.0. HPNPP was added to give an initial concentration of 1 mM and, as before, the release rate of PNP was measured monitoring the absorbance at 400 nm. A plot of the initial rate (v_1) normalized with the respect to initial rate in the absence of inhibitor (v_0) gave the inhibition curves depicted in Figure 7.1d. Unfortunately, the obtained profiles are identical, showing that the system is not able to differentiate between structure having three (ADP) or more negative charges (ATP).

Having in mind that the binding of anionic species on the surface of Au NP **1**•Zn^{2+} is sensitive to subtle changes in the molecular structure, we reasoned that by tailoring the structure of HPNPP it would be possible to obtain different Michaelis-Menten parameters. As mentioned before, taking into account that k_{cat} refers to the rate of the reaction while K_m concerns the binding with the catalytic active sites, a substrate with a lower K_m should be, in principle, more competitive toward highly charged oligoanions as ATP and ADP. From these consideration, we have designed the molecule 2-hydroxypropyl 3-trifluoromethyl-4-nitrophenyl phosphate (HTFMP), which possesses 3-trifluoromethyl-4-nitrophenol (TFM) as leaving group (Scheme 7.1). The presence of a trifluoromethyl moiety in position 3 of the phenol ring decreases the leaving group acidity (pK_a from 7.1 to 6.1),[17] while assuring an higher hydrophobic contribution to the overall molecular structure. For these reasons, an higher k_{cat} and a lower K_m were expected for HTFMP.

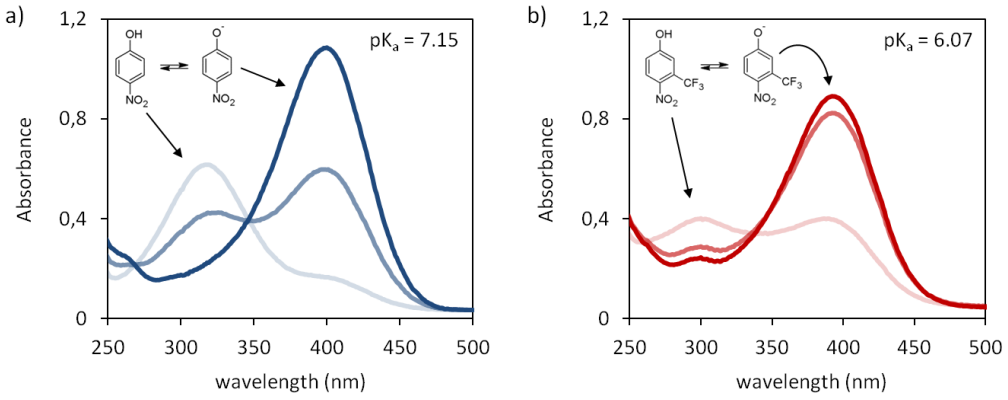

Figure 7.2. Comparison of PNP and TFM absorption spectra at different pH: due to the lower pK_a, the corresponding absorption band at longer wavelength of TFM has a higher extinction coefficient over almost the entire range of pH. (a) Absorption spectra of PNP at pH 6.0 (light blue), 7.0 (blue) and 8.0 (dark blue). (b) Absorption spectra of TFM at pH 6.0 (light red), 7.0 (red) and 8.0 (dark red). Experimental conditions: [PNP] = [TFM] = 100 µM, [HEPES] = 10 mM, pH = 7.0 and 8.0, [MES] = 10 mM pH = 6.0, 40 °C.

In addition, it is very important to notice that the pK_a of phenols determines their optical properties. In general phenols show two characteristic absorption bands in water. The band at shorter wavelength is referred to the protonated form while the band at longer wavelength is associated to the deprotonated form. At a given pH, the equilibrium is shifted toward one of two depending on the pK_a. Consequently, operating at physiological pHs (i.e. 6-8) with TFM as reporter molecule create an important advantage, which is the higher output signal (i.e. the absorption of the deprotonated band) compared to PNP (Figure 7.2)

7.2.2 Synthesis of HTFMP

HTFMP (**5a**) has been synthesized following a slightly modified literature protocol.[17] The synthesis involves few steps, starting from 3-trifluoromethyl-4-nitrophenol (**1a**) and ethyl (S)-(−)-2-(tert-butyldimethylsilyloxy)propionate (**3**) as commercially available compounds (Scheme 7.1).

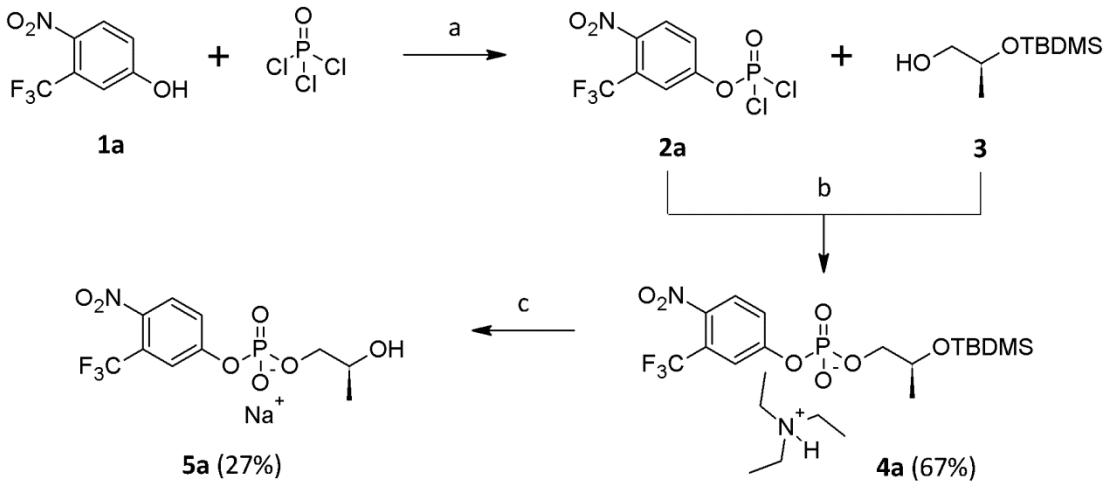

Scheme 7.1. Reagent and conditions for the synthesis of HTFMP: (a) pyridine, Tol, 95 to 110 °C, 45 min; b) TEA, 0 °C, 4 hr; TEA/H_2O, 0 °C, 30 min; c) TEA·3HF, 0°C to RT, overnight; TEA/H_2O till pH ~ 5; Sephadex-C50 (Na^+); preparative-reversed phase HPLC.

The first step (a) is a mono-phosphorylation using $POCl_3$. Both **1a** and $POCl_3$ are suspended in dry toluene and heated to 95 °C, while dry pyridine (1 eq.) is added by a syringe pump over a period of 30 min. The reaction mixture was refluxed for further 15 min, cooled to RT and filtered off to remove pyridinium chloride. **2a** is

obtained as yellow oil after evaporation and used in the next step without further purification. The second step (b) is the coupling of **2a** with the commercially available monoprotected diol **3**. A solution of **3** and TEA (1 eq.) in dry THF is added dropwise over a period of 1 h at 0 °C. The reaction is allowed to stir from 0 °C to RT for further 3 h, then TEA/H_2O is added to hydrolyze the intermediate (phospho monochloridate). THF is evaporated under reduced pressure and the product extracted into CH_2Cl_2 (3×30 mL), washed with water and brine and dried over $MgSO_4$. The product **4a** is obtained as an yellow to orange oil after column chromatography ($CHCl_3$/MeOH 95:5 with 0.5% Et_3N).

The final step (c) is the cleavage of the tert-butyldimethyl silyl protective group (TBDMS). For this purpose, the reaction goes to completeness using an excess of commercially available TEA·3HF overnight in dry THF. A mixture of TEA/H_2O is added to quench the excess of HF. Since the TBDMS-fluoride generated during the reaction is volatile, it can be removed under reduced pressure together with THF. The product (as triethylammonium salt) is then extracted into CH_2Cl_2, passed through through an ion exchange resin (Sephadex C-50 Na^+) and purified by preparative reverse-phase HPLC (gradient, t(min), %ACN]: 0, 0; 10, 33; 15, 90; 20, 100; λ=294 nm). **5a** is obtained as a white solid lyophilizing the fractions isolated at t_R = 13 min (see experimental section for more details).

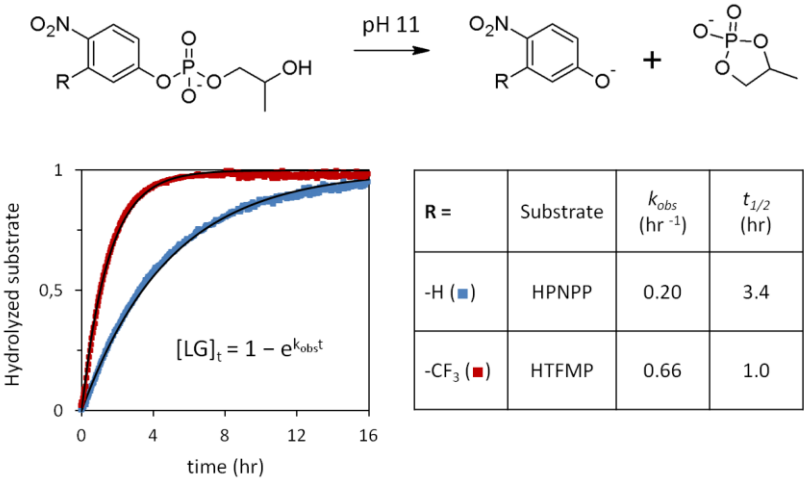

R =	Substrate	k_{obs} (hr^{-1})	$t_{1/2}$ (hr)
-H (■)	HPNPP	0.20	3.4
-CF_3 (■)	HTFMP	0.66	1.0

Figure 7.3. Hydrolysis of HTFMP (red) and HPNPP (blue) at pH 11.0. The solid lines represent fits to a first order kinetic. The corresponding values of k_{obs} and $t_{1/2}$ obtained for the two substrates are reported on the right. Experimental conditions: [TFM] = 0-100 µM, [HTFMP] = [HPNPP] = 50 µM, [CAPS] = 10 mM, pH 11.0, 40 °C.

7.2.3 Reactivity of HTFMP

The lower acidity of TFM should result in a higher reactivity of the new substrate compared to HPNPP. Preliminary proofs to test this hypothesis have been obtained by comparing the hydrolysis rates at pH 11.0 (Figure 7.3). In both cases, the reaction was followed spectrophotometrically, monitoring the absorbance of PNP or TFM at 400 and 392 nm, respectively (see figure 3). A quantitative analysis of the kinetic profiles revealed the first order constant for the hydrolysis: HTFMP hydrolyzes around 3 times faster than HPNPP ($t_{1/2}$: 1.0 *vs* 3.4 hr), confirming the expected higher reactivity.

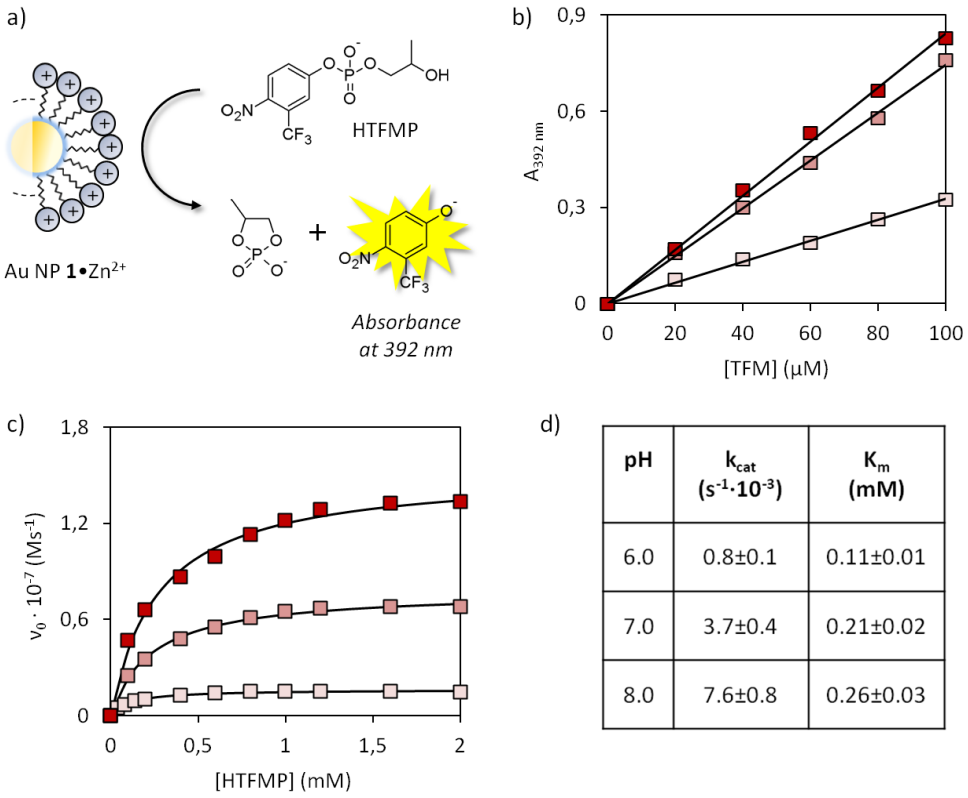

pH	k_{cat} ($s^{-1}\cdot10^{-3}$)	K_m (mM)
6.0	0.8±0.1	0.11±0.01
7.0	3.7±0.4	0.21±0.02
8.0	7.6±0.8	0.26±0.03

Figure 7.4. (a) Schematic representation of the transphosphorylation reaction of HTFMP promoted by Au NP **1**•Zn^{2+}. (b) calibration curves of TFM at pH 6.0 (light red), 7.0 (red) and 8.0 (dark red). Experimental conditions: [TFM] = 0-100 μM, [HEPES] = 10 mM, pH = 7.0 and 8.0, [MES] = 10 mM, pH 6.0, 40 °C. (c) Initial rate for the cleavage of HTFMP as function of the substrate concentration at pH 6.0 (light red), 7.0 (red) and 8.0 (dark red). (d) Michaelis-Menten parameters obtained for HTFMP. Experimental conditions: [TACN•Zn^{2+}] = 20 μM, [HTFMP] = 0-2.0 mM, [HEPES] = 10 mM, pH = 7.0 and 8.0, [MES] = 10 mM, pH 6.0, 40 °C.

Subsequently, we moved to test the catalytic activity of Au NP **1**•Zn^{2+} toward HTFMP (Figure 7.4a). Kinetic measurements were carried out at three different pHs,

monitoring the catalytic production of TFM as a function of the concentration of HTFMP (Figure 7.4c). At each pH, a calibration curve is used to convert the kinetic evolution of TFM into the corresponding initial rate (Figure 7.4b). From these experiments three sets of Michaelis-Menten parameters were obtained (Figure 7.4d): as the pH increase, both k_{cat} and K_m increases. Remarkably, all the K_m values are less than or equal to the K_m determined for HPNPP (0.25 mM at pH 7.0, see above), showing that HTFMP has a higher binding affinity compared to HPNPP over the entire range of pH. These results are important also from a purely analytical point of view as they indicate that a better competition can be associated with a faster kinetic (k_{cat}) as well as a stronger signal.

7.2.4 ATP/ADP differentiation

The new substrate HTFMP is more effective than HPNPP both in terms of rate (k_{cat}) and binding (K_m). In particular, the hypothesis was that a substrate with a lower K_m should compete with ATP from ADP more efficiently, resulting in different inhibition profiles. In order to see whether it is the case, we performed inhibitions studies by adding increasing amount of ATP or ADP to a solution containing Au NP **1**•Zn^{2+}. HTFMP was added to give an initial concentration of 1 mM and the release rate of TFM was measured monitoring the absorbance at 392 nm. A plot of the initial rate (v_1) normalized with the respect to initial rate in the absence of inhibitor (v_0) gave the corresponding inhibition curve for ATP or ADP. In order to associate the results to each pair of Michaelis-Menten parameters, the same experiment was repeated at the same three different pHs used before (Figure 7.5a-c).

In all cases, the system achieves the best differentiation at a concentration of inhibitors equal to 6.4 μM (see the yellow rectangles). In addition, the ratio of the relative initial rates (v_{ADP}/ v_{ATP}) (i.e the differentiation power) correlates very nicely with the corresponding K_m: the higher differentiation is observed at pH 6.0 (v_{ADP}/ v_{ATP} = 7.2) where the K_m has is minimum (0.11 mM), while the worse one is observed at pH 8.0 (v_{ADP}/ v_{ATP} = 2.3) where the K_m becomes closer to that of HPNPP (0.26 vs 0.25 mM).

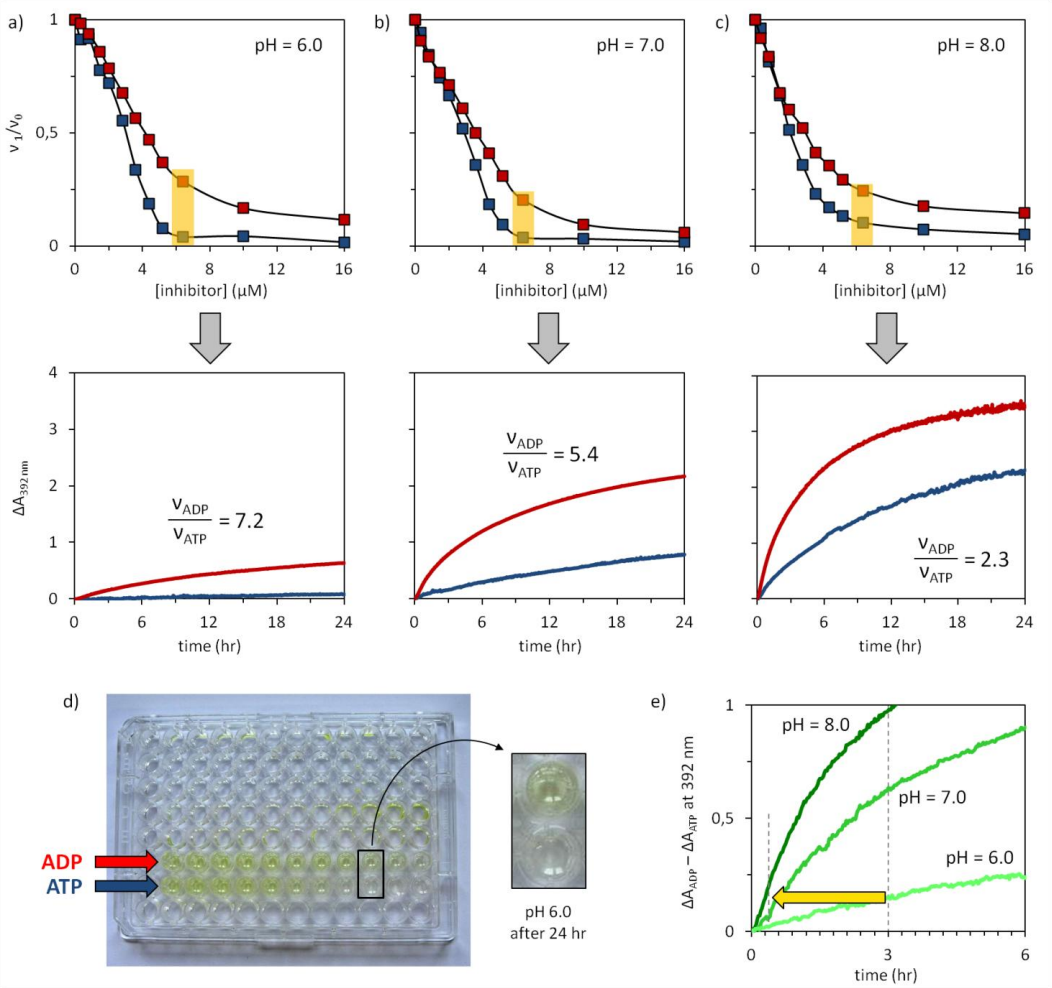

Figure 7.5. Inhibition curves of ATP (blue) and ADP (red) at pH 6.0 (a), pH 7.0 (b) and pH 8.0 (c). On the bottom: time courses of ΔA corresponding to the concentration at which the difference between ATP (blue) and ADP (red) is maximized (6.4 μM). (d) Representative inhibition experiment at pH 6.0. The zoom indicates the wells containing 6.4 μM of ADP (top) or ATP (bottom) after 24 hr at pH 6.0. (e) Signal amplification at the three different pHs in the presence of 6.4 μM of inhibitors. Experimental conditions: [TACN•Zn^{2+}] = 20 μM, [HTFMP] = 1 mM, [HEPES] = 10 mM, pH = 8.0 or 7.0, [MES] = 10 mM, pH 6.0, [ATP or ADP] = 0-16 μM, 40 °C.

Nonetheless, the combination of faster kinetics together with a stronger signal is able to compensate the worse competition at pHs above 6.0: for example, the same level of amplification obtained after 3.0 hr at pH 6.0 (ΔΔA ≈ 0.14) is reached almost 10 times faster (after ca. 20 min) at pH 8.0 (figure 7.5e). These results show clearly how a subtle change in the substrate's chemical structure can affect dramatically its behaviour, both in terms of transesterification rate and binding affinity. Importantly, ATP can now be differentiated from ADP with a catalytic signal amplification using HTFMP. Currently we are developing a new protocol for detecting kinase activity.

7.3 Experimental section

7.3.1 Instrumentation

NMR-Analysis

^{1}H, ^{13}C and ^{31}P-NMR spectra were recorded using a Bruker AV300 spectrometer operating at 75, 121 and 300 MHz for ^{13}C, ^{31}P and ^{1}H, respectively. Chemical shifts (δ) are reported in ppm using $CDCl_3$ or D_2O residual solvent values as internal reference. (REF) ^{31}P-NMR spectra were calibrated using a solution of H_3PO_4 80% as external standard. The coupling constants (*J*) are listed in Hertz (Hz), while the multiplicity of the signals are shown as follow: s: singlet, d: doublet, t: triplet, q: quartet, sp: septet, m: multiplet.

ESI-MS Analysis

ESI-MS measurements were performed on an Agilent Technologies 1100 Series LC/MSD Trap-SL spectrometer equipped with an ESI source, hexapole filter and ionic trap. All the sample solutions were prepared in neutral solvents (ACN or MeOH). In all cases the mass of the anionic species were characterized operating in the negative mode.

HPLC

HPLC purifications were performed on a preparative HPLC Shimazu LC-8A equipped with a Shimazu SPD-20A UV detector. The column used for separation was a Jupiter Proteo 4u 90A 250 x 21.20 mm, 4 µm. All the runs were carried out using a flow of 17 mL/min. Eluents: neutral H_2O (A) and ACN (B).

pH measurements and UV-Vis spectroscopy

For pH measurements see chapter 1. UV-Vis measurements were recorded on a TECAN M1000 PRO micro-plate reader using UV-Star® Greiner Bio-one microtiter plates (cycloolefine 96-WELL).

7.3.2 Materials

Reagents and solvents

For Au NP **1**, $Zn(NO_3)_2$ ATP and ADP see previous chapters. 2-(N-morpholino)ethanesulfonic acid (MES), 4-(2-hydroxyethyl)-1-piperazineethanesulfonic acid (HEPES), N-cyclohexyl-3-aminopropanesulfonic acid (CAPS) were purchased from Sigma Aldrich and used without further purification. For the syntheses, all commercially available reagents were purchased from Sigma-Aldich and used as received (table 8.1). Anhydrous solvents were used without further purification. Chromatographic columns were packed silica gel Machery-Nagel 230÷400 mesh, while TLC analyses were performed with silica gel 60-F254 plates.

Table 8.1. List of reagents and solvents used in this part

Reagent/Solvent	**Product code (Sigma Aldrich)**
Ethyl (S)-(−)-2-(tert-butyldimethylsilyloxy)propionate	424951
(S)-(+)-1,2-propanediol	540250
BH_3·THF (solution 1.0 M THF)	176192
tert-butyldimethylsilyl chloride (1.0 M CH_2Cl_2)	384429
Imidazole	I0250
Phosphorus(V) Oxychloride	201170
Triethylamine (Carlo Erba)	489556
TEA·3HF	344648
4-nitrophenyl phosphodichloridate	155403
4-nitrophenol (10 mM H_2O)	N7660
3-trifluromethyl-4-nitrophenol	N27802
4-methylumbelliferone	M1381
Toluene (dry)	89677
Pyridine (dry)	82704
Dichlorometane (dry)	66749
Tetrahydrofurane (dry)	87371
SP Sephadex C-50 Na^+	SPC50120

7.3.3 Synthesis and characterization

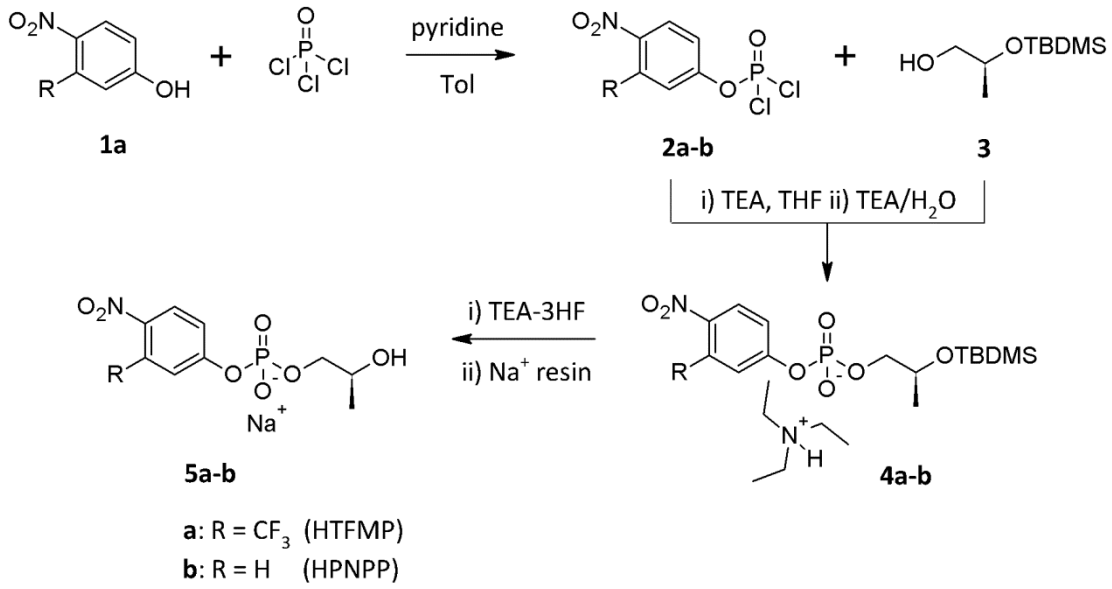

Scheme 7.2 General scheme for the synthesis of HTFM and HPNPP (sodium salts).

7.3.3.1 Synthesis of 2-[(tert-Butyldiphenylsilyl)oxy]-1-propanol (3)

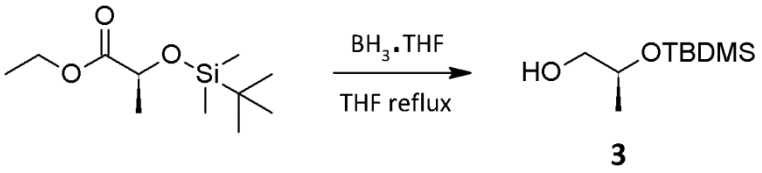

All glassware was dried several times by nitrogen-vacuum. In a three-necked flask, commercially available ethyl (S)-(-)-2-(*tert*-butyldimethylsilyloxy) propionate (5.4 mL, 20.4 mmol) was dissolved in anhydrous THF (30 mL) and cooled to 0 °C under nitrogen. A solution of BH_3·THF 1.0 M (50 mL, 50 mmol) was added dropwise over a period of 30 min. After complete addition, the resulting solution was then refluxed for 5 hours. The reaction was cooled and quenched by slow addition of water until bubbling ceased. After removal of THF by rotary evaporation the product was dissolved in Et_2O and was washed with water and brine. The ether solution was dried over $MgSO_4$, filtered, and concentrated. The desired product **3** was obtained as colorless oil after purification by column chromatography (SiO_2, Hexane/AcOEt, 8:2) yielding 3.38 g of colorless oil (87%).

^{1}H-NMR ($CDCl_3$), δ (ppm): 3.95-3.73 (m, 1H, -C*H*-), 3.50-3.25 (m, 2H, -CH_2-), 2,25 (s, 1H, -O*H*), 1.09-1.06 (d, 3H, ^{3}J = 6.2 Hz, -CH-CH_3), 0.85 (s, 9H, -C-(CH_3)$_3$), 0.04 (s, -Si-(CH_3)$_2$).

^{13}C-NMR ($CDCl_3$), δ (ppm): 77.89, 77.47, 77.04, 69.53, 68.66, 26.29, 20.29, 18.52, -2.82-, -3.82 (m), -4.15 (d, *J* = 30.8 Hz).

7.3.3.2 Synthesis of 3-trifluoromethyl-4-nitrophenyl phosphodichloridate (2a)

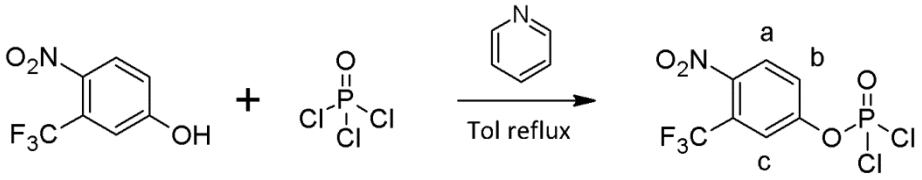

1a **2a**

All glassware was dried several times by nitrogen-vacuum cycles before the use. In a dry 3-necked flask equipped with a condenser, commercially available **1a** (1.76 g, 8.5 mmol) was suspended in anhydrous toluene (50 mL) and freshly distilled $POCl_3$ (1.82 mL, 19.6 mmol) was added. The reaction mixture was heated to 95 °C and pyridine (680 µL) was added by syringe pump over a period of 30 min. The reaction was refluxed (110 °C) for further 15 min after the complete addition and then the salts removed by filtration of the cooled reaction mixture. The obtained filtrated solution (pale yellow) was concentrated under reduced pressure and the resulting yellow oil was used in the next steps without further purification.

^{1}H-NMR ($CDCl_3$), δ (ppm): 8.05-8.02 (m, 1H, H_b), 7.76-7.71 (m, 2H, H_a, H_c).

^{31}P-NMR ($CDCl_3$), δ (ppm): 4.84 (s).

7.3.3.3 Synthesis of 2-[(tert-Butyldimethylsilyl)oxy]propyl 3-trifluoromethyl-4-nitrophenyl phosphate, TEA salt (4a)

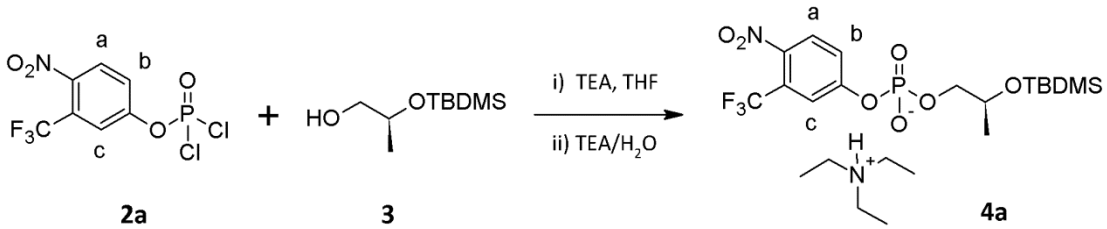

2a **3** **4a**

Phosphodichloridate **2a** (8.5 mmol) was dissolved in anhydrous THF (20 mL) under nitrogen and cooled to 0 °C. A solution of **3** (1.6 g, 8.5 mmol) and TEA (1.2 mL, 8.5 mmol) in anhydrous THF (20 mL) was added by a siringe pump over a period of 1 h. After addition was complete, the mixture (white precipitate into a peach-clored solution) was allowed to stir at R.T. for 3h. Finally, a mixture of TEA/cold water (2.5/15 mL) was added to hydrolyze the intermediate (monochloridate) and the solution was stirred for further 30 minutes. THF was evaporated and the product extracted into CH_2Cl_2 (3×30 mL), washed with H_2O and brine and dried over $MgSO_4$. The organic solvent was then removed under reduced pressure to give 4.0 g of a dark orange oil (crude). A small portion of the crude product (200 mg) was purified by column chromatography (SiO_2, $CHCl_3$/MeOH 95:5 with 0.5% TEA) to give 160 mg of yellow oil (scaled yield = 67 %).

^{1}H-NMR ($CDCl_3$), δ (ppm): 7.82-7.79 (d, 1H, ^3J = 9.0 Hz, H_a), 7.64-7.63 (d, 1H, ^4J =2.5 Hz , H_c), 7.51 (m, 1H, H_b), 3.68 (m, 2H+1, -C*H*-CH_2), 3.01-2.93 (q, 6H, ^3J = 7.3 Hz, -CH_2-CH_3), 1.25-1.20 (t, 9H, ^3J = 7.3 Hz, -CH_2-CH_3), 1.02-1.00 (d, 3H, ^3J = 7.1 Hz, -CH-CH_3), 0.72 (s, 9H, -C-(CH_3)$_3$), -0.09- -0.10 (d, 6H, ^4J =3.1 Hz, -Si-(CH_3)$_2$).

^{13}C-NMR ($CDCl_3$), δ (ppm): 157.24 (d, *J* = 73 Hz), 141.97, 127.21, 123.15 (d, *J* = 4.8 Hz), 119.33 (m), 77.4(m), 76.75, 71.25 (d, *J* = 6.3 Hz), 67.51 (d, *J* = 9.2 Hz), 45.85, 25.65, 20.48, 17.97, 8.54, -4.90.

^{31}P-NMR ($CDCl_3$), δ (ppm): -5.14 (t, *J*(P,H) = 6.1 Hz).

MS-ESI (FIA,(-)-mode, ACN), m/z: calcd. for $C_{16}H_{24}F_3NO_7PSi^-$: 458.42; found: 458.0

7.3.3.4 Synthesis of 2-hydroxypropyl 3-trifluoromethyl-4-nitrophenyl phosphate, sodium salt (5a)

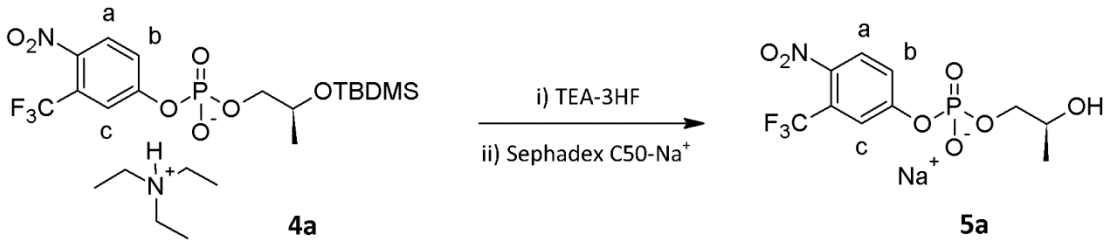

To a solution of **6b** (0.5 g, 0.9 mmol) in anhydrous THF (2 mL), TEA·3HF complex (1.0 mL, 6.2 mmol) was added at R.T. and the resulting mixture was stirred overnight before the addition of H_2O (5 mL) and TEA until pH∽5. THF and the resulting volatile *tert*-butyldimethylsilyl fluoride were removed by rotary evaporation. The crude product was then extracted several times into CH_2Cl_2 (3×25 mL), washed with H_2O to remove undesired triethylammonium salts, passed through an ion exchange resin (Sephadex C-50, Na^+). The water was removed by rotary evaportation and the following addition of EtOH have not led to any precipitation. The crude was then purified by HPLC. The lyophilization of the portion isolated at t_R = 13 min furnished 70 mg of the desired product as a white solid (27 %).

HPLC (Column: Phenomenex RP Jupiter 4U Proteo 90 Å. Gradient [t(min), %ACN]: 0, 0; 10, 33; 15, 90; 20, 100; λ=294 nm) t_R : 13 min.

^{1}H-NMR (D_2O, 300 K, 300 MHz) δ (ppm): 8.18 (d, 1H, ^{3}J=9.0 Hz, H_a), 7.79 (d, 1H, ^{4}J=2.2 Hz, H_c), 7.65 (dd, 1H, ^{3}J=9.0 Hz, ^{4}J=2.2 Hz, H_b), 4.14-3.79 (m, 2+1H, -CH_2-CH-), 1.20 (d, 3H, ^{3}J=6.4 Hz, -CH-CH_3).

^{13}C-NMR (D_2O, 300 K, 75 MHz) δ (ppm): 155.62 (d, J(C,P) = 6.0 Hz), 142.70 (s), 128.19 (s), 123.93 (s), 119.98 (m), 71.13 (d, J(C,P) = 6.1 Hz), 66.43 (d, J(C,P) = 8.1 Hz), 17.72 (s).

^{31}P-NMR (D_2O, 300K, 121 MHz) δ (ppm): -4.12 (t, ^{3}J(P,H) = 6.1 Hz)

MS-ESI (FIA,(-)-mode, ACN), m/z: Calcd. for $C_{10}H_{10}F_3NO_7P^-$: 344.16, found: 343.8

7.3.3.5 Synthesis of 2-[(tert-Butyldimethylsilyl)oxy]propyl 4-nitrophenyl phosphate, TEA salt (4b)

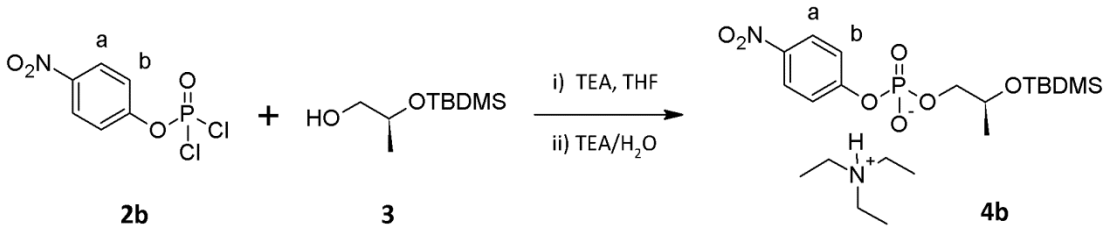

2b **3** **4b**

Commercially available 4-nitrophenyldichlorophosphate **2b** (1.40 g, 5.5 mmol) was dissolved in anhydrous THF (30 mL) under nitrogen and cooled to 0°C. A solution of **3** (1.04 g, 5.5 mmol) and TEA (0.77 mL, 5.5 mmol) in anhydrous THF (20 mL) was added drop-wise over a period of 30 min. After addition was complete, the mixture was allowed to stir at R.T. for 2 h. Finally, a mixture of TEA/cold water (2/10 mL) was added to hydrolyze the intermediate (monochloridate) and the solution was stirred for further 30 minutes. THF was evaporated and the product extracted into CH_2Cl_2 and washed with H_2O and brine, dried over $MgSO_4$ and the organic solvent removed under reduced pressure. The product was purified by column chromatography (SiO_2, MeOH from 0 to 10% / $CHCl_3$ with 0.5% TEA). After purification two main products were isolated: **4b** (SiO_2, MeOH/$CHCl_3$ 95:5 with 0.5% TEA) and the final product **5b** (SiO_2, MeOH/$CHCl_3$ 90:10 with 0.5% TEA) both as TEA salt.

^{1}H-NMR ($CDCl_3$), δ (ppm): 8.14-8.11 (d, 2H, ^3J = 9.1 Hz, H_a), 7.41-7.38 (d, 2H, ^3J = 9.1 Hz, H_b), 3.95-3.63 (m, 2H+1, -C*H*-CH_2), 3.05-2.98 (q, 6H, ^3J = 7.3 Hz, -CH_2-CH_3), 1.31-1.26 (t, 9H, ^3J = 7.3 Hz, -CH_2-CH_3), 1.10-1.08 (d, 3H, ^3J = 6.0 Hz, -CH-CH_3), 0.82 (s, 9H, -C-(CH_3)$_3$), 0.00 (s, 6H, -Si-(CH_3)$_2$).

^{13}C-NMR ($CDCl_3$), δ (ppm): 125.28, 120.01 (d, *J* = 5.6 Hz), 77.47, 77.04, 76.62, 71.24 (d, *J* = 6.6 Hz), 67.63 (d, *J* = 9.3 Hz), 45.76, 25.77, 18.09, 8.65.

^{31}P-NMR ($CDCl_3$), δ (ppm): -7.47 (t, *J*(P,H) = 10.3 Hz).

MS-ESI (FIA,(-)-mode, ACN), m/z: Calcd. for $C_{15}H_{25}NO_7PSi^-$: 390.42; found 390.5

7.3.3.6 Synthesis of 2-hydroxypropyl 4-nitrophenyl phosphate, sodium salt (5b)

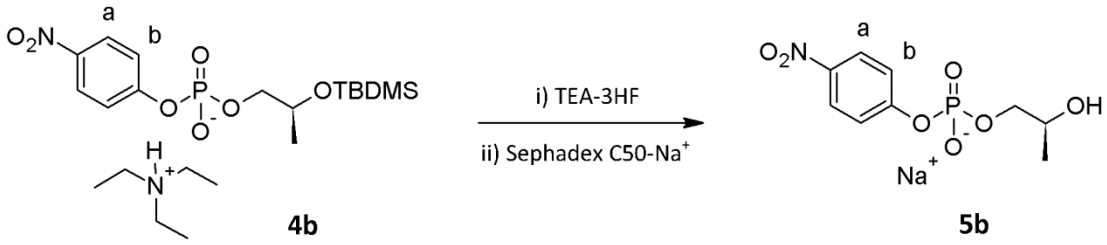

To a solution of **4b** (0.50 g, 1.0 mmol) in anhydrous THF (5 mL) was added a solution of TEA·3HF complex (0.65 mL, 8.4 mmol) in THF (1 mL) at room temperature and the resulting mixture was stirred for 5 h before the addition of H_2O (7 mL) and TEA until pH∽5. THF and the resulting volatile *tert*-butyldimethylsilyl fluoride were removed by rotary evaporation. The crude product was then extracted several times into CH_2Cl_2 (3×25 mL), washed with H_2O to remove undesired triethylammonium salts and passed through an ion exchange resin (Sephadex C-50, Na^+). The water was removed by rotary evaporation. EtOH was added and undissolved inorganic salts were removed by filtration. EtOH was removed under reduced pressure and the crude purified by HPLC. The lyophilization of the portion isolated at t_R = 9 min furnished 90 mg of the desired product as a white solid (30 %).

HPLC (Column: Phenomenex RP Jupiter 4U Proteo 90 Å. Gradient [t(min), %ACN]: 0, 0; 10, 33; 15, 90; 20, 100; λ=294 nm) t_R : 9 min.

^{1}H-NMR (D_2O), δ (ppm): 8.35-8.32 (d, 2H, ^3J = 9.2 Hz, H_a), 7.45-7.41 (d, 2H, ^3J = 9.3 Hz, H_b), 4.09-3.86 (m, 2H+1, -C*H*-CH_2-), 1.23-1.21 (d, 3H, ^3J = 6.4 Hz, -CH-CH_3).

^{13}C-NMR (D_2O), δ (ppm): 157.45 (d, *J* = 6.4 Hz), 142.53, 125.87, 120.50 (d, *J* = 5.1 Hz), 71.04 (d, *J* = 6.3 Hz), 66.50 (d, *J* = 8.2 Hz), 17.68.

^{31}P-NMR (D_2O), δ (ppm): -3.94 (t, *J*(P,H) = 6.00 Hz).

MS-ESI (FIA,(-)-mode, ACN), m/z: Calcd. for $C_9H_{11}NO_7P^-$: 276.16, found: 276.0

7.3.4 UV-Vis kinetics

Calibration curves

The calibration curves were carried out by measuring the absorbance at 400 nm (or 392 nm) and 40 °C of increasing amount of the leaving group PNP (or TFM) (final concentration: from 0 to 100 µM) added to a aqueous solution (buffered at the desired pH, [buffer] = 10 mM) containing Au NP **1**•Zn^{2+} (20 µM) (V_{well} = 250 µL). Taking into account the Lambert-Beer law, the slope of the curve represents ε·l. The obtained values are listed in table 2 and were used to convert kinetic signals, i.e. dA/dt, into dC/dt.

Table 7.2. List of all the ε·l values used in this part

Leaving group	**pH**	**ε·l (M^{-1})**
PNP	7.0	5820
	11.0	12966
TFM	6.0	3276
	7.0	7394
	8.0	8471
	11.0	9745

Hydrolysis of the substrates

The hydrolysis was carried out by monitoring the of the corresponding leaving group of a aqueous solution ([CAPS] = 10 mM, pH = 11.0) containing HPNPP (or HTFMP) at a final concentration of 50 µM. (V_{well} = 250 µL, 40 °C). In order to avoid volume changes during the analysis, a transparent plastic strip on the top of the wells was applied before the measurement. The obtained profiles were nicely fitted with a first order kinetic:

$$[\mathrm{PNP}]_t = 1 - e^{-kt}$$

(Origin 8 Pro, function: MnMolecular1 A_1-A_2e^{-kt}, constrains; $A_1 = A_2 = 1$). Stock solution of substrates were prepared by weight from the final product of synthesis. This experiment was used to determine accurately their concentration using the plateau value (full conversion) and the corresponding ε·l listed in table 2.

Activity of Au NP **1** as a function of Zn^{2+}

The activity of Au NP **1** as a function of the concentration of Zn^{2+} was assayed by monitoring the release rate of PNP of different aqueous solutions ([HEPES] = 10 mM, pH = 7.0) containing Au NP **1** (20 μM) and $Zn(NO_3)_2$ (from 0 to 1.5 equivalents, i.e. 30 μM of Zn^{2+}). The evolution of the absorbance at 400 nm was monitored after adding HPNPP (1 mM).

Michaelis-Menten kinetics

The catalytic activity of Au NP **1**•Zn^{2+} was measured by monitoring the release rate of PNP (or TFM) in different aqueous solutions (buffered at the desired pH, [buffer] = 10 mM) containing Au NP **1**•Zn^{2+} (20 μM) and increasing amounts of substrate. The evolution of the absorbance at 400 nm (or 392 nm) was monitored at 40 °C after adding HPNPP (or HTFMP, final concentration: from 0 to 2.0 mM) (V_{well} = 250 μL). In order to avoid volume changes during the analysis, a transparent plastic strip on the top of the wells was applied immediately after the additions of the substrate. Initial rates (v_0) were calculated converting the absorbance signals into concentration using the corresponding ε·l listed in table 2. Michaelis-Menten parameters were extrapolated by fitting the corresponding saturation profile with the Michaelis Menten model:

$$v = \frac{\boldsymbol{V_{max}} \cdot [\text{Substrate}]}{\mathbf{K_m} + [\text{Substrate}]}$$

(Origin 8 Pro, function: Hill, constrains; n = 1, i.e. Michaelis-Menten kinetic). k_{cat} values were obtained by dividing V_{max} to the concentration of TACN•Zn^{2+} (20 μM).

inhibition experiments with ATP and ADP

The catalytic activity of Au NP **1**•Zn^{2+} was measured by monitoring the release rate of PNP (or TFM) in different aqueous solutions (buffered at the desired pH, [buffer] = 10 mM) containing Au NP **1**•Zn^{2+} (20 μM) and increasing amounts of ATP or ADP (final concentration = from 0 to 16 μM). The evolution of the absorbance at 400 nm (or 392 nm) was monitored at 40 °C after adding HPNPP (or HTFMP, final

concentration = 1 mM). In order to avoid volume changes during the analysis, a transparent plastic strip on the top of the wells was applied immediately after the additions of the substrate. Initial rates were scaled to the initial rate observed in the absence of inhibitor (i.e. ν_1/ν_0). The kinetic of points at which the differentiation is maximized (6.4 μM of inhibitors) were repeated using a well-volume of 50 μL. On this way it was possible to record the full kinetics, avoiding the saturation of the detector.

7.5 References

(1) Rakow, N. A.; Suslick, K. S. *Nature* **2000**, *406*, 710.
(2) Janata, J.; Josowicz, M. *Nat. Mater.* **2003**, *2*, 19.
(3) Nguyen, B. T.; Anslyn, E. V. *Coord. Chem. Rev.* **2006**, *250*, 3118.
(4) Hunt, H. K.; Armani, A. M. *Nanoscale* **2010**, *2*, 1544.
(5) Scrimin, P.; Prins, L. J. *Chem. Soc. Rev.* **2011**, *40*, 4488.
(6) Das, G.; Talukdar, P.; Matile, S. *Science* **2002**, *298*, 1600.
(7) Zhu, L.; Anslyn, E. V. *Angew. Chem. Int. Ed.* **2006**, *45*, 1190.
(8) Gianneschi, N. C.; Nguyen, S. T.; Mirkin, C. A. *J. Am. Chem. Soc.* **2005**, *127*, 1644.
(9) Sella, E.; Shabat, D. *J. Am. Chem. Soc.* **2009**, *131*, 9934.
(10) Manea, F.; Houillon, F. B.; Pasquato, L.; Scrimin, P. *Angew. Chem. Int. Ed.* **2004**, *43*, 6165.
(11) Martin, M.; Manea, F.; Fiammengo, R.; Prins, L. J.; Pasquato, L.; Scrimin, P. *J. Am. Chem. Soc.* **2007**, *129*, 6982.
(12) Zaupa, G.; Scrimin, P.; Prins, L. J. *J. Am. Chem. Soc.* **2008**, *130*, 5699.
(13) Zaupa, G.; Mora, C.; Bonomi, R.; Prins, L. J.; Scrimin, P. *Chem. Eur. J.* **2011**, *17*, 4879.
(14) Bonomi, R.; Cazzolaro, A.; Sansone, A.; Scrimin, P.; Prins, L. J. *Angew. Chem. Int. Ed.* **2011**, *50*, 2307.
(15) Diez-Castellnou, M; Mancin, F.; Scrimin, P. *J. Am. Chem. Soc.* **2014**, *136*, 1158-1161.
(16) Tehan, B. G.; Lloyd, E. J.; Wong, M. G.; Pitt, W. R.; Montana, J. G.; Manallack, D. T.; Gancia E. *Quant. Struct.-Act. Relat.* **2002**, 21, 457
(17) Humphry, T.; Iyer, S.; Iranzo, O.; Morrow, J. R.; Richard, J. P.; Paneth, P.; Hengge, A. C. *J. Am. Chem. Soc.* **2008**, *130*, 17858.

Chapter 8

Transient signal generation in a self-assembled nanosystem fueled by ATP

A fundamental difference exists in the way signal generation is dealt with in natural and synthetic systems. Whereas Nature uses the transient activation of signaling pathways to regulate all cellular functions, chemists rely on sensory devices that convert the presence of an analyte into a steady output signal. The development of chemical systems that bear a closer analogy to living ones (i.e. require energy for functioning, are transient in nature and operate out-of-equilibrium) requires a paradigm shift in the design of such systems. Herein, a straightforward strategy that enables transient signal generation in a self-assembled system is reported. It will be shown that it can be used to mimic key features of natural signaling pathways, which are: control over the output signal intensity and decay rate, the concentration-dependent activation of different signaling pathways and the transient down-regulation of catalytic activity. In general terms, the reported methodology provides for a straightforward way to gain temporal control over supramolecular processes.

8.1 Introduction

Communication is an essential feature of all living systems as it permits coordination, organization and adaptation.[1] To achieve this, Nature has evolved elaborate signaling pathways relying on circular enzymatic networks to regulate all intra- and extracellular functions.[2,3] In such networks, a trigger can up- or downregulate an enzymatic cascade reaction leading to the transient generation of an output signal, after which the system returns to the original state. The circular nature of enzymatic networks implies that signal generation is a process that requires energy consumption. Over the past decades, chemists have developed a wealth of supramolecular sensory systems able to generate an output signal in response to an external trigger.[4-8] A common feature of these systems is that signal generation is thermodynamically driven, *i.e.* the system adapts to a trigger-induced change in the energetic landscape developing into a new, energetically more favorable, resting state. This change is accompanied with a change in a property (fluorescence, current, catalysis, solubility, etc.) that can be measured and correlated to the strength of the trigger. This approach is exemplified in Figure 8.1a (step *i*) for an indicator-displacement assay in which an analyte displaces a receptor-bound indicator.[9]

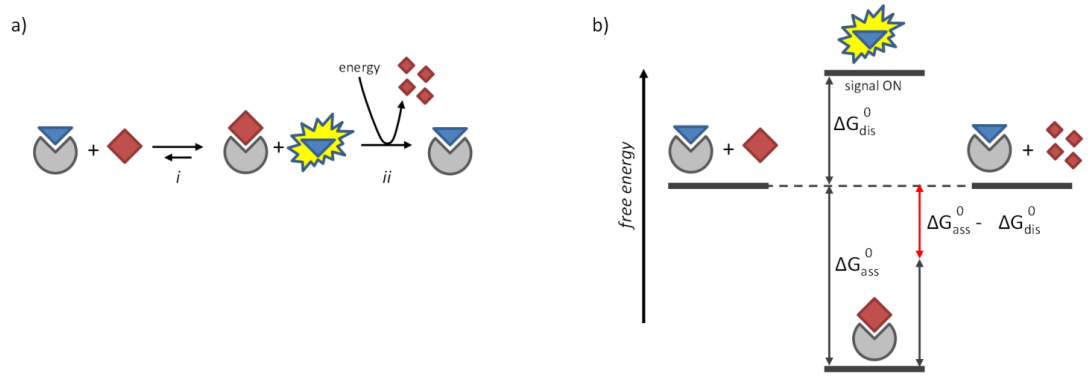

Figure 8.1. (a) Schematic representation of an indicator displacement assay (step *i*). An additional energy-consuming step (*ii*) is required to revert the system back to the original state. b) Schematic energy diagram indicating the changes in free energy related to steps *i* and *ii* of the indicator displacement assay depicted in Figure 1a.

The energy cost required for dissociation of the indicator ($\Delta G°_{diss}$) is more than compensated for by the energy gain resulting from formation of the receptor-

analyte complex ($\Delta G°_{ass}$) (Figure 8.1b). Overall this process is energetically downhill and generates a signal that is stable in time. For applications in sensing this is obviously a highly attractive property and, consequently, a wide variety of supramolecular sensing systems have been developed based on this principle.[4-8,10] However, the absence of a return to the original state, which would require an amount of energy equal to $\Delta G°_{ass}$-$\Delta G°_{diss}$, makes it fundamentally different from the way Nature deals with signal generation. Indeed, there is currently an enormous interest in the development of synthetic systems that require energy consumption to remain in a functional state.[11] Such systems have properties that are more similar to living systems and are expected to offer new applications in the field of materials and nanotechnology[12]. Examples of dissipative self-assembled systems, [13-15] transient catalyst formation,[16] molecular transport systems,[17] and molecular motors[18-20] are emerging.

Here, we demonstrate a general strategy that permits transient signal generation in a self-assembled system.[21-23] The approach relies on the addition of an additional step to the scheme depicted in Figure 1a (step *ii*) that provides the necessary energy ($\Delta G°_{ass}$-$\Delta G°_{diss}$) to convert the system back to the original state. It will be shown that this gives the possibility to perform multiple signaling cycles with the same system and, importantly, allows for temporal control over signal intensity. It is then demonstrated that this approach can be used to mimic features of natural signaling pathways, such as the activation of one or two signaling pathways depending on the initial trigger concentration and the transient regulation of catalytic activity.

8.2 Results and discussion

8.2.1 Components and conditions

The interaction of a given oligoanion with Au NP **1**•Zn^{2+} strongly depends on the number of negative charges present in its molecular structure. This emerges in a clear manner from a series of displacement experiments in which increasing amounts of A*X*P (*X* = T, D, M) are added to Au NP **1**•Zn^{2+} saturated with fluorescent probe **F**. When bound to Au NP **1**•Zn^{2+}, the fluorescence of **F** is quenched by the gold nanoparticle, but is turned on upon its displacement by nucleotides A*X*P (*X* = T, D, M) as depicted in Figure 8.2a. Measurement of the fluorescence intensity as a

function of the concentration of A*X*P provides information on the relative affinity, K_{rel}, of A*X*P for Au NP **1**•Zn^{2+} compared to **F** (Figure 8.2c). Fitting of the measured curves yielded K_{rel} values of 1.8, $9.2x10^{-2}$ and $2.8x10^{-4}$ for ATP, ADP and AMP respectively, demonstrating once again the importance of multivalent interactions. As described in previous chapters, this attractive differentiation has been exploited for the development of assays based on an analyte-induced change in the thermodynamic equilibrium (analogous to step *i* in Figure 8.1).

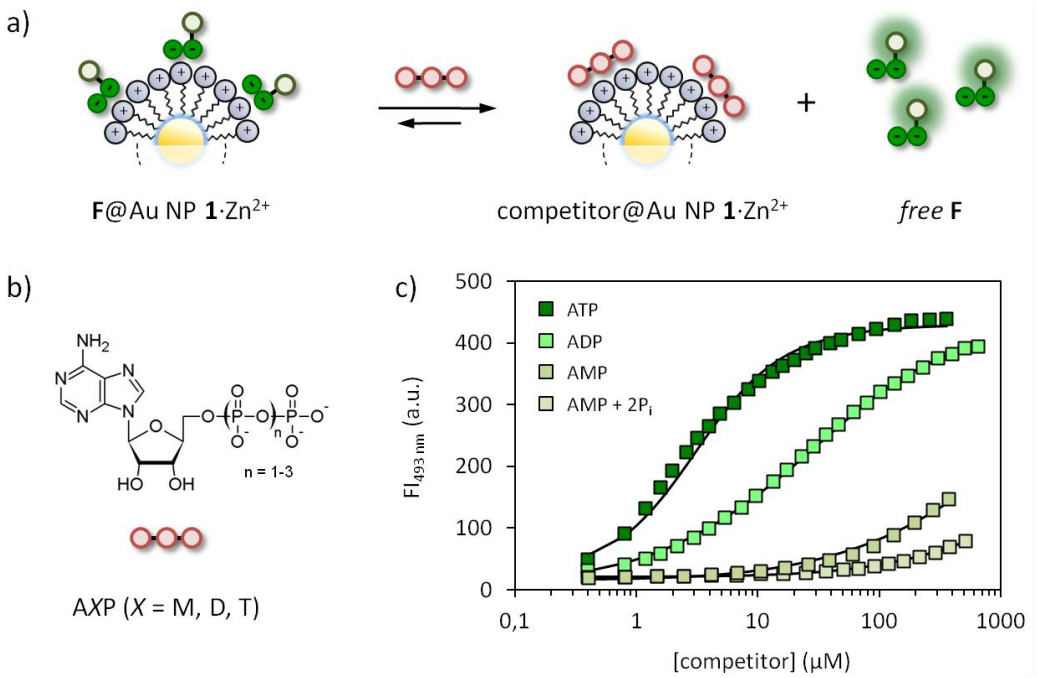

Figure 8.2. (a) Displacement of probe **F** from Au NP **1**•Zn^{2+} upon the addition of a competitor. (b) Structure of the competitors used in this chapter. (c) Fluorescent intensity at 493 nm as a function of the concentration of competitor. The solid lines represent the best fit to model. Experimental conditions: [TACN•Zn^{2+}] = 10 ± 1 µM, [**F**] = 3.7 µM, [HEPES] = 10 mM, pH = 7.0 [$CaCl_2$] = 1 mM, 37 °C.

Nonetheless, here we are intrigued by the question of whether this system would be able to generate a fluorescent signal that is transient in nature. This would rely on the initial displacement of **F** by the strong competitor ATP after which the irreversible destruction of ATP into weaker competitors would results in re-formation of the complex between **F** and Au NP **1**•Zn^{2+}, and thus, a disappearance of the signal (Figure 8.3a). The enzyme potato apyrase very efficiently hydrolyses ATP into AMP and 2 equivalents of inorganic phosphate P_i, which makes it very suitable for the purpose given above.[24] Potato apyrase requires metal ions for its

hydrolytic activity, typically Ca^{2+}. Consequently, we have verified the stability of the **F**@Au NP **1**•Zn^{2+} complex toward both Ca^{2+} and PA by monitoring the fluorescence intensity of **F** upon the addition of increasing amounts of Ca^{2+} or PA (see experimental section). The presence of both Ca^{2+} (up to 1.0 mM) and PA (at a fixed [Ca^{2+}] = 1.0 mM) hardly induced the displacement of **F** from Au NP **1**•Zn^{2+}, showing that the system is stable and thus it is possible to work with PA *in situ*. Finally, we determined the K_{rel}-value of the AMP+2P_i mixture rather than just AMP (Figure 8.2c). As expected, a slightly higher value ($1.6x10^{-3}$) was obtained, but still around 3 orders of magnitude lower than that of ATP.

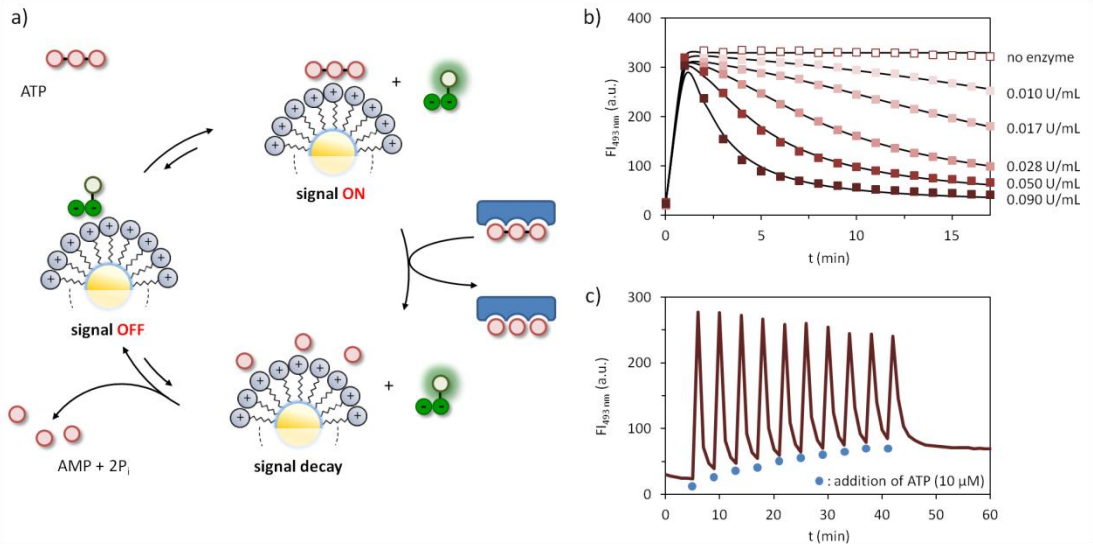

Figure 8.3. (a) Schematic representation of the system for transient signal generation. (b) Fluorescent intensity at 493 nm as a function of time upon the addition ATP (10 µM) to Au NP **1**•Zn^{2+} (10 µM) and **F** (3.7 µM) in the presence of different concentrations of potato apyrase. The solid lines represent fits to the kinetic model shown in Figure 4. (c) Fluorescent intensity at 493 nm upon 10 repetitive additions of ATP (10 µM) to a solution of Au NP **1**•Zn^{2+} (10 µM) and **F** (3.7 µM) in the presence of potato apyrase (0.3 U/ml).

8.2.2 Transient signal generation

Kinetic measurements showed that in the absence of enzyme, the addition of ATP (10 µM) to a solution of **F**@Au NP **1**•Zn^{2+} led to a rapid increase in fluorescence intensity which then remained constant in time (Figure 8.3b). We were very pleased to observe that repetition of the same experiment in the presence of increasing amounts of enzyme (from 0.01 up to 0.09 U/ml) resulted in the same initial increase in fluorescence intensity, but this time followed by a signal decay with rates

depending on the concentration of enzyme (Figure 8.3b). At the highest concentration of enzyme, the fluorescence intensity returned to the starting value after just 15 minutes. The reproducibility of transient signal generation by the system was demonstrated by performing 10 cycles with the same sample adding new batches of ATP (10 μM) each time the signal had returned to the starting value (Figure 8.3c). It is noted that the higher fluorescent intensity after 10 cycles (69 a.u.) originates from the accumulation of waste (AMP+2P_i) in the system (72 a.u. expected for 100 μM of AMP and 200 μM of P_i based on the displacement curves).

8.2.3 Signal-response curve and kinetic model

The most important feature of any signaling system is the signal-response curve, as it correlates the output signal to the intensity of the input signal. We determined the response curves of our system at 4 different concentrations of ATP (10, 50, 100 and 150 μM) at a constant concentration of enzyme (0.01 U/ml). Measurement of the fluorescence intensity as a function of time clearly showed strong differences between the 4 samples (Figure 8.4b). In all cases, the addition of ATP caused a rapid increase of the fluorescence intensity. The maximum intensity was lower for $[ATP]_0$ = 10 μM (FI_{493} = 306 a.u.), compared to the other three samples which reached a nearly identical intensity of around 410 a.u. These values correspond to the fluorescence intensities measured in the competition experiments between probe **F** and ATP (Figure 8.2c). The nature of the displacement curve indeed confirms that a fluorescence intensity of around 410 a.u. is the maximum intensity of the output signal that can be generated by the system as it represents the situation at which (nearly) all of probe **F** is displaced from Au NP **1**•Zn^{2+}. However, although the addition of 50, 100 or 150 μM of ATP gives the same initial signal, the signal decay is much different, being much slower for high concentrations of ATP. Although this can be intuitively explained based on the displacement curve, we were interested in a quantitative description of the signal generation process in order to have detailed information on the concentration of all species in the system. For that purpose we developed a model taking into account all relevant kinetic processes that occur within the system (Figure 8.4a, see experimental section for more details).

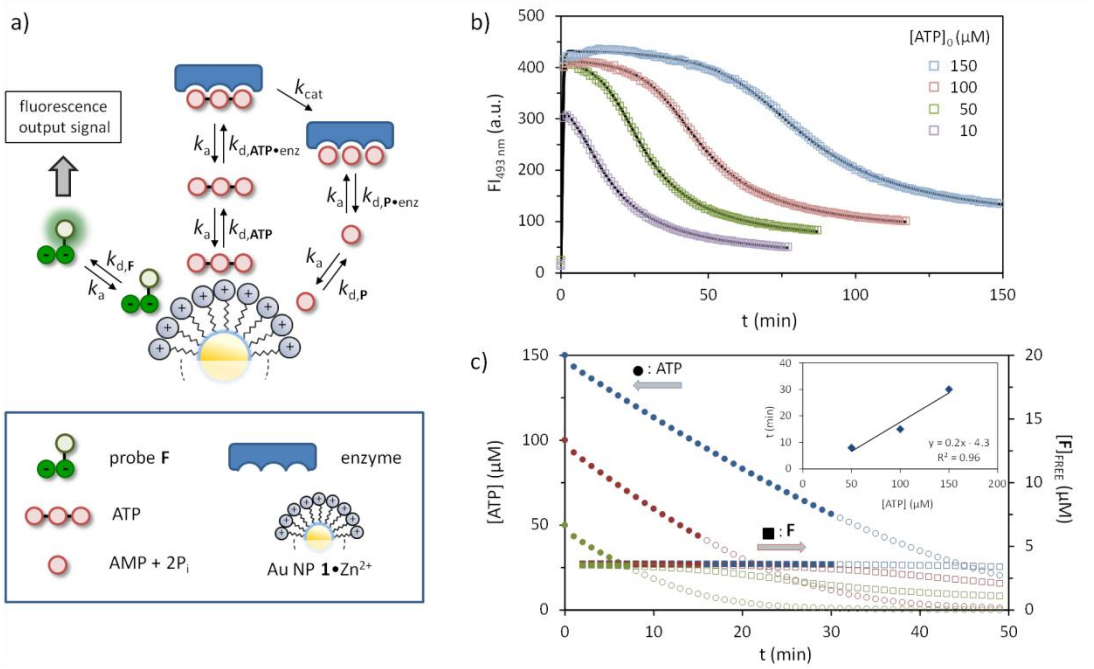

Figure 8.4. (a) Kinetic model used for fitting the experimental data. A full description is given in the Supporting Information. (b) Fluorescent intensity at 493 nm as a function of time upon the addition of different amounts of ATP to a solution containing Au NP **1**•Zn^{2+}, probe **F** and a constant concentration of potato apyrase. The solid lines represent the fit to a kinetic model. (c) Plots of the concentration of ATP (left axis) and free **F** (right axis) as a function of time for three different initial concentrations of ATP. The solid points indicate the period at which the concentration of free **F** is constant (<2% decrease with respect to the maximum value). The inset gives the duration of the time interval with a steady concentration of free **F** as a function of the initial amount of ATP.

The relative affinities, K_{rel}, were used to define the dissociation rate constants of all complexes involving Au NP **1**•Zn^{2+}, assuming that all association rate constants are very high. Dissociation rate constants for the complexes involving the enzyme were varied to fit the experimental data to the model. As illustrated by the solid lines the model neatly describes the experimental data (Figure 8.4b). Analysis of the concentrations of ATP and **F** as a function of time illustrates the most interesting feature of this system, which is the possibility to develop a steady fluorescent signal with a duration that depends on the initial concentration of ATP. Interestingly, during the period in which the concentration of free **F**, and thus the output signal, remains constant (< 2% decrease), a significant consumption of ATP takes place (see filled symbols in Figure 4c). However, not until the concentration of ATP falls below a certain threshold value at which **F** can effectively compete with the remaining ATP for binding to Au NP **1**•Zn^{2+}, the signal starts to decay. The correlation between the duration of this lag time and the initial concentration of ATP demonstrates that it is

possible to control this time interval, which may last up to 30 minutes (inset Figure 8.4c). As will be discussed in the next section, signaling pathways in Nature rely heavily on this control mechanism.

8.2.4 ATP-dependent activation of two different signals

Having developed a robust system for transient signal generation, we were curious to find out whether it would be possible to mimic other features of natural signaling pathways. In particular, we were inspired by the purinergic signaling pathway as it bears a strong resemblance to our system. The purinergic signaling pathway is involved in the regulation of various physiological functions in the circulatory,[25] immune,[26] and nervous system,[27] amongst others. It operates through the activation of purinergic receptors in the cell-membrane by extracellular nucleotides and nucleosides. It is known that all receptors belonging to the P2X family, which is one out of the three known distinct classes of purinergic receptors, respond only to ATP.[28] However, they require different concentrations of ATP for activation and exhibit different desensitization kinetics. For example, the P2X1 receptor has a high affinity for ATP (K_D ≈ 0.01-1 μM) and a desensitization rate less than 1 s, whereas activation of the P2X7 receptor requires ATP concentrations > 100 μM but has a much slower desensitization rate (>20 s).[28] Thus, the overall response of the signaling pathway (both in terms of output signal diversity and decay rate) is dependent on the intensity of the trigger (ATP). We argued that this property could be mimicked by adding a second fluorescent probe **G** (dipeptide Ac-WD-OH) to the system (Figure 8.5a and d). Dipeptide **G** has a much lower affinity and surface saturation concentration compared to **F** (0.6 μM for [TACN•Zn^{2+}] = 10 μM, Figure 8.5b) and, in addition, has a fluorescent tryptophan moiety (λ_{ex} = 280 nm, λ_{em} = 360 nm) which can be monitored independently from probe **F**. The displacement of probes **F** (0.5 μM) and **G** (0.5 μM) from Au NP **1**•Zn^{2+} by either ATP or the waste mixture AMP+2P_i was studied at a slightly higher concentration of Au NP **1** (20 μM) in order to ensure that both probes were initially (nearly) quantitatively bound. As a result of the lower valency of probe **G** the margin between ATP and the waste mixture is much reduced. Nonetheless, the difference between probes **F** and **G** is sufficiently large to test the abovementioned hypothesis (Figure 8.5c).

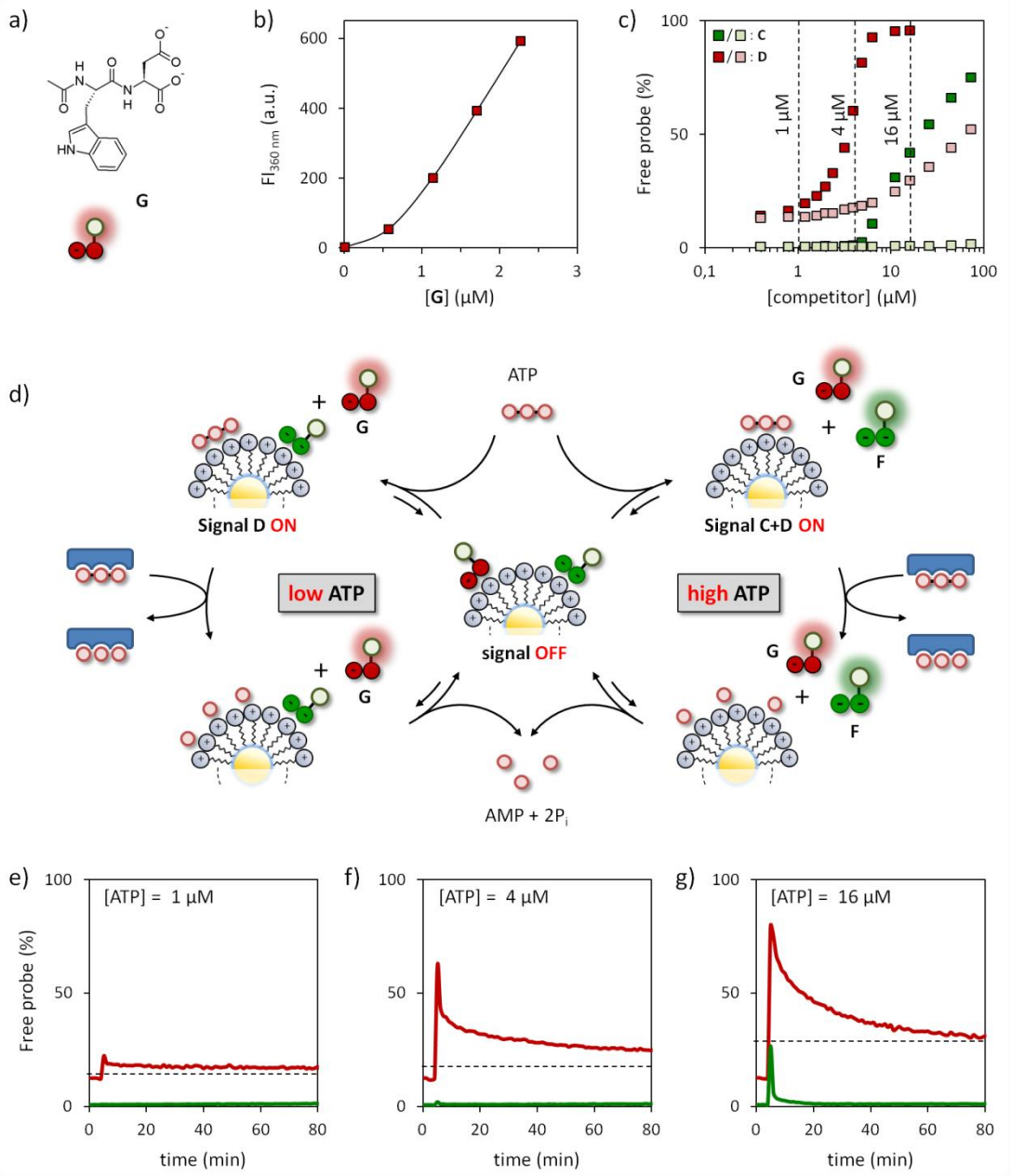

Figure 8.5. (a) Structure of Ac-WD-OH (**G**). (b) Fluorescence intensity at 360 nm as a function of the concentration of **G** added to a solution of Au NP **1**•Zn^{2+} at pH 7.0. (c) Amount of displaced probe **F** (green) or **G** (red) as a function of the concentration of either ATP (filled squares) or the waste mixture AMP + $2P_i$ (empty squares). (d) Schematic representation of the ATP-dependent transient generation of one or two signals. (e-f) Amount of displaced probe **F** (green) and **G** (red) as a function of time upon the addition of ATP at 1 (e), 4 (f) or 16 (g) μM concentrations. The dotted lines mark the expected end value expected for probe **G** in the presence of the respective amount of waste formed. Experimental conditions: [TACN•Zn^{2+}] = 20 ± 1 μM, [**F**] = [**G**] = 0.5 μM, [HEPES] = 10 mM, pH 7.0, [$CaCl_2$] = 1.0 mM, [potato apyrase] = 0.3 U/ml, 37 °C.

In particular, three concentrations of ATP were identified at which the system was expected to generate a different response: 1 μM of ATP should not result in any signal, 4 μM of ATP should generate a signal from **G** but not **F**, whereas at 16 μM of ATP, signals from both **F** and **G** should emerge. It is noted that higher

concentrations of ATP could not be used because the accumulation of waste would block the re-formation of the complex between **G** and Au NP **1**•Zn^{2+} after ATP hydrolysis. Also, it was found that high concentrations of ATP (> 20 μM) caused a quenching of the fluorescence of free **G** (data not shown). Transient signal generation by the system was studied by measuring the fluorescence intensities of probe **F** and **G** in time upon the addition of ATP at 1, 4, or 16 μM concentrations to the system in the presence of potato apyrase (Figure 8.5e-g). The obtained curves clearly demonstrate that, just as in the purinergic signaling pathway, the initial concentration of ATP determines whether none, one or two signals are generated.[29] Importantly, the system also displays a similar correlation between probe affinity and signal duration. Thus, activation of probe **F** requires high concentrations of ATP, but the resulting signal decays rapidly (k_{obs} = 1.5 min^{-1}). On the other hand, low concentrations of ATP are sufficient to activate probe **G**, but that signal persists for a much longer time (23x, k_{obs} = 0.07 min^{-1}). The inverted relation between binding affinity and signal duration originates directly from the competition between the probes and ATP for binding to Au NP **1**•Zn^{2+}. For example, low-affinity probe **G** requires a near complete hydrolysis of ATP in order to be able to return to Au NP **1**•Zn^{2+}. Here, this takes a particular long time because the ATP hydrolysis by the enzyme slows down significantly upon depletion of ATP.

8.2.5 Transient down-regulation of catalytic activity

Another feature of natural signaling pathways is that they consist of cascades of enzymatic reactions that are either up- or downregulated by an initial trigger. This permits the system to transform a weak input signal into a strong output signal by means of catalytic signal amplification. We were interested to find out whether we could exploit the potato apyrase-driven consumption of ATP for the transient regulation of the catalytic activity of Au NP **1**•Zn^{2+}. In the previous chapter we have seen that Au NP **1**•Zn^{2+} are highly efficient catalysts for the transphosphorylation of 2-hydroxypropyl-4-nitrophenylphosphate (HPNPP). As for enzymes, the catalytic activity of Au NP **1**•Zn^{2+} is inhibited in the presence of species able to compete with HPNPP for binding (see previous chapter). Indeed, kinetic studies at varying concentrations showed that ATP is a very effective inhibitor already at low

micromolar concentrations (Figure 8.6b). However, a significantly lower inhibitory effect of the AMP+2P_i waste mixture was observed (Figure 8.6b). This difference raised the possibility to temporarily downregulate the catalytic activity of Au NP **1**•Zn^{2+} by ATP in the presence of potato apyrase. This was verified by adding 3 µM of ATP to a solution containing Au NP **1**•Zn^{2+} (10 µM), HPNPP (1 mM) and potato apyrase (0.06 U/ml). This caused an immediate inhibition of the transphosphorylation reaction evidenced by the constant absorbance at 400 nm (Figure 8.6c).

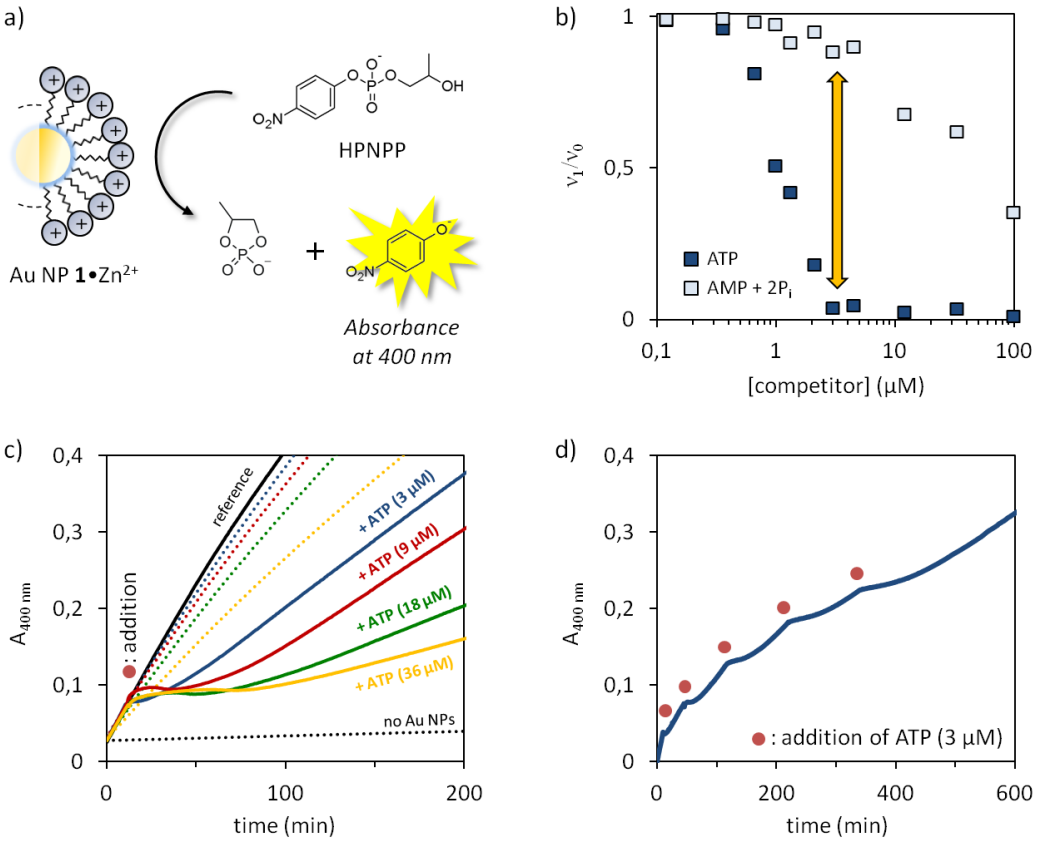

Figure 8.6. (a) Catalysis of the transphosphorylation of HPNPP by Au NP **1**•Zn^{2+}. (b) Relative reaction rates (v/v0) as a function of the concentration of either ATP or the mixture AMP+2P_i. Experimental conditions: [TACN•Zn^{2+}] = 10 ± 1 µM, [HPNPP] = 1 mM, [HEPES] = 10 mM, pH 7.0, [$CaCl_2$] = 1.0 mM, 37 °C. c) Absorbance at 400 nm (originating from the reaction product *p*-nitrophenolate) as a function of time for different mixtures. The red dot indicates the time at which inhibitors were added. Experimental conditions: : [TACN•Zn^{2+}] = 10 ± 1 µM µM, [HPNPP] = 1 mM, [HEPES] = 10 mM, pH 7.0, [$CaCl_2$] = 1.0 mM, [potato apyrase] = 0.06 U/mL, 37 °C. d) Absorbance at 400 nm as a function of time upon the sequential additions of ATP (5x3 µM). The red dots indicate the time of addition. Experimental conditions: same as for 6c.

However, after a period of around 5 minutes, the absorbance started to increase again clearly indicating the re-activation of Au NP **1**•Zn^{2+}. It is noted that even after

prolonged times the catalytic activity of Au NP **1**•Zn^{2+} was not restored to the level expected in the presence of AMP+2P_i (see dotted line in Figure 8.6c). This could indicate that potato apyrase is inhibited by HPNPP causing a further reduction of the already slow hydrolysis rate of ATP at these concentrations. Nonetheless, the observation that the duration of the inhibition lag time depends on the amount of ATP added, demonstrates that ATP indeed functions as transient regulatory element for the down-regulation of Au NP **1**•Zn^{2+} (Figure 8.6c) The transient nature emerged in a clear manner from a kinetic experiment in which 5 cycles were performed by sequentially adding ATP (3 μM each) (Figure 8.6d).

8.3 Conclusion

In conclusion, we have developed a strategy that permits transient signal generation in a self-assembled system. Signal formation is triggered by an input in the form of ATP, the consumption of which returns the system back to the original state. The initial concentration of ATP regulates the intensity of the output signal and its duration and determines also whether one or two signals are generated in the case where two reporter molecules are used. The same mechanism is evoked when applied to the transient downregulation of the catalytic activity of the nanoparticles.

In more general terms, though, we have developed straightforward methodology to gain temporal control over supramolecular processes, *i.e.* all these processes rely on noncovalent interactions between molecules. In our particular case, ATP shifts the equilibrium between Au NP **1**•Zn^{2+} and **F** away from the free energy minimum and continues to do so as long as its concentration remains above a certain threshold value. Although we have focused on transient signal generation, one can envision that the same strategy may also be applied to control the temporal stability of self-assembled systems, such as nanoarchitectures or materials, in which the degradable compound plays an essential role as building block or as stabilizing unit. As such, it may provide an important new tool for the design of synthetic systems with 'life-like' properties, such as adaptation, self-healing, evolution, etc.

8.4 Experimental section

8.4.1 Instrumentation

See Chapter 1

8.4.2 Materials

For Au NP **1**, probe **F**, $Zn(NO_3)_2$, ATP, ADP, AMP and buffers see previous chapters. Probe **G** was already present in the laboratories of prof. Prins. Na_3PO_4 (namely, P_i) and $CaCl_2$ was obtained from Carlo Erba Reagenti and BDH Prolabo, respectively, and used as received. The enzyme potato apyrase (PA) was obtained from Sigma Aldrich and used without further purification. In particular, PA was dissolved in 1.0 mL of mQ-water and divided in 10 working aliquots of 100 µL, which were stored at -20 °C. In order to avoid harmful freeze-thaw cycles, all the experiments were carried out using fresh solutions of PA. All these solutions were prepared by diluting one of above mentioned aliquots to the desired concentration and used within a day.

8.4.3 Determination of the stock solution concentrations

For the nucleotides see previous chapters. The concentration of $CaCl_2$ and Na_3PO_4 stock solutions was determined by weight. For the enzyme PA the concentration is addressed to the units (U) declared in the batch of PA purchased (100 U). One unity is defined as the quantity of enzyme that will liberate 1.0 µmol of P_i from ATP or ADP per minute at pH 6.5 and 30 °C (see the DataSheet of the product - A6237 *Sigma* - for more details).

8.4.4 Displacement experiments

The displacement experiments were performed by monitoring the change in fluorescence intensity at 493 nm upon the addition of increasing amounts of a stock solution of ATP, ADP or AMP + 2Pi to a 3-mL aqueous solution ([HEPES] = 10 mM, pH = 7.0, $[CaCl_2]$ = 1.0 mM) containing Au NP **1**•Zn^{2+} (10 µM) coated with **F** (3.7 µM) at 37°C. The time course of the fluorescence intensity after each addition was monitored at the emission maximum of the C343-probe (λ_{ex} = 450 nm, λ_{ex} = 493 nm,

slits = 2.5/5 nm). K_{rel} values were obtained by fitting the corresponding displacement curve with the model described in chapter 3.

Displacement experiments were repeated using a heteromeric surface composed by probes **F** and **G** (1:1). In this case, the experiments were carried out by adding consecutive amounts of a stock solution of ATP or AMP + 2Pi to a 3-mL aqueous solution ([HEPES] = 10 mM, pH = 7.0, [$CaCl_2$] = 1.0 mM) containing Au NP **1**•Zn^{2+} (20 μM) coated with **F** (0.5 μM) and **G** (0.5 μM) at 37°C. The optical settings were optimized in order to follow the two probes simultaneously ($\lambda_{ex,\,F}$ = 370 nm, $\lambda_{em,\,F}$ = 493 nm, $\lambda_{ex,\,G}$ = 280 nm, $\lambda_{em,\,G}$ = 360 nm, slits = 10/10 nm)

8.4.5 Compatibility of PA

Compatibility studies were performed by monitoring the change in fluorescence intensity at 493 nm upon the addition of increasing amounts of either $CaCl_2$ (a) or PA (b) to a 3-mL aqueous solution ([HEPES] = 10 mM, pH = 7.0) containing Au NP **1**•Zn^{2+} (10 μM) coated with probe **F** (3.7 μM) at 37 °C. In the case of PA (b), $CaCl_2$ was already present in the solution at a constant concentration equal to 1.0 mM. The optical settings were the same used in the first displacement experiments.

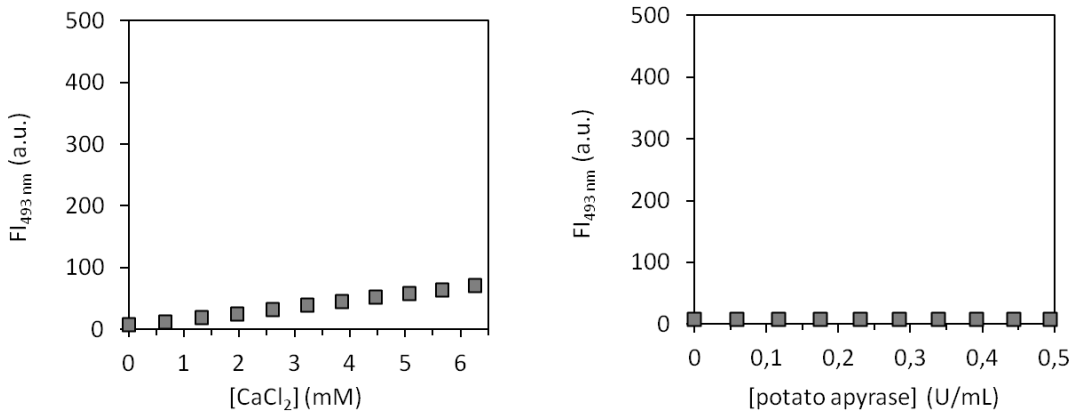

Figure 7.7. Fluorescent intensity at 493 nm as a function of the concentration of (a) $CaCl_2$ or (b) PA in the presence of $CaCl_2$ (1.0 mM).

8.4.6 Kinetic model

The model was used to fit the data depicted in Figures 7.3 and 7. by varying the parameters related to the interactions of ATP and P with enzyme E ($k_{d,ATP•enz}$, $k_{d,P•enz}$ and k_{cat}) and parameter X (Figure 7.8).

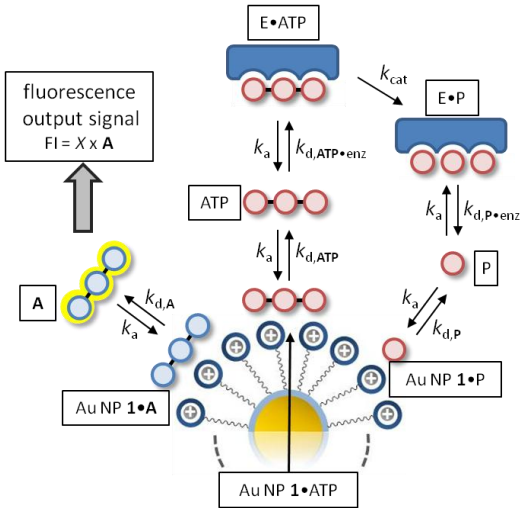

Figure 7.8. Kinetic model used to describe the fluorescence intensity as a function of time upon the addition of ATP

The model was implemented in Micromath Scientist for Windows, version 2.01:

```
// MicroMath Scientist Model File
//
// FI = fluorescence intensity; X = factor to correlate [A] to the fluorescence intensity (free)
// A = [A]; ATP = [ATP]; P = [P]
// NP = [Au NP 1]; NPA = [Au NP 1•A]; NPATP = [Au NP 1•ATP]; NPP = [Au NP 1•P]
// E = [E]; EATP = [E•ATP]; EP = [E•P]
// ka = ka  = 1x10^7 (fixed); kda = kd,A = 2.5 (fixed); fatp = kd,A/kd,ATP = 1.79 (fixed); fp = kd,A/kd,P = 0.00163 (fixed)
// kd = kd,ATP•E  (free); kdep = kd,P•E (free); kcat = kcat (free)
//
//variables and parameters
        IndVars:    T
        DepVars:    FI, NPA, NPATP, NPP, NP, A, ATP, P, EATP, E, EP, NPTOT, ETOT
        Params:     ka, kda, fatp, fp, kd, kdep, kcat, X, NPA0, A0, NP0, ATP0, E0
//model
        kdatp=kda/fatp
        kdp=kda/fp
        NPA'=ka*NP*A-kda*NPA
        NPATP'=ka*NP*ATP-kdatp*NPATP
        NPP'=ka*NP*P-kdp*NPP
        NP'=-ka*A*NP+kda*NPA-ka*ATP*NP+kdatp*NPATP-ka*NP*P+kdp*NPP
        A'=-ka*A*NP+kda*NPA
        ATP'=-ka*NP*ATP+kdatp*NPATP-ka*E*ATP+kd*EATP
        EATP'=ka*E*ATP-kd*EATP-kcat*EATP
        EP'=ka*E*P-kdep*EP
        E'=-ka*E*ATP+kd*EATP+kcat*EATP-ka*E*P+kdep*EP
        P'=-ka*P*NP+kdp*NPP+kcat*EATP-ka*E*P+kdep*EP
        FI=X*A
//initial conditions
```

T=0
NPA=NPA0
NPATP=0
A=A0
NP=NP0
ATP=ATP0
P=0
NPP=0
E=E0
EP=0
EATP=0
***

8.5 References

(1) Ricard, J.; Bernardi, G. *Emergent Collective Properties, Networks and Information in Biology*; Elsevier Science, 2006.
(2) Krauss, G. *Biochemistry of Signal Transduction and Regulation*; Wiley-VCH Verlag GmbH & Co: Weinheim, 2008.
(3) Behar, M.; Hoffmann, A. *Curr. Opin. Genet. Dev.* **2010**, *20*, 684.
(4) Valeur, B.; Leray, I. *Coord. Chem. Rev.* **2000**, *205*, 3.
(5) Beer, P. D.; Gale, P. A. *Angew. Chem. Int. Edit.* **2001**, *40*, 486.
(6) Rogers, C. W.; Wolf, M. O. *Coord. Chem. Rev.* **2002**, *233-234*, 341.
(7) Anslyn, E. V. *J. Org. Chem.* **2007**, *72*, 687.
(8) Wu, J.; Liu, W.; Ge, J.; Zhang, H.; Wang, P. *Chem. Soc. Rev.* **2011**, *40*, 3483.
(9) Nguyen, B. T.; Anslyn, E. V. *Coord. Chem. Rev.* **2006**, *250*, 3118.
(10) Wright, A. T.; Anslyn, E. V. *Chem. Soc. Rev.* **2006**, *35*, 14.
(11) Grzybowski, B. A.; Wilmer, C. E.; Kim, J.; Browne, K. P.; Bishop, K. J. M. *Soft Matter* **2009**, *5*, 1110.
(12) Stuart, M. A. C.; Huck, W. T. S.; Genzer, J.; Mueller, M.; Ober, C.; Stamm, M.; Sukhorukov, G. B.; Szleifer, I.; Tsukruk, V. V.; Urban, M.; Winnik, F.; Zauscher, S.; Luzinov, I.; Minko, S. *Nat. Mater.* **2010**, *9*, 101.
(13) Fialkowski, M.; Bishop, K. J. M.; Klajn, R.; Smoukov, S. K.; Campbell, C. J.; Grzybowski, B. A. *J. Phys. Chem. B* **2006**, *110*, 2482.
(14) Boekhoven, J.; Brizard, A. M.; Kowlgi, K. N. K.; Koper, G. J. M.; Eelkema, R.; van Esch, J. H. *Angew. Chem. Int. Edit.* **2010**, *49*, 4825.
(15) Debnath, S.; Roy, S.; Ulijn, R. V. *J. Am. Chem. Soc.* **2013**, *135*, 16789.
(16) Fanlo-Virgos, H.; Alba, A.-N. R.; Hamieh, S.; Colomb-Delsuc, M.; Otto, S. *Angew. Chem. Int. Edit.* **2014**, *53*, 11346.
(17) Dambenieks, A. K.; Vu, P. H. Q.; Fyles, T. M. *Chemical Science* **2014**, *5*, 3396.
(18) Fletcher, S. P.; Dumur, F.; Pollard, M. M.; Feringa, B. L. *Science* **2005**, *310*, 80.
(19) Cheng, C.; McGonigal, P. R.; Liu, W.-G.; Li, H.; Vermeulen, N. A.; Ke, C.; Frasconi, M.; Stern, C. L.; Goddard, W. A., III; Stoddart, J. F. *J. Am. Chem. Soc.* **2014**, *136*, 14702.
(20) Ragazzon, G.; Baroncini, M.; Silvi, S.; Venturi, M.; Credi, A. *Nat. Nanotechnol.* **2014**, doi:10.1038/nnano.2014.260.

(21) For an example of transient signal generation in the context of enzyme assay development see:; Ghale, G.; Kuhnert, N.; Nau, W. M. *Nat. Prod. Commun.* **2012**, *7*, 343.
(22) A related strategy has been applied for studying the conformational dynamics of proteins; White, H. D. *J. Biol. Chem.* **1985**, *260*, 982.
(23) For anentirely different approach towards (irreversible) transient signal gene ration see:; Thomas, S. W., III; Chiechi, R. C.; LaFratta, C. N.; Webb, M. R.; Lee, A.; Wiley, B. J.; Zakin, M. R.; Walt, D. R.; Whitesides, G. M. *Proc. Natl. Acad. Sci. USA* **2009**, *106*, 9147.
(24) Molnar, J.; Lorand, L. *Arch. Biochem. Biophys.* **1961**, *93*, 353.
(25) McIntosh, V. J.; Lasley, R. D. *J. Cardiovasc. Pharmacol. Ther.* **2012**, *17*, 21.
(26) Junger, W. G. *Nat. Rev. Immunol.* **2011**, *11*, 201.
(27) Abbracchio, M. P.; Burnstock, G.; Verkhratsky, A.; Zimmermann, H. *Trends Neurosci.* **2009**, *32*, 19.
(28) Jarvis, M. F.; Khakh, B. S. *Neuropharmacol.* **2009**, *56*, 208.

Summary

Supramolecular chemistry is the chemistry of the non-covalent bond, *i.e.* all those chemical processes relying on non-covalent interactions between molecules. In the last decades, chemists have learned to exploit non-covalent interactions for the construction of sensors, catalysts and materials. In particular self-assembly, defined as the spontaneous organization of small molecules into a well-defined structure has emerged as the most attractive way to prepare highly complex molecular architectures of nanosized dimensions. In this Thesis, the self-assembly of small molecules on the surface of monolayer protected gold nanoparticles (Au NPs) is introduced as an approach toward the realization of complex chemical systems with minimal synthetic efforts. An essential role is played by Au NPs as they provide a robust multivalent surface for the binding of external molecules. The unique features of Au NPs such as stability, biocompatibility, ease of preparation and optoelectronic properties have led to their wide-spread use in a variety of functional supramolecular systems. The Au NPs used in this Thesis have a monolayer composed of thiols terminating with a 1,4,7-triazacyclononane (TACN)•Zn^{2+} complex. The resulting multivalent cationic surface provides a scaffold for the binding of small anionic molecules (*e.g.* peptides and nucleotides). In the first part, the attention is focused on understanding the interactions that drive the self-assembly of small oliogoanions on the monolayer surface. This process was studied by means of fluorescence spectroscopy, taking advantage of the well-known ability of gold clusters to quench the fluorescence of bound fluorophores. It emerged that the high affinity is determined by i) the number of negative charges of the oligoanion, ii) the chemical nature of the anionic groups and iii) the presence of hydrophobic moieties able to penetrate into the apolar part of the monolayer. These studies also showed that the metal ions in the monolayer acts as regulatory elements of the self-assembly process. It was shown that the valency of the self-assembled system, *i.e.* the number of bound molecules , can be precisely controlled in a reversible manner by the addition and removal of Zn^{2+} from the monolayer. The ability to control the self-assembly process was demonstrated by showing that a mixture of two different oligoanions, with the same number of negative charges but

with different anionic groups (phosphate *vs* carboxylate), spontaneously self-sorted on two different monolayer surfaces, thus creating two discrete topological domains in a homogeneous system. In the second part of the thesis, the obtained knowledge was used for the development of supramolecular sensors for the detection of small molecules and enzymes. The self-assembly of multiple fluorescence indicators on the monolayer surface resulted in a dynamic responsive surface able to generate finger-print patterns upon the addition of eight different di- and tri-nucleotides. The ability of the system to discriminate between ATP and ADP was then used for the development of a protein kinase assay relying on the monitoring of ATP→ADP conversion. With the aim to improve the sensitivity of this assay, an alternative system was subsequently developed in which ATP→ADP conversion led to activation of the catalytic activity of Au NPs. Also in this case a crucial role was played by the Zn^{2+} metal ions in the monolayer, by the formation of catalytic pockets able to catalyze a chromogenic reaction generating the output signal. In the final chapter all concepts were used to set up a dissipative system able to generate a transient signal, whose duration is determined by the amount of ATP added to the system. This last methodology provides for a straightforward way to gain temporal control over supramolecular processes, showing important analogies with the behaviours of natural systems.

Sommario

La chimica supramolecolare è definita come la chimica del legame non covalente, ovvero la chimica di tutti quei processi chimici che dipendono da interazioni non-covalenti tra molecole. Negli ultimi decenni, i chimici hanno imparato a sfruttare le interazioni non covalenti nello sviluppo di sensori, catalizzatori e materiali. In particolare, l'autoassemblaggio, definito come l'organizzazione spontanea di piccole molecole in una struttura ben definita, si è dimostrato essere il modo più conveniente per preparare architetture molecolari molto complesse e di dimensioni nanometriche. In questa Tesi, l'auto-assemblaggio di piccole molecole sulla superficie di nanoparticelle d'oro funzionalizzate (Au NPs) è usato come approccio per la realizzazione di sistemi chimici complessi, senza l'ausilio di complicate vie di sintesi. Le Au NPs svolgono un ruolo fondamentale, in quanto forniscono una robusta superficie polivalente per il legame con molecole esterne. Le caratteristiche uniche delle Au NPs, quali la stabilità, la biocompatibilità, la facilità di preparazione e le proprietà optoelettroniche, hanno portato ad una loro larga diffusione. Le Au NPs utilizzate in questa Tesi sono ricoperte da un monostrato organico composto da tioli la cui unità periferica è un legante (1,4,7-triazaciclononano) in grado di complessare ioni metallici come lo Zn^{2+}. La superficie cationica multivalente che ne deriva fornisce un'ottima piattaforma per il legame di piccole molecole anioniche (per esempio peptidi e nucleotidi). Nella prima parte di questa Tesi, l'attenzione è stata focalizzata sulla comprensione delle interazioni che guidano l'auto-assemblaggio di piccoli oliogoanioni sulla superficie del monostrato. Questo processo è stato studiato mediante spettroscopia di fluorescenza, sfruttando le note capacità dei cluster d'oro di spegnere la fluorescenza di fluorofori ad essi legati. Da questi studi è emerso che l'alta affinità è determinata i) dal numero di cariche negative dell'oligoanione, ii) dalla natura chimica dei gruppi anionici e iii) dalla presenza di porzioni idrofobiche in grado di penetrare nella parte apolare del monostrato. Questi studi hanno inoltre dimostrato che gli ioni metallici nel monostrato sono in grado di regolare il processo di auto-assemblaggio. È stato dimostrato che la valenza del sistema auto-assemblato, ovvero il numero di molecole legate, può essere controllata con precisione in modo reversibile

attraverso l'aggiunta e la rimozione di Zn^{2+}. La capacità di controllare il processo di auto-assemblaggio è stato confermato dimostrando come due oligoanioni differenti, aventi lo stesso numero di cariche negative ma diversi gruppi anionici (fosfato *vs* carbossilato), siano capaci di auto-organizzarsi spontaneamente sulla superficie di due monostrati differenti, creando due domini topologici in un sistema omogeneo. Nella seconda parte della Tesi, la conoscenza acquisita è stata utilizzata per lo sviluppo di sensori supramolecolari atti alla rivelazione di piccole molecole ed enzimi. Attraverso l'auto-assemblaggio di più indicatori di fluorescenza sulla superficie di un unico monostrato è stato possibile realizzare una superficie in grado di generare segnali specifici in risposta all'aggiunta di otto diversi nucleotidi. La capacità del sistema di discriminare tra ATP e ADP è stata poi fruttata per lo sviluppo di un saggio per protein-chinasi, basato sul monitoraggio della conversione ATP→ADP. Al fine di migliorare la sensibilità di questo saggio, è stato successivamente sviluppato un sistema alternativo, in cui la conversione ATP→ADP porta all'attivazione dell'attività catalitica delle Au NPs. Anche in questo caso, gli ioni Zn^{2+} presenti nel monostrato giocano un ruolo cruciale, formando dei siti catalitici in grado di catalizzare una reazione cromogena e quindi di generare un segnale rilevabile. Nel capitolo finale, questi concetti sono stati usati per sviluppare un sistema dissipativo in grado di generare un segnale transiente, la cui durata dipende dalla quantità di ATP aggiunto al sistema. Quest'ultima metodologia fornisce un modo semplice per controllare processi supramolecolari a livello temporale, mostrando importanti analogie proprie dei sistemi naturali.

Acknowledgements

Here we are, it's time to thank all the people I will never forget. Let me first thank my supervisor, Prof. Leonard J. Prins. He is the one who guided me during these years with an impressive dose of competence, devotion and patience. Leonard, thank you for the confidence and all the opportunities you gave me. Nothing could have been realized without your outstanding support.

Special thanks go to Dr. Grégory Pieters for all the tricks he taught me and his genuine friendship. For the amazing moments that we have spent together both in and outside the laboratory. Mercy beaucoup Greg, it was simply unique to work with you. I hope to see you soon!

I wish to thank also Prof. Kay Severin (EPFL, Switzerland) for his kindness and his collaboration in some of the results reported. Even if shortly, he accepted me in his amazing laboratory, where I had the opportunity to meet brilliant people like Albert Ruggi (I will never forget that lunch man!) and Boram Lee. Bo, thank you for your amazing statistical analyses!

I have to thank also my two undergraduate students Massimiliano Martinelli and Michela Salvi. They have tolerated my fussiness and worked very hard. Massimiliano, the red wine is still there, I will drink it soon! Michela, thanks for the work you carried out, I will never forget it.

Very specials thanks go to all the people I saw in the labs and with whom I shared the office. They are still suffering the effects of my mild form of autism, anyway they were always there, supporting me when it was needed, joking, discussing about life, dreaming, drinking "coffee" or smoking downstairs. Among others: Elisa, Enrico, Federico, Patrizia, Edmondo, Subha, Luca, Matteo, Jack, Antonio. Thank to all of you guys,"...we shall fight in the fields and in the streets, we shall fight in the hills, we shall never surrender...".

Final but not least, I thank my family because they love me and they will continue to do so.